IOP Publishing Plasma Sources Science and Technology
Plasma Sources Sci. Technol. **30** (2021) 085008 (11pp) https://doi.org/10.1088/1361-6595/ac17ca

Electron induced elastic and inelastic processes for perfluoroketone (PFK) molecules

Nirav Thakkar[1], Mohit Swadia[2], Minaxi Vinodkumar[3], Nigel Mason[4] and Chetan Limbachiya[5,*]

[1] M.N. Science College, Patan, 382 120, India
[2] H. V. H. P. institute of Science, Kadi, 382 443, India
[3] V. P. Science College, Vallabh Vidyanagar, 382 120, India
[4] School of Physical Sciences, The University of Kent, Canterbury, CT2 7NH, United Kingdom
[5] The M.S. University of Baroda, Vadodara, 390 001, India

E-mail: cglimbachiya-apphy@msubaroda.ac.in

Received 23 February 2021, revised 9 July 2021
Accepted for publication 26 July 2021
Published 18 August 2021

Abstract

We report the results of calculations of elastic and inelastic (ionization and excitation) cross sections for electron scattering from perfluoroketone molecules, $C_xF_{2x}O$ ($x = 1$–6) over a wide energy range, from ∼the ionization potential to 5 keV. These molecules have been determined to have extremely low global warming potentials and therefore may have applications in next generation gas discharges and plasma reactors. The results are derived using the complex scattering potential-ionization contribution method to investigate ionization cross sections Q_{ION} and are found to be in good agreement with the available data. The spherical complex optical potential formalism is used to evaluate elastic (Q_{EL}), inelastic (Q_{INEL}) and total cross sections (Q_T). This study is a maiden effort to report summed total excitation cross section ($\sum Q_{EXC}$), Q_{ION} and Q_{INEL} for CF_2O and C_2F_4O, and Q_{EL} and Q_T for $C_xF_{2x}O$ ($x = 1$–6). The study includes various correlation analyses and a prediction of the dipole polarizability.

Keywords: perfluoroketone, total cross sections, ionization, polarizability

S Supplementary material for this article is available online

(Some figures may appear in colour only in the online journal)

1. Introduction

The perfluoroketones (PFKs), $C_xF_{2x}O$ ($x = 1$–6) are a group of molecules that contain carbon–fluorine bonds and a ketone (figure 1). They have been found to have a low global warming potential (GWP) and thus PFK gases are being widely adopted by industry, e.g. as an insulating medium in high-voltage equipment and as cleaning, etching, doping gas agents in plasma reactors [1, 2] to replace sulphur hexafluoride (SF_6) which is commonly used as the gas insulating medium in various industrial electrical applications due to its good insulating capacity [3, 4]. SF_6 is also prominent greenhouse gas owing to its long lifetime (3200 years) in the terrestrial atmosphere and high GWP value of 23 500 over a 100 years time horizon [5–7]. The Kyoto protocol guidelines require reduction of global warming gases and hence emissions of SF_6 [8]. One of the four methods to treat SF_6 involves decomposition through plasma or electrical discharge leading to 100% removal of SF_6 [9]. In this situation due to the high dielectric strength, gases containing PFK molecules are considered as good substitute for SF_6 and could replace it as the insulating medium in high-voltage power apparatus.

The smallest PFK molecules e.g. CF_2O and C_2F_4O are also important by-products in inductively coupled plasma

* Author to whom any correspondence should be addressed.

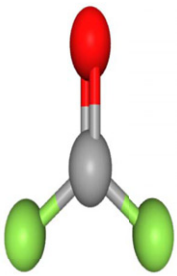

3D structure image of CID 9623 (CF_2O)
Pubchem Identifier: **CID 9623**
URL: https://pubchem.ncbi.nlm.nih.gov/compound/9623#section=3D-Conformer

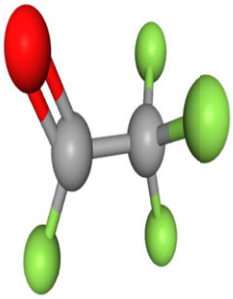

3D structure image of CID 67716 (C_2F_4O)
Pubchem Identifier: **CID 67716**
URL: https://pubchem.ncbi.nlm.nih.gov/compound/67716#section=3D-Conformer

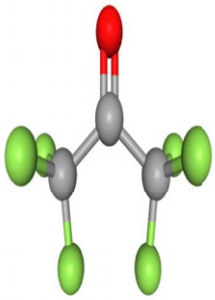

3D structure image of CID 12695 (C_3F_6O)
Pubchem Identifier: **CID 12695**
URL: https://pubchem.ncbi.nlm.nih.gov/compound/12695#section=3D-Conformer

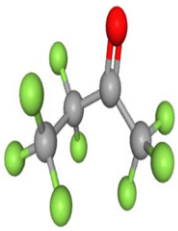

3D structure image of CID 3429852 (C_4F_8O)
Pubchem Identifier: **CID 3429852**
URL: https://pubchem.ncbi.nlm.nih.gov/compound/3429852#section=3D-Conformer

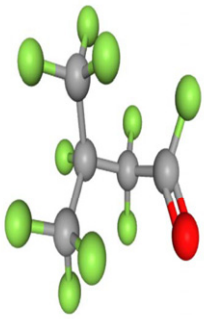

3D structure image of CID 14175377 ($C_5F_{10}O$)

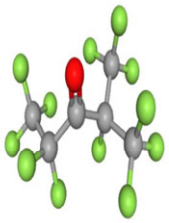

3D structure image of CID 14175377 ($C_6F_{12}O$)

Figure 1. Schematic diagrams of PFK molecules.

processes, such as Ar–CF_4–O_2 plasmas [10]. The low GWP value (100) of C_3F_6O has led it to being a replacement for SF_6 in the dry etching process of silicon compounds in the semiconductor as well as display industries [11]. C_4F_8O is now being used as a plasma processing gas in Cherenkov detectors and as cleaning agent for chemical vapour deposition chambers [12, 13] and in high-voltage gaseous insulation processes [12] and has low GWP (33% of SF_6) [12].

Owing to high dielectric strength (E_r), good arc quenching ability, low GWP and other applications in gas insulated switchgear (GIS) and gas insulated transmission line (GIL), $C_5F_{10}O$ and $C_6F_{12}O$ also have been preferred as alternative to SF_6. The dielectric strength of $C_5F_{10}O$ is twofold and GWP 1/23 900 times that of SF_6 [14]. Similarly $C_6F_{12}O$ has a higher dielectric strength (about 2.7 times) and a GWP around 1/23 500 times that of SF_6. Furthermore, it has low toxicity

Table 1. Dielectric Strength (E_r) and GWP relative to SF_6 of PFK molecules.

Molecule	E_r	GWP
SF_6	1 [15]	23 900 [16]
CF_2O	—	—
C_2F_4O	—	—
C_3F_6O	1 [18]	<100 [2]
C_4F_8O	1.2–1.4 [19]	8000 [12]
$C_5F_{10}O$	1.5–2.0 [15]	<1 [15]
$C_6F_{12}O$	2.7 [15]	1 [15]

(LC50 > 100 000 ppm) [15]. $C_6F_{12}O$ with air or CO_2 as the background gas is now deemed as a good replacement for SF_6 [16, 17]. However PFK molecules can provide effective economic and environmental alternative to SF_6. For ready reference we show in table 1 the dielectric strengths and GWP of the studied molecules relative to SF_6.

In plasma processes, electron driven ionisation of the PFK molecules is an important major process resulting in the initiation of the avalanche of electrons that determines whether the discharge is self-sustained. Electron induced ionization cross-sections for PFK molecules are basic inputs for the Boltzmann equation analysis and Monte Carlo simulations [20, 21] to calculate the dielectric strength of the gases. These models are used to determine swarm factors for electrons such as, coefficient of effective ionization, drift velocity and diffusion coefficient.

Thus in order to model the efficiency of the PFKs in the industrial gas discharges, GIS, GIL and plasma reactors it is necessary to compile a comprehensive set of electron scattering cross sections. However, to date electron interaction studies with PFKs are limited (table 2) and in particular data on inelastic processes including the determination of ionisation probabilities are scarce, while the investigation for elastic cross sections, Q_{EL} and the total (complete) cross sections, Q_T have not been reported. All allowed molecular phenomena upon the electron impact are encompassed by Q_T that confirms the event of the e-molecule collision [22, 23]. Hence, in this paper we compute Q_{EL} and Q_T for these important plasma relevant molecules for the first time.

The only experimental evaluation of Q_{ION} for PFK molecules is that of Chachereau *et al* [12] for C_4F_8O (<30 eV) using an electron beam method. For $C_xF_{2x}O$ ($x = 1$ to 5), theoretical Q_{ion} are reported by Zhong *et al* [2] through both the binary-encounter Bethe (BEB) and Deutsch Meark (DM) methods. $C_5F_{10}O$ was also studied by Wang *et al* [26] using the BEB method. Szmytkowski *et al* [24] reported Q_{ion} with BEB method for e-C_3F_6O scattering. Xiong *et al* [27] studied e-$C_5F_{10}O$ using a DM and modified DM method. Two different groups, Wang *et al* [26] and Wang *et al* [28] computed Q_{ion} for $C_6F_{12}O$. Wang *et al* [26] used the BEB method and Wang *et al* [28] investigated $C_6F_{12}O$ using Mulliken population analysis (MPA), natural atomic orbital (NAO) and C-squared population analysis (SCPA) techniques. All these groups have undertaken their work up to a maximum of 1000 eV. Recently Sinha *et al* [25] have computed Q_{INEL}, Q_{ION} and $\sum Q_{EXC}$ for C_3F_6O, C_4F_8O, $C_5F_{10}O$ and $C_6F_{12}O$ using the CSP-icN method.

The present work is the first attempt to determine the summed total excitation cross section $\sum Q_{EXC}$ and Q_{INEL} for CF_2O and C_2F_4O. We also note that there is no previous work, either experimental or theoretical reported on elastic (Q_{EL}) or total cross sections (Q_T) for these ketones. This prompted us to take up this exhaustive study on electron collision with these environmentally important plasma relevant, PFK ($C_xF_{2x}O$; $x = 1$–6) molecules from ionization potential (IP) to 5 keV.

2. Theoretical methodology

The calculations of the electron driven molecular processes employed in this work make use of two distinct methodologies, the spherical complex optical potential (SCOP) method [29–32] and the complex scattering potential-ionization contribution (CSP-ic) method [33–35].

2.1. SCOP method

All electron–molecule interactions except the elastic are related to the loss of projectile energy and are broadly encompassed into the inelastic channel. These interaction processes are described through an interaction potential called the optical potential, $V_{opt}(E_i, r)$ within the SCOP formalism under the fixed nuclei approach such that,

$$V_{opt}(E_i, r) = V_{st}(r) + V_{ex}(E_i, r) + V_{pol}(E_i, r) + iV_{abs}(E_i, r). \quad (1)$$

Here E_i is the incident energy and the short ranged static potential (V_{st}), which is a measure of the unperturbed molecular charge cloud, can be obtained using the Hartree Fock wave functions [36]. The exchange between the incident electron and one of the target electrons is given by the exchange potential (V_{ex}). Hara [37, 38] treated the Fermi gas of electrons as the total wave function being anti-symmetrized while the exchange energy is calculated from all momentum states up to Fermi level. The transient distortion of the molecular charge cloud in presence of the projectile electron is because of induced multipole moments and is accounted for by the polarization potential (V_{pol}). The imaginary term, the absorption potential (V_{abs}) corresponds to the transfer of projectile flux into inelastic scattering channels describing electronic excitation and ionization. In this work we have used the improved absorption potential [34, 39] given in a.u. as,

$$V_{abs} = -\frac{1}{2}\rho(r)v_{loc}\sigma_{ee}. \quad (2)$$

Here, v_{loc} is velocity of the projectile electron and σ_{ee} is mean probability of the binary impact between the projectile and a molecular electron. This absorption potential V_{abs} is given as,

$$V_{abs}(r, E_i) = -\rho(r)\left(\frac{T_{loc}}{2}\right)^{\frac{1}{2}}\left(\frac{8\pi}{10{k_F}^3 E_i}\right)\theta(p^2 - {k_F}^2 - 2\Delta) \times (A_1 + A_2 + A_3). \quad (3)$$

Table 2. Previous work on electron—PFK scattering study.

Target	Quantity	Impact energy range	Reference
CF_2O	Q_{ION}	Threshold to 1000 eV	Zhong *et al* (2018) [2]
C_2F_4O	Q_{ION}	Threshold to 1000 eV	Zhong *et al* (2018) [2]
C_3F_6O	Q_{ION}	Threshold to 1000 eV	Zhong *et al* (2018) [2]
			Szmytkowski *et al* (2011) [24]
	Q_{ION}, Q_{INEL}, $\sum Q_{EXC}$	Threshold to 5000 eV	Sinha *et al* (2020) [25]
C_4F_8O	Q_{ION}	Threshold to 1000 eV	Zhong *et al* (2018) [2]
		Threshold to 30 eV	Chachereau *et al* (2016) [12]
	Q_{ION}, Q_{INEL},$\sum Q_{EXC}$	Threshold to 5000 eV	Sinha *et al* (2020) [25]
$C_5F_{10}O$	Q_{ION}	Threshold to 1000 eV	Zhong *et al* (2018) [2]
		Threshold to 400 eV	Wang *et al* (2019) [26]
		Threshold to 2000 eV	Xiong *et al* (2017) [27]
	Q_{ION}, Q_{INEL}, $\sum Q_{EXC}$	Threshold to 5000 eV	Sinha *et al* (2020) [25]
$C_6F_{12}O$	Q_{ION}	Threshold to 400 eV	Wang *et al* (2019) [26]
		Threshold to 2000 eV	Wang *et al* (2020) [28]
	Q_{ION}, Q_{INEL}, $\sum Q_{EXC}$	Threshold to 5000 eV	Sinha *et al* (2020) [25]

The local kinetic energy of the incident electron is obtain from

$$T_{loc} = E_i - V_R = E_i - (V_{st} + V_{ex} + V_p).$$

In equation (3), $p^2 = 2E_i$, k_F is the Fermi wave vector and Δ is an energy parameter, $\theta(x)$ is the Heaviside step function, such that $\theta(x) = 1$ for $x > 0$, and is zero otherwise. The dynamic functions A_1, A_2 and A_3 depend differently on $\rho(r)$, I, Δ and E_i. The parameter Δ assumed to be fixed in the original model determines a threshold below which $V_{abs} = 0$, and the ionization or excitation is prevented energetically [39]. Here, we have modified Δ such that at impact energies close to the ionization threshold, excitations to the discrete states also take place, but as E_i increases valence ionization becomes dominant, together with possibility of ionization from the inner electronic shells.

All these model potentials make use of the molecular charge density $\rho(r)$ making its representation critical. We have used parameterized atomic charge densities obtained from the Hartree–Fock wave functions [36]. We have adopted the modified additivity rule to find the molecular charge density which is then used to develop the interaction potentials [32].

The SCOP formalism involves a partial wave approach under the spherical approximation leading to complex phase shifts $\delta_l(k)$ which carry the signature of the interaction between the incident electrons and molecule. At low impact energies only a few (<10) phase shifts are needed but as the impact energy increases more phase shifts are required for convergence [23, 31]. The scattering matrix is given as,

$$S_l(k) = \exp[2i\,(\mathrm{Re}\,\delta_l + i\,\mathrm{Im}\,\delta_l)]. \tag{4}$$

The imaginary term accounts for the 'inelasticity' or the absorption factor causing the inelastic effects during the interactions. We obtain the elastic and inelastic cross sections through the complex scattering amplitudes obtained from the scattering matrix $S_l(k)$.

2.2. CSP-ic method

A quantity of great applied interest is the total ionization cross section. The CSP-ic method was developed by some of the authors to compute Q_{ion} by defining a ratio $R(E_i)$ such that [33, 34]

$$R\,(E_i) = \frac{Q_{ion}\,(E_i)}{Q_{inel}\,(E_i)}.$$

The ratio $R(E_i)$ is expressed as a function of impact energy given as

$$R\,(E_i) = 1 - C_1\left(\frac{C_2}{U+a} + \frac{\ln U}{U}\right). \tag{5}$$

where, $U = \frac{E_i}{I}$ where E_i is impact energy and I is the IP of the target. We require three conditions to evaluate the three constants C_1, C_2 and 'a' as follows,

$$R(E_i)\begin{cases} = 0 & \text{for } E_i \leqslant I \\ = R_p & \text{for } E_i = E_p \\ \cong 1 & \text{for } E_i \gg E_p \end{cases}.$$

The ionization channel opens at the ionization threshold (I) of the molecule and is accompanied by discrete excitations given by $\sum Q_{EXC}$. However, at very high energies ionization dominates and excitation cross sections diminish greatly as required by the third condition. At the peak of inelastic cross sections, the $R(E_i) = R_p$. Thus, R_p is the value of the ratio $R(E_i)$ that is set at the impact energy E_p at which the inelastic cross sections attain peak. The value of R_p is close to 0.7–0.8 as observed through many experimental results for stable molecules such as H_2O, CH_4 [22, 40, 41] etc and noted theoretically [42, 43]. This feature renders the theory to be semi-empirical in nature and introduces an overall uncertainty of the order of 10%–15% [44]. Evaluating these conditions for $R(E_i)$ to find the constant C_1, C_2 and a enables us to compute the Q_{ION} and summed total excitation cross sections $\sum Q_{EXC}$ at least to within the accuracy required by users [34].

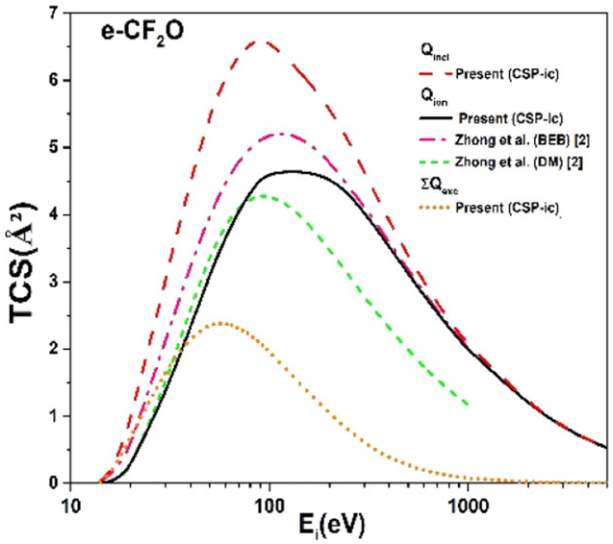

Figure 2. TCS for e-CF_2O collision solid line: present Q_{ION}; dash line: present Q_{INEL}; dash dot line: Zhong *et al* [2] Q_{ION} (BEB); short dash line: Zhong *et al* [2] Q_{ION} (DM); dot line: present $\sum Q_{EXC}$.

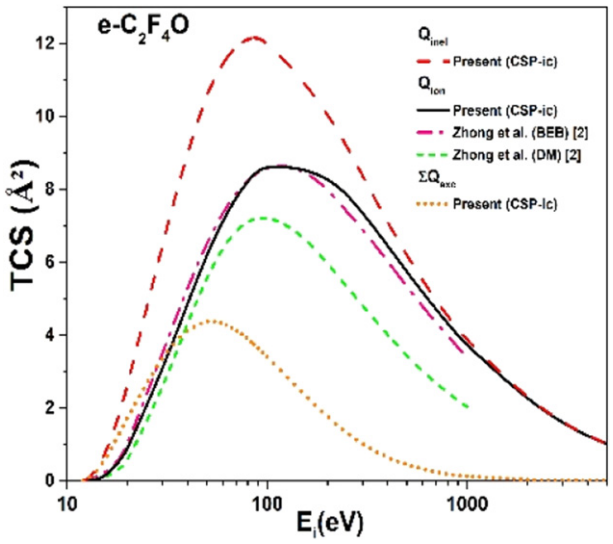

Figure 3. TCS for e-C_2F_4O collision solid line: present Q_{ION}; dash line: present Q_{INEL}; dash dot line: Zhong *et al* [2] Q_{ION} (BEB); short dash line: Zhong *et al* [2] Q_{ION} (DM); dot line: present $\sum Q_{EXC}$.

The target properties that we use for these computations are the IP and polarisability and they are taken from literature [2, 14, 25, 45]. From the relation of total cross sections with polarizability of the molecule we predict in this work the polarizability of three molecules, C_2F_4O, $C_5F_{10}O$ and $C_6F_{12}O$.

3. Results and discussion

In this work we have undertaken the first exhaustive study of electron interactions with six environmentally important PFK molecules, $C_xF_{2x}O$ ($x = 1$–6) and reported numeric (in supplementary data (https://stacks.iop.org/PSST/30/085008/mmedia)) as well as graphical data on various total cross sections. We present our results along with accessible data from literature in three subsections,

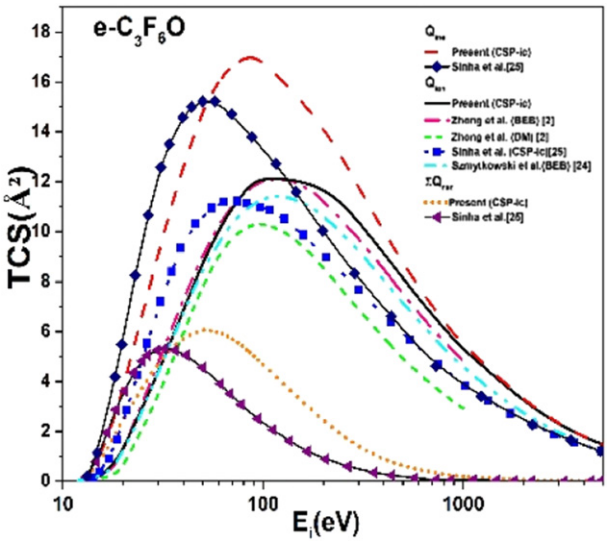

Figure 4. TCS for e-C_3F_6O collision solid line: present Q_{ION}; dash line: present Q_{INEL}; dash dot line: Zhong *et al* [2] Q_{ION} (BEB); short dash line: Zhong *et al* [2] Q_{ION} (DM); short dot line: present $\sum Q_{EXC}$; -■- line: Sinha *et al* [25] Q_{ION} (CSP-icN); dash dot dot line: Szmytkowski *et al* [24] Q_{ION} (BEB); -♦- line: Sinha *et al* [25] Q_{INEL} (CSP-icN); -◀- line: Sinha *et al* [25] $\sum Q_{EXC}$ (CSP-icN).

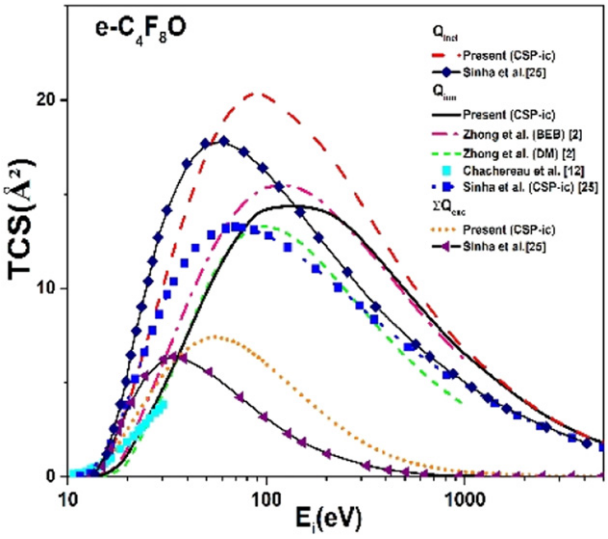

Figure 5. TCS for e-C_4F_8O collision solid line: present Q_{ION}; dash line: present Q_{INEL}; dash dot line: Zhong *et al* [2] Q_{ION} (BEB); short dash line: Zhong *et al* [2] Q_{ION} (DM); dot line: present $\sum Q_{EX}$; ■ Chachereau *et al* [12] Q_{ION}; -■- line: Sinha *et al* [25] Q_{ION} (CSP-icN); -♦- line: Sinha *et al* [25] Q_{INEL} (CSP-icN); -◀- line: Sinha *et al* [25] $\sum Q_{EXC}$ (CSP-icN).

(1) Inelastic processes (2) elastic process and (3) various correlations in derived cross sections and a prediction of polarizability.

3.1. Inelastic processes

In this sub section we show present Q_{INEL}, Q_{ION} and $\sum Q_{EXC}$ through figures 2–7 for $C_xF_{2x}O$ ($x = 1$–6) respectively and compare with previous work.

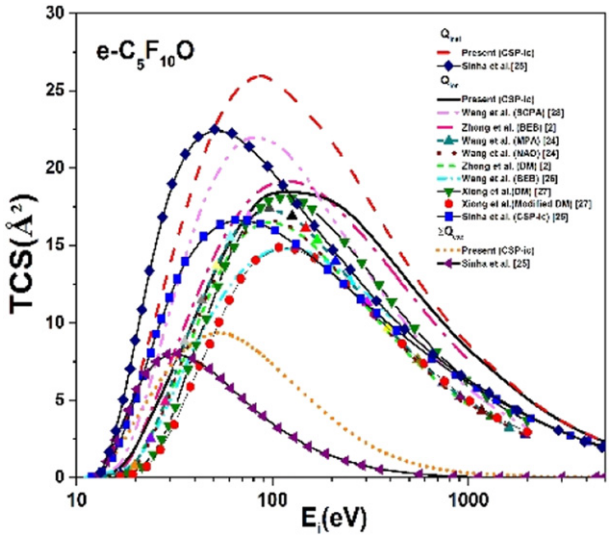

Figure 6. TCS for e-$C_5F_{10}O$ collision solid line: present Q_{ION}; dash line: present Q_{INEL}; dash dot line: Zhong *et al* [2] Q_{ION} (BEB); short dash line: Zhong *et al* [2] Q_{ION} (DM); short dot line: present $\sum Q_{EXC}$; dash dot dot line: Wang *et al* [28] Q_{ION} (SCPA); -▲- line: Wang *et al* [28] Q_{ION} (MPA); dot line: Wang *et al* [28] Q_{ION} (NAO); short dash dot line: Wang *et al* [26] Q_{ion} (BEB); -▼- line: Xiong *et al* [27] Q_{ION} (DM); -●- line: Xiong *et al* [27] Q_{ION} (modified DM); -■- line: Sinha *et al* [25] Q_{ION} (CSP-icN); -♦- line: Sinha *et al* [25] Q_{INEL} (CSP-icN); -◀- line: Sinha *et al* [25] $\sum Q_{EXC}$ (CSP-icN).

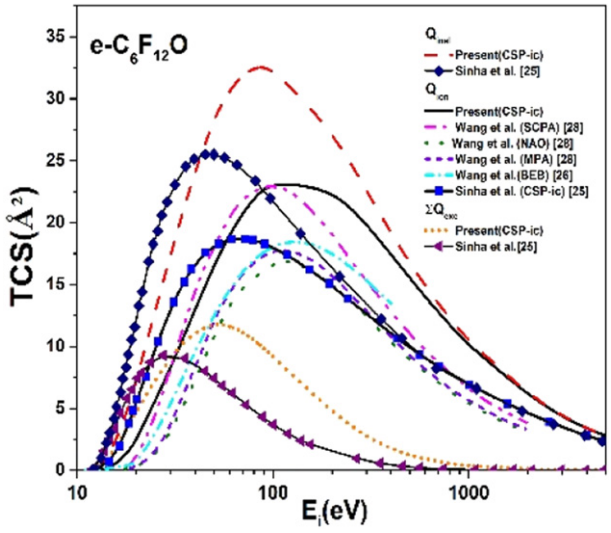

Figure 7. TCS for e-$C_6F_{12}O$ collision solid line: present Q_{ION}; dash line: present Q_{INEL}; short dot line: present $\sum Q_{EXC}$; dash dot dot line: Wang *et al* [28] Q_{ION} (SCPA); short dash line: Wang *et al* [28] Q_{ION} (MPA); dot line: Wang *et al* [28] Q_{ION} (NAO); short dash dot line: Wang *et al* [26] Q_{ION} (BEB);-■- line: Sinha *et al* [25] Q_{ION} (CSP-icN); -♦- line: Sinha *et al* [25] Q_{INEL} (CSP-icN); -◀- line: Sinha *et al* [25] $\sum Q_{EXC}$ (CSP-icN).

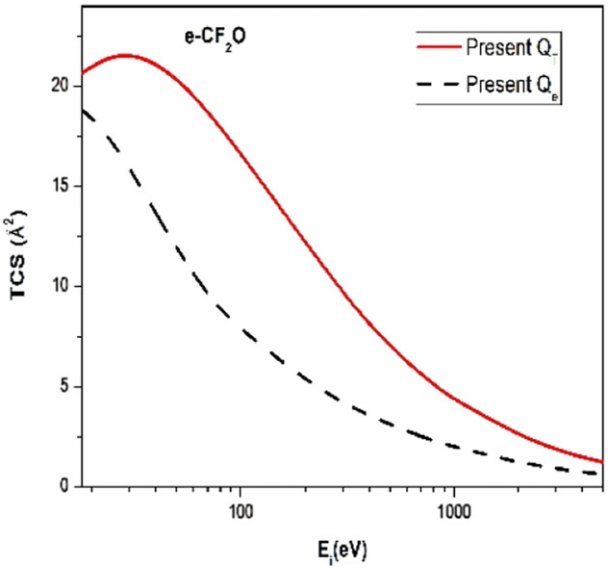

Figure 8. TCS for e-CF_2O collision.

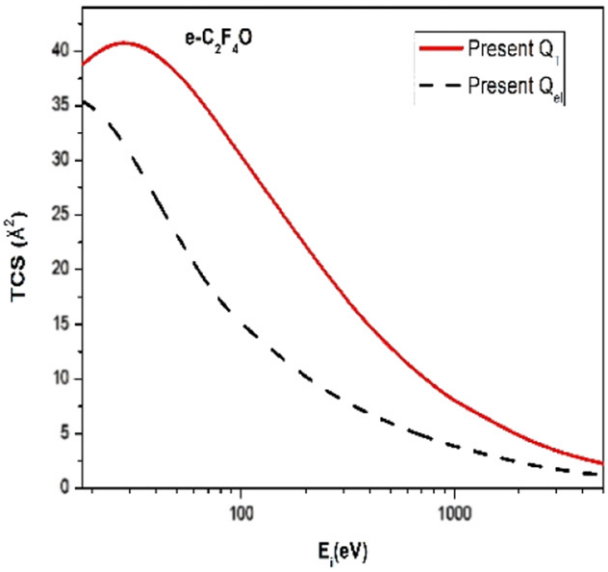

Figure 9. TCS for e-C_2F_4O collision.

As shown in figure 2, our Q_{ION} for e-CF_2O are in good agreement with the Zhong *et al* [2] derived using the BEB approximation over the higher energy range. However, our Q_{ION} values rise rather slower at the threshold and are smaller than the BEB results at the peak albeit within the quoted uncertainty of about 10% for BEB results [33, 46, 47]. While the present results of Q_{ION} are higher than the DM results of Zhong *et al* [2] and they do not include indirect ionization such as auto-ionization etc beyond the peak value, they are in agreement at lower energies below 80 eV. The top most curve shows present Q_{INEL} that contains all electronic excitations and ionization and the lower most is $\sum Q_{EXC}$ for which we do not find any comparison in the literature.

As shown in figure 3 present Q_{ION} data for e-C_2F_4O is in excellent agreement with the BEB data throughout the entire energy range [2]. The DM results of Zhong *et al* [2] are relatively lower than the present results as well as the BEB results of Zhong *et al* [2] beyond 50 eV. For C_2F_4O also Q_{inel} and $\sum Q_{exc}$ are computed for the first time in this work.

In figure 4, we show cross sections for electron scattering from C_3F_6O. When we compare Q_{INEL} (top most curve) and

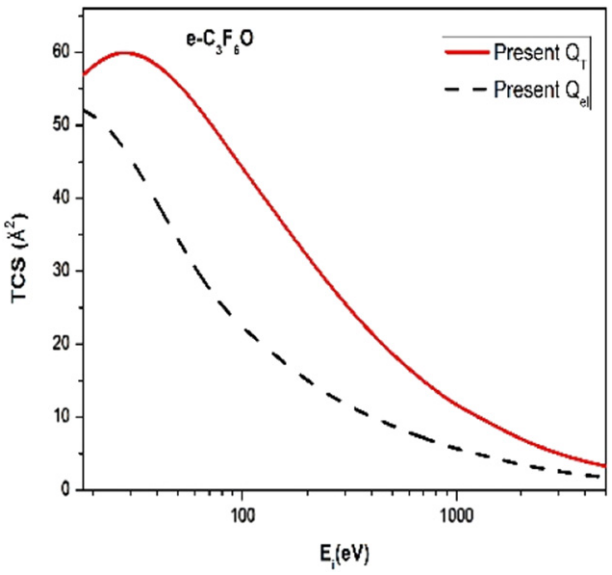

Figure 10. TCS for e-C_3F_6O collision.

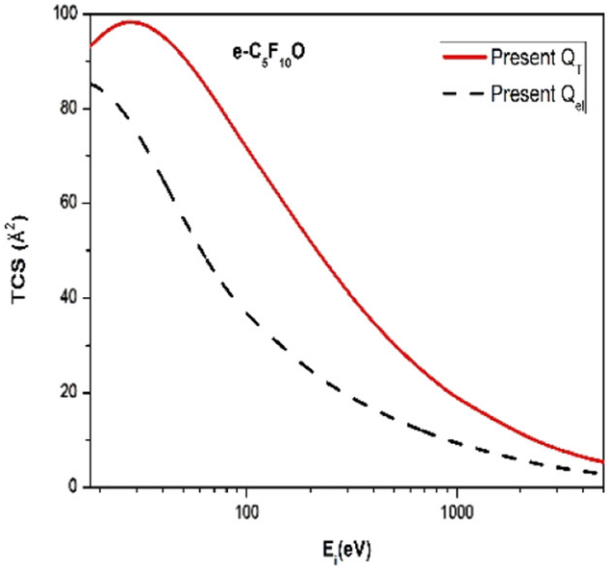

Figure 12. Q_T and Q_{el} for e-C_4F_8O scattering.

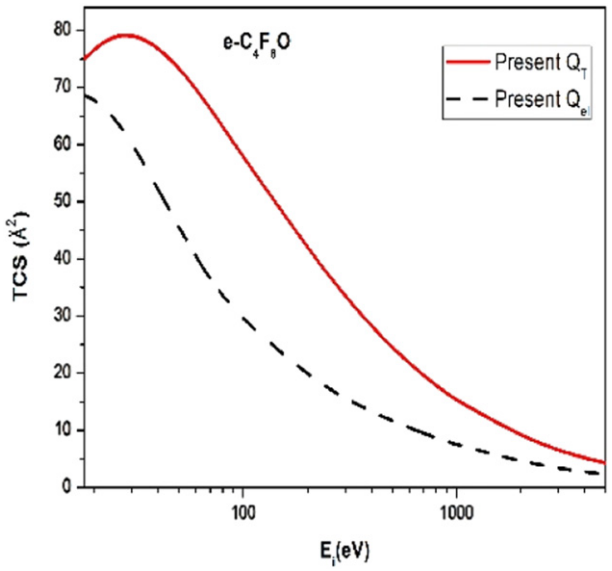

Figure 11. TCS for e-C_4F_8O collision.

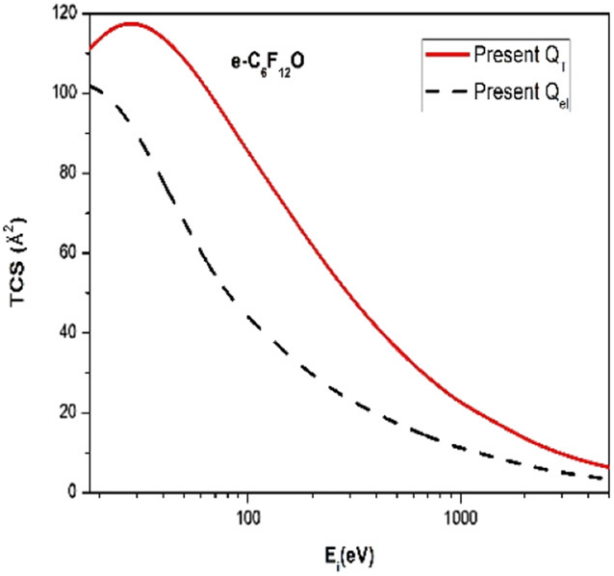

Figure 13. Q_T and Q_{el} for e-$C_6F_{12}O$ scattering.

$\sum Q_{EXC}$ (lower most curve) we observe that the present data are higher in magnitude than the data of Sinha *et al* [25] and their peaks are at lower energies.

The Q_{ION} data obtained by Sinha *et al* [25] is slightly lower compared to the present results as well as BEB data and their peak value occurs at lower energy as compared to all the other results. This shift may be due to the inclusion of nuclear charge for computation which affects the peak value and its position as pointed out by Sinha *et al* [25]. The present Q_{ION} are in excellent agreement with results of BEB calculations reported by Zhong *et al* [2] throughout the energy range of investigation. The DM results once again are consistently lower than both the present and BEB results [2] beyond the peak of Q_{ION} while showing reasonable accord up to the peak of Q_{ION}.

Similar trend is observed for e-C_4F_8O for present Q_{INEL}, Q_{ION} and $\sum Q_{EXC}$ with respect to the results of Sinha *et al* [25] as shown in figure 5. The present Q_{ION} values are in good agreement with those determined by Zhong *et al* using the BEB method [2]. The present results and BEB results are once more higher than those derived using the DM method beyond the peak of Q_{ION} but at low energies the present data is in good agreement. The present data also shows good agreement with the only experimental study, Chachereau *et al* [12] available only for low energies (<30 eV).

In figure 6, present Q_{INEL} and $\sum Q_{EXC}$ for $C_5F_{10}O$ are compared with Sinha *et al* [25] and we observe similar behaviour as discussed earlier. Present Q_{ION} are in excellent agreement with cross sections derived by Zhong *et al* [2] using the BEB

Table 3. Target properties and predicted polarizability.

			Polarizability (10^{-24} cm^{-3})		
N	Target	IP (eV)	Available	Predicted	Computed through www.chemspider.com
32	CF_2O	13.89 [2]	1.88 (www.cccbdb.gov.in)	—	2.8
56	C_2F_4O	12.84 [2]	—	4.21	4.6 (deviation 8.4%)
80	C_3F_6O	12.05 [2]	5.62 [14], 7.5 [25]	—	6.7
104	C_4F_8O	12.84 [2]	7.47 [14], 7.96 [25]	—	8.6
128	$C_5F_{10}O$	12.02 [2]	8.83 [25]	9.84	10.6 (deviation 7.1%)
152	$C_6F_{12}O$	11.41 [45]	11.44 [25]	12.54	12.6 (deviation 0.4 %)

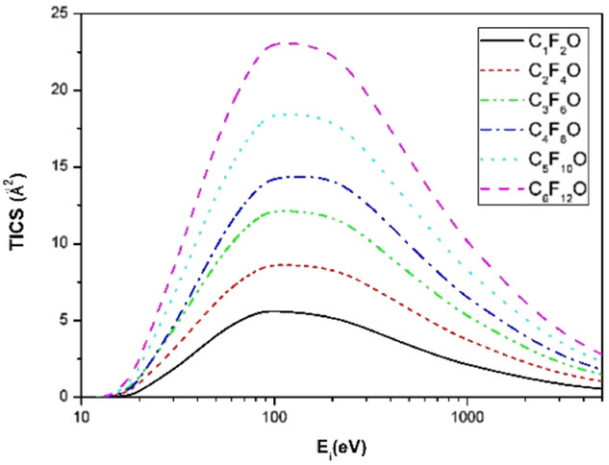

Figure 14. Present Q_{ION} for e-$C_xF_{2x}O$ ($x = 1$–6) collision.

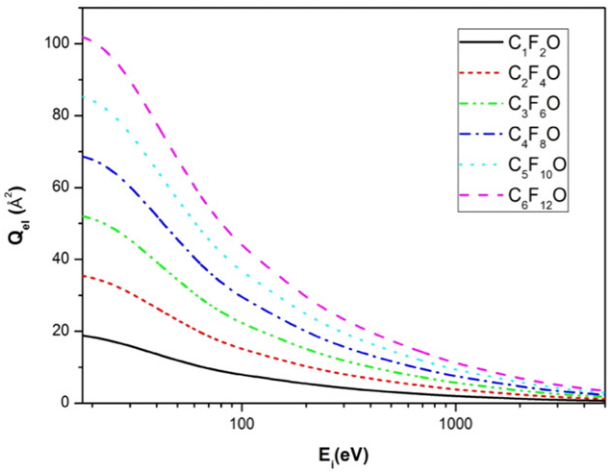

Figure 15. Present Q_{EL} for e-$C_xF_{2x}O$ ($x = 1$–6) collision.

method throughout the energy range (IP-5000 eV). The DM results of Q_{ION} are systematically lower than both the present and BEB results beyond the peak of Q_{ION} [2]. The BEB results of Q_{ION} obtained by Wang *et al* [26] underestimate the present results and BEB results of Zhong *et al* [2]. The present Q_{ION} are in good agreement with the results reported by Wang *et al* [28] using MPA and NAO methods for low energies i.e. below Q_{ION} (peak). However the Wang *et al* [28] results using the SCPA (C-squared population analysis) method overestimate all the results of Q_{ION}. The present results are also in good agreement with those of Xiong *et al* [27] derived using the DM method while their modified DM results [27] appear to underestimate the cross sections. The present results along with the BEB results of Zhong *et al* [2] overestimate the data of Sinha *et al* [25] with the peak value of Sinha *et al* [25] at a lower energy.

Similar behaviour as discussed earlier is observed for e-$C_6F_{12}O$ for present Q_{INEL}, Q_{ION} and $\sum Q_{EXC}$ with respect to the results of Sinha *et al* [25] as shown in figure 7. The present Q_{ION} show relatively good agreement with results given by Wang *et al* [28] using the SCPA method for energies up to Q_{ION} peak beyond which the present data tends to be higher than the calculations of Wang *et al* (SCPA) [28]. The present results of Q_{ION} are also higher than those derived using NAO as well as MPA methods by Wang *et al* [28]. The BEB results of Q_{ION} obtained by Wang *et al* [26] are systematically lower than our results. However the position of the Q_{ION} (peak) is same for present and the BEB data of Wang *et al* [26].

3.2. Elastic process

In this sub section we show present Q_{EL} and Q_T through figures 8–13 for $C_xF_{2x}O$ ($x = 1$–6) respectively.

The method of SCOP enables us to compute Q_{EL} along with Q_{INEL} as follows,

$$Q_T(E_i) = Q_{EL}(E_i) + Q_{INEL}(E_i).$$

In these figures the upper curves show Q_T for $C_xF_{2x}O$ ($x = 1$–6) molecules. Q_T represents probability of occurrence of all the electron induced molecular phenomena and it has applications in various modelling techniques [22, 31]. As can be seen Q_T falls as $\frac{\ln E_i}{E_i}$ at higher energies following the Born–Bethe trend. The lower curves in all these figures show the Q_{el} for $C_xF_{2x}O$ ($x = 1$–6) molecules.

This work presents the first attempt to report Q_{EL} and Q_T for these important molecules relevant to environmental and plasma sciences upon electron impact.

3.3. Various correlations in derived cross sections and a prediction of polarizability

Various target properties are listed in table 3 along with the polarizability of three molecules, C_2F_4O, $C_5F_{10}O$ and $C_6F_{12}O$ as predicted in this work. The size of the molecular cloud depends on the number of electrons (N) of the molecule.

The SCOP formalism describes the electron interacting with the molecular charge cloud and allows for the quantitative evaluation of probabilities of various electron assisted

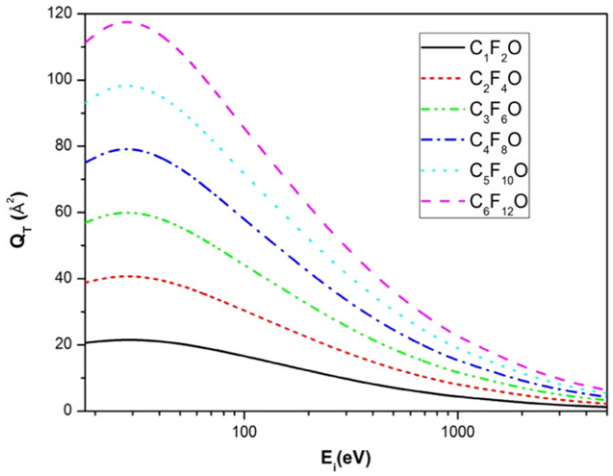

Figure 16. Present Q_T for e-$C_xF_{2x}O$ ($x = 1$–6) collision.

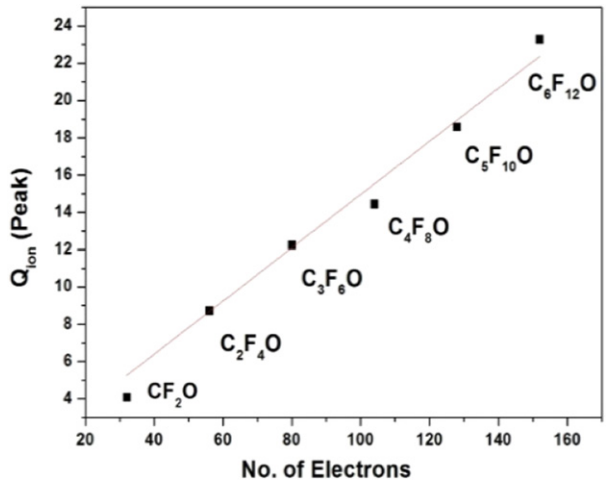

Figure 17. Correlation between Q_{ION} (peak) and number of electrons (N).

molecular phenomena. Hence it is sensitive to the size of the cloud through the number of electrons (N) of the target molecule. This feature can be seen in figure 14, where Q_{ION} of all the molecules are plotted. As the size of the charge cloud increases, the magnitudes of these cross sections also increase for given impact energy. A similar trend is observed in figures 15 and 16 where Q_{EL} and Q_T are shown respectively.

Apart from the size of the molecular cloud, the Q_{ION} are also sensitive to the first IP which does not show great deviation for these large molecules (table 3). Hence the peaks of Q_{ION} show linear relation with N (figure 17). The slight deviation in IPs of CF_2O and $C_6F_{12}O$ is reflected in figure 17. The point for CF_2O is below the line due to slightly higher IP and that for $C_6F_{12}O$ is above the line owing to marginally lower IP (table 3).

We have also observed a linear relationship between Q_{ION} (peak) with polarizability, α (figure 18) as well as $\sqrt{\alpha/I}$ (figure 19) as proposed by Bart *et al* [48]. This has enabled us to predict the polarizability for three molecules, C_2F_4O, $C_5F_{10}O$ and $C_6F_{12}O$. We then compared the predicted α with that computed using an online software, www.chemspider.com

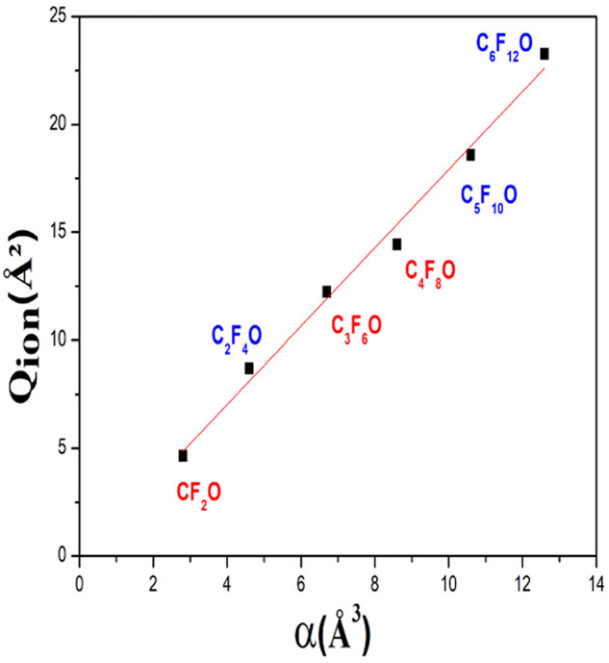

Figure 18. Correlation between Q_{ION} (peak) and polarizability α.

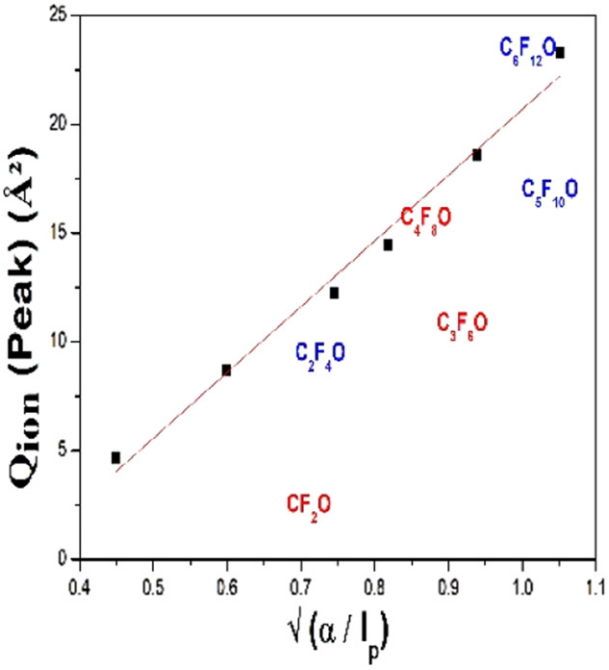

Figure 19. Correlation between Q_{ION} (peak) and $\sqrt{\alpha/I_p}$.

and found excellent accord with matching up to 91.6% for C_2F_4O, 92.9% for $C_5F_{10}O$ and 99.6% for $C_6F_{12}O$ as shown in table 3.

The combination of SCOP and CSP-ic enables us to compute total cross sections for many complex molecules under the same methodology with a slight uncertainty of about 10% due to the spherical approximation and semi-empirical nature of evaluation of Q_{ION}. We display comparative magnitudes of various TCS computed in this work for e-C_3F_6O at $E_p = 90$ eV

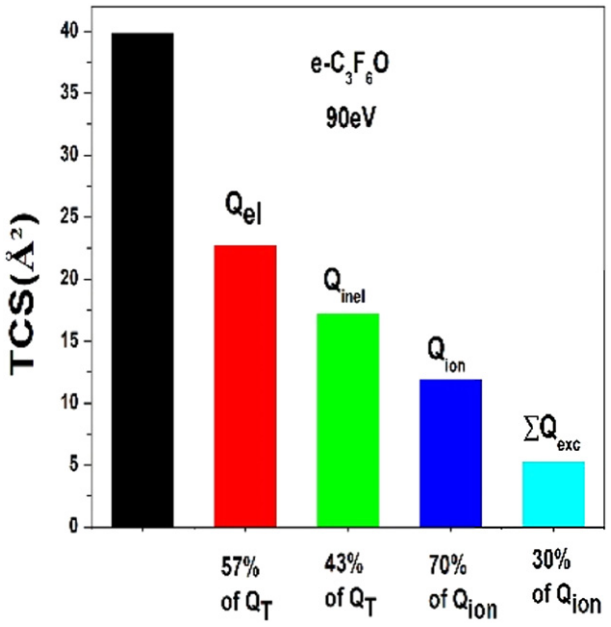

Figure 20. Relative total cross sections.

(figure 20). While Q_T show the upper bound for the electron induced phenomena, Q_{el} is 57% of Q_T and Q_{INEL} is 43% of Q_T. Although as pointed out by Joachain [49], Q_{EL} should be equal to Q_{INEL} at E_p, slight deviation in the present case is due to the approximations involved in the theory. The contribution of Q_{ION} in Q_{INEL} is 70% and $\sum Q_{EXC}$ are 30% of Q_{INEL} as expected. All these applied quantities are calculated purely under the quantum framework. This renders reliability and consistency to the results and validates the robustness of the theory.

4. Conclusion

We have carried a comprehensive theoretical study of electron scattering from PFK molecules, $C_xF_{2x}O$ ($x = 1$–6) over a wide energy range from ∼the molecular IP to 5 keV. We have used the SCOP formalism to evaluate total elastic (Q_{EL}), total inelastic (Q_{INEL}) and total cross sections (Q_T) and used CSPic method to derive total ionization (Q_{ION}) and summed total excitation cross sections ($\sum Q_{EXC}$). The computed results are shown graphically (figures 2–13) and as well as numerically in supplementary data. We have found the computed Q_{ION} to be in good agreement with the available BEB data [2, 22] and often the SCPA data of Wang *et al* [28] but while the DM results [2] tend to match well up to 70–80 eV for $C_xF_{2x}O$ ($x = 1$–4) these cross sections are in general lower than the values we have derived.

We correlated the cross sections with the size of the molecular cloud through the total number of electrons, N (figures 14–16) and found that the TCSs increase with the number of electrons of the target. We observed the sensitivity of Q_{ION} with the IP and found linear relation for Q_{ION} (peak) with N in absence of much deviation in IP for these targets (figure 17). We also correlated the Q_{ION} (peak) with IP and polarizability (figures 18–19) and observe the linear relation as predicted by Bart *et al* [48]. Using these correlation analyses we predicted the dipole polarizability for $C_xF_{2x}O$ ($x = 2, 5, 6$) and found that our predicted polarizabilities are in excellent agreement with those computed using online software www.chemspider.com.

This study is the first attempt to report $\sum Q_{EXC}$ and Q_{INEL} for CF_2O and C_2F_4O and Q_{EL}, and Q_T for all these important environmental and plasma relevant molecules whose extremely low GWPand higher dielectric strength make them attractive candidates for use by industry. We hope this work may encourage experimentalists and other theoreticians to pursue similar work.

Acknowledgments

Minaxi Vinodkumar acknowledges DST-SERB, New Delhi for the Major research Project [EMR/2016/000470] for financial support under which part of this work is carried out.

Data availability statement

All data that support the findings of this study are included within the article (and any supplementary files).

ORCID iDs

Nirav Thakkar https://orcid.org/0000-0002-0303-5175
Minaxi Vinodkumar https://orcid.org/0000-0002-1227-4717
Chetan Limbachiya https://orcid.org/0000-0003-2845-1244

References

[1] Kesari S, Behr F E, Costello M G, Flynn R M, Minday R M, Owens J G and Zazzera L A 2003 *US Patent* 6540930 (Washington, DC: US Patent and Trademark Office)
[2] Zhong L, Wang J, Wang X and Rong M 2018 *Plasma Sources Sci. Technol.* **27** 095005
[3] Tang J, Rao X, Tang B, Liu X, Gong X, Zeng F and Yao Q 2017 *IEEE Trans. Dielectr. Electr. Insul.* **24** 2066–75
[4] Dervos C T, Vassiliou P and Mergos J A 2007 *J. Phys. D: Appl. Phys.* **40** 6942–52
[5] Maiss M and Brenninkmeijer C A M 1998 *Environ. Sci. Technol.* **32** 3077–86
[6] Fu Y, Wang X, Li X, Yang A, Han G, Lu Y, Wu Y and Rong M 2016 *AIP Adv.* **6** 085305
[7] Wu Y *et al* 2017 *J. Phys. D: Appl. Phys.* **50** 385202
[8] Oberthür S and Ott H E 1999 *The Kyoto Protocol: International Climate Policy for the 21st Century* (Berlin: Springer)
[9] Zhang J, Zhou J Z, Liu Q, Qian G and Xu Z P 2013 *Environ. Sci. Technol.* **47** 6493–9
[10] Ide A, Furuya K, Okumura H and Harata A 2007 *The 28th Int. Conf. Phenomena in Ionized Gases (ICPIG)* (Prague, Czech Republic) pp 1572–5
[11] Kim I J, Moon H K, Lee J H, Lee N-E, Jung J W and Cho S H 2012 *Microelectron. Reliab.* **52** 2970–4
[12] Chachereau A, Fedor J, Janečková R, Kočišek J, Rabie M and Franck C M 2016 *J. Phys. D: Appl. Phys.* **49** 375201
[13] Kim K J, Oh C H, Lee N-E, Kim J H, Bae J W, Yeom G Y and Yoon S S 2004 *J. Vac. Sci. Technol.* B **22** 483–8

[14] Zhong L, Rong M, Wang X, Wu J, Han G, Han G, Lu Y, Yang A and Wu Y 2017 *AIP Adv.* **7** 075003
[15] Rabie M and Franck C M 2018 *Environ. Sci. Technol.* **52** 369–80
[16] Mantilla J D, Gariboldi N, Grob S and Claessens M 2014 *IEEE Electrical Insulation Conf. (EIC)* (IEEE) pp 469–73
[17] Linteris G T, Babushok V I, Sunderland P B, Takahashi F, Katta V R and Meier O 2013 *Proc. Combust. Inst.* **34** 2683–90
[18] Yu X, Hou H and Wang B 2017 *J. Comput. Chem.* **38** 721–9
[19] Gao Z, Wang Y, Wang S, Peng R, Zhou W, Yu P and Luo Y 2020 *IEEE Access* **8** 3007–15
[20] Vinodkumar M, Bhutadia H, Limbachiya C and Joshipura K N 2011 *Int. J. Mass Spectrom.* **308** 35–40
[21] Joshipura K N, Vaishnav B G and Limbachiya C G 2006 *Pramana J. Phys.* **66** 403–14
[22] Vinodkumar M, Limbachiya C, Barot A and Mason N 2013 *Phys. Rev.* A **87** 012702
[23] Limbachiya C, Vinodkumar M and Mason N 2011 *Phys. Rev.* A **83** 042708
[24] Szmytkowski C, Możejko P and Ptasińska-Denga E 2011 *J. Phys. B: At. Mol. Opt. Phys.* **44** 205202
[25] Sinha N, Patel V M and Antony B 2020 *J. Phys. B: At. Mol. Opt. Phys.* **53** 145101
[26] Wang F, Dun Q, Chen S, Zhong L, Fan X and Li L 2019 *IEEE Trans. Dielectr. Electr. Insul.* **26** 1693–700
[27] Xiong J, Li X, Wu J, Guo X and Zhao H 2017 *J. Phys. D: Appl. Phys.* **50** 445206
[28] Wang Y, Tian S, Zhang X, Liu W, Wang Y and Zhang G 2020 *AIP Adv.* **10** 035217
[29] Jain A 1986 *Phys. Rev.* A **34** 3707–22
[30] Jain A and Baluja K L 1992 *Phys. Rev.* A **45** 202–18
[31] Vinodkumar M, Limbachiya C, Desai H and Vinodkumar P C 2014 *Phys. Rev.* A **89** 062715
[32] Limbachiya C, Chaudhari A, Desai H and Vinodkumar M 2015 *RSC Adv.* **5** 103964–76
[33] Limbachiya C, Vinodkumar M, Swadia M and Barot A 2013 *Mol. Phys.* **112** 101–6
[34] Joshipura K, Vinodkumar M, Limbachiya C and Antony B 2004 *Phys. Rev.* A **69** 022705
[35] Swadia M, Thakar Y, Vinodkumar M and Limbachiya C 2017 *Eur. Phys. J.* D **71** 85
[36] Cox H L and Bonham R A 1967 *J. Chem. Phys.* **47** 2599–608
[37] Hara S 1967 *J. Phys. Soc. Japan* **22** 710–8
[38] Vinodkumar M, Limbachiya C and Bhutadia H 2009 *J. Phys. B: At. Mol. Opt. Phys.* **43** 015203
[39] Staszewska G, Schwenke D W, Thirumalai D and Truhlar D G 1983 *Phys. Rev.* A **28** 2740–51
[40] Vinodkumar M, Joshipura K N, Limbachiya C G and Antony B K 2003 *Nucl. Instrum. Methods Phys. Res.* B **212** 63–6
[41] Joshipura K N, Gangopadhyay S, Limbachiya C G and Vinodkumar M 2007 *J. Phys.: Conf. Ser.* **80** 012008
[42] Turner J E, Paretzke H G, Hamm R N, Wright H A and Ritchie R H 1982 *Radiat. Res.* **92** 47
[43] Vinodkumar M, Korot K and Vinodkumar P C 2010 *Eur. Phys. J.* D **59** 379–87
[44] Rahman M A, Gangopadhyay S, Limbachiya C, Joshipura K N and Krishnakumar E 2012 *Int. J. Mass Spectrom.* **319–320** 48–54
[45] Zhang X, Tian S, Xiao S, Deng Z, Li Y and Tang J 2017 *Energies* **10** 1170
[46] Kim Y and Desclaux J 2002 *Phys. Rev.* A **66** 012708
[47] Kim Y and Stone P 2001 *Phys. Rev.* A **64** 052707
[48] Bart M, Harland P W, Hudson J E and Vallance C 2001 *Phys. Chem. Chem. Phys.* **3** 800–6
[49] Joachain C J 1983 *Quantum Collision Theory* (Amsterdam: North-Holland) p 107

Radiation Physics and Chemistry 214 (2024) 111248

Contents lists available at ScienceDirect

Radiation Physics and Chemistry

journal homepage: www.elsevier.com/locate/radphyschem

Scattering of electrons with aqueous biomaterials

Smruti Parikh [a], Dhaval Chauhan [a], Nirav Thakkar [b], Chetan Limbachiya [a,*]

[a] Department of Applied Physics, The Maharaja Sayajirao University of Baroda, Vadodara, 390001, India
[b] Sheth M. N. Science College, Patan, 384265, India

ARTICLE INFO

Handling Editor: Dr. Chris Chantler

Keywords:
Aqueous DNA compounds
Cross-sections
Dielectric constant
Polarisability

ABSTRACT

The aqueous phase of DNA, which is more realistic phase due to the presence of H-bonds is studied in this work for various molecular processes upon electron impact. We report computed probabilities of various interaction processes taking place during the collision of electrons with DNA molecules, viz., Adenine, Guanine, Cytosine, Thymine and Uracil in their aqueous phase. Modified spherical complex potential approach has been employed for the quantification of various (N+1) elastic and inelastic including ionisation interactions through the cross-sections. Since no study for electron scattering with aqueous DNA is available, we compared our results with condensed phase and also a new approach for estimating the elastic and total cross-sections has been proposed in the present work for larger and complex molecules ($55 < Z < 95$) like the DNA compounds and encouraging results are observed. Correlations of molecular ionisation with dielectric constant and polarisability of the compounds have also been investigated.

1. Introduction

The application of ionising radiation in the field of medicine is extremely common. It is frequently utilised in the medical field as a therapeutic agent and in the field of radio diagnostics as a probe. Ballistic impact was traditionally thought to be the mechanism that was responsible for the majority of the damage that high-energy incident radiation caused to living tissue. However, secondary species that result from primary ionisation are responsible for a significant radiation damage (Boudaïffa et al., 2002). The majority of the energy is deposited by the primary ionising particles once they enter the biological medium through several collision processes, including excitations and ionisations. Large amounts of secondary electrons are released as a result of this significant energy transfer, and these electrons can interact with a variety of biological substances causing the radiation damage. Among all the living tissues, DNA molecules are thought to be most sensitive to radiations. Exposure of DNA species to radiations result in multiple types of DNA damage (Nikjoo et al., 2016) through secondary species including electrons.

As primary as well as secondary species induces the radiation damage, it is essential to model their tracks through a biological medium. This makes it possible to anticipate and comprehend the type, location, and severity of cell damage. The route taken by the primary and secondary particles as they move through the medium is depicted by the charged-particle track structures (Goodhead, 1994). The entire range of interaction between the primary and secondary species at the level of each atom or molecule, is modelled in these aleatory (stochastic) simulations using the cross-section values. Hence, accurate cross-sections are crucial to the validity of these types of simulations.

Till now a lot of cross-sectional data has been reported for the DNA constituents upon electron impact in their gaseous phase (Mozejko and Sanche, 2005; Mokrani et al., 2020; Vinodkumar and Limbachiya, 2013; Rahman and Krishnakumar, 2016; Shafranyosh et al., 2015; Champion, 2013; Bull et al., 2014; Aouina and Chaoui, 2018; van der Burgt et al., 2014; Minaev et al., 2014; Zein et al., 2021). Such cross-sections (CSs) are also available for the condensed phase interaction processes but only for the low energy below 20 eV (Toburen, 1998; Bass and Sanche, 1998). But aqueous phase of the DNA rather than gaseous or condensed phase, presents more realistic picture, as they are always found covered with the water molecules through hydrogen bonding (Khesbak et al., 2011; Helmholtz Association of German Research Centres). This has motivated us to take up the work on electron interactions with aqueous DNA constituents. We have computed the ionisation CSs (Q_{ion}), inelastic CSs (Q_{inel}), elastic CSs (Q_{el}), and total CSs (Q_T) for all the five DNA constituents, viz. Adenine, Guanine, Thymine, Cytosine and Uracil upon electron collisions by considering their aqueous phase. This is the maiden attempt to investigate the electron induced processes for the aqueous DNA constituents for the energies from ionisation threshold of the

* Corresponding author.
E-mail address: cglimbachiya-apphy@msubaroda.ac.in (C. Limbachiya).

https://doi.org/10.1016/j.radphyschem.2023.111248
Received 3 May 2023; Received in revised form 22 August 2023; Accepted 27 August 2023
Available online 1 September 2023

molecules to 5000 eV.

Tan et al. (Tan et al., 2004) have reported the Q_{inel} data for the case of DNA in water using dielectric response theory and Penn's approximation for energy range from 20 to 10,000 eV. Recently, Vera et al. (De Vera et al., 2021) and Tan et al. (Tan et al., 2018) have reported the ionisation CSs data for DNA compounds by considering their condensed phase for impact energies from 1 to 10,000 eV and 10–500 eV, respectively. All of these groups (Tan et al., 2004, 2018; De Vera et al., 2021) have used a method that underlines the concept of dielectric response theory.

Since, to the best of our knowledge no work is available for the aqueous phase of DNA molecules; we have developed a new 2-parameter Semi-empirical method (2p-SEM) for computing the Q_T and Q_{el} for these applied biomaterials.

2. Theoretical methodology

The methodologies involved in the present study for the computations of inelastic and elastic interaction events as a result of electron interactions with the aqueous DNA constituents, have been described in this section.

2.1. Spherical complex optical potential approach (SCOP)

The energy-dependent modified complex potential is precisely treated in partial wave decomposition method (Vinodkumar et al., 2013a, 2013b, 2014a; Limbachiya et al., 2011, 2015) with respect to the DNA constituents in their aqueous phase in order to determine the CSs. In essence, a local version of the absorption potential (V_{ab}) (Staszewska et al., 1984) have been modified by keeping $\Delta = IE + E_{gap}$, due to the fact that when dealing with the aqueous or condensed phase, ionisation only occur when the projectile energy exceeds the ionisation energy, IE by an amount equal to the energy-band gap, E_{gap} (Pandya et al., 2012; Joshipura et al., 2007). Table 2 shows the target properties used for the present calculations.

This modified potential is given by,

$$V_{abs}(r, E_i) = -\rho(r)\sqrt{\frac{T_{loc}}{2}}\left(\frac{8\pi}{10{k_F}^3 E_i}\right)\Theta\left(p^2 - {k_F}^2 - 2\Delta\right) \times (A_1 + A_2 + A_3) \tag{1}$$

where, k_F is the appropriate fermi vector, and p is the incident momentum. The A_1, A_2 and A_3 are dynamic parameters, details of which already have been mentioned in our previous articles (Limbachiya et al., 2014, 2015; Vinodkumar et al., 2006, 2011; Joshipura et al., 2006). The local kinetic energy of the incident electron is, $T_{loc} = E_i - (V_s + V_e + V_p)$. Here, V_s is calculated using the Hartree-Fock wave functions (Cox and Bonham, 1967), is used to measure the undeformed molecule charge cloud. The exchange effect that took place between the target electrons and the incoming electrons, is taken into account through V_e (Hara, 1967). The charge cloud of the target system temporarily deforms in the response of the incoming electron. This polarisation effect has been considered through V_p (Zhang et al., 1992).

Since all of these potentials are constructed using the charge density of the molecule under study, it is crucial to represent it. The parameterized charge densities of constituent atomic systems to generate the total $\rho(r)$ of the target molecules have been introduced, which is input to the complex potential (Parikh et al., 2023; Parikh and Limbachiya, 2023).

The inelastic and elastic CSs, are computed by determining the scattering complex phase shifts (δ_l) (Parikh and Limbachiya, 2023). This Q_{inel} totals all the possible ionisations and electronic excitations:

$$Q_{inel} = Q_{ion} + \Sigma Q_{exc} \tag{2}$$

where, Q_{ion} stands for the total ionisation CSs for all permittable ionisations of the molecule and $\sum Q_{exc}$ represents all permitted electronic transitions that are influenced by low-lying states, which is less important than Q_{ion} for the incident energy higher than IE, hence,

$$Q_{inel} \geq Q_{ion} \tag{3}$$

2.2. Complex scattering potential-ionisation contribution (CSP-ic) method

Above inequality (equation (3)) is the cornerstone of this CSP-ic approach (Limbachiya et al., 2015; Vinodkumar et al., 2006; Thakkar et al., 2021) and implies to the ratio,

$$R(E_i) = \frac{Q_{ion}}{Q_{inel}} \tag{4}$$

The boundary conditions of which are as follows,

$$R(E_i) = \begin{cases} 0, for\ E_i \leq \Delta \\ R_P, for\ E_i = E_P \\ \sim 1, for\ E_i \gg \Delta \end{cases} \tag{5}$$

The ionisation events which are dominant part in the inelastic channel, begins to occur at the target's ionisation threshold, which is equal to Δ in this aqueous case. The inelastic CSs attains its peak at energy E_P. However, at high incident energy, ionisation dominates, and excitation CSs drastically drop, as seen by the final condition in equation (5). According to both experimental and theoretical results (Parikh et al., 2023; Swadia et al., 2017; Turner et al., 1982) of the stable targets, the value R_P will be within 0.7–0.8 when the impinging energy reaches E_P. This feature lends uncertainty of 10–15%.

2.3. 2-Parameter semi-empirical method (2p-SEM)

The impact energy dependence of the Q_T for the intermediate energy (Nishimura and Tawara, 1991a; Zecca et al., 1992) and high energy (Joshipura and Vinodkumar, 1996; García and Manero, 1997) have been previously studied and the proposed formula was as follows,

$$Q_T = \frac{A}{E^B} \tag{6}$$

where, parameter A is governed by the molecular characteristics such as molecular size and its polarisability. The value of B for the high energies, above 500 eV will be ~ 0.7, as proposed by Joshipura and Vinodkumar (1996) and García and Manero (1997) only for smaller molecules i.e., for ten electrons ($Z = 10$) and up to $Z = 22$ electrons systems respectively. However, Nishimura and Tawara (1991b) proposed the value of B ~ 0.5 for the intermediate energy range, 50–500 eV. In this work we have derived a single expression from our previous work (Vinodkumar et al., 2014b) and our current results for C_4F_7N, for the wide energy range, 50 $\leq E_i \leq$ 5000 eV and which is applicable for the complex and larger molecules with $55 < Z < 95$.

In Table 3, both the parameters A and B have been tabulated for the larger molecules whose Z ranges from 56 to 94, and it is seen that the

Table 2
Molecular characteristics.

DNA constituents	Aqueous phase IE (eV) (Crespo-Hernández et al., 2004; Fernando et al., 1998)	E_{gap} (eV)
Adenine	5.00	5.25 (Gop et al., 2019)
Cytosine	5.50	5.35 (Baei et al., 2014)
Guanine	4.80	4.80 (Di Felice et al., 2002)
Thymine	5.40	5.20 (MacNaughton et al., 2005)
Uracil	5.55	5.70 (Baei et al., 2014)

Table 3
Parameters vide equation (6).

Parameter	Adenine ($C_5H_5N_5$) (I)	Perfluoroisobutyronitrile (C_4F_7N) (II)	Thymine ($C_5H_6N_2O_2$) (III)	Cytosine ($C_4H_5N_3O$) (IV)	Uracil ($C_4H_4N_2O_2$) (V)
A	43.47	53.64	40.75	31.70	28.33
B	0.61	0.60	0.60	0.59	0.60

value of B (~0.6) is nearly same for all the molecules. However, the value of A is different for each molecule, suggesting its dependency on the number of target electrons (Z) and polarisability (α).

To observe this relation, we plotted the graph of A vs Z as shown in Fig. 1. The linear relationship observed in Fig. 1 is represented through the following equation,

$$A(Z) = 0.6413Z - 4.8016 \text{ (Correlation r = 95\%)} \quad (7)$$

However, for a given Z, the precision can be enhanced by inclusion of polarisability by considering the difference between the actual values of 'A' (from Table 3) and those derived from equation (7) for each molecule. We have observed the dependency of this deviation (A - $A(Z)$) on the molecular size through the polarisability (α). The linear relationship thus obtained from Fig. 2 is,

$$A - A(Z) = 0.1431\alpha - 10.5712 \text{ (Correlation r = 76\%)} \quad (8)$$

Hence, from the equations (6)–(8), a two-parameter expression for Q_T can be formulated for the wider energy range from 50 to 5000 eV for large molecules.

$$Q_T(E_i, Z, \alpha) = \frac{0.6413Z + 0.1431\alpha - 15.3728}{E_i^{0.60}} \quad (9)$$

We note the impact energy dependency as, $E_i^{0.60}$. Equation (9) provides the two-parameter expression for Q_T, which is applicable for the larger molecules with $55 < Z < 95$ and for the wider impact energy 50 eV $\leq E_i \leq$ 5000 eV. This 2p-SEM method provides total cross sections as well as total elastic cross sections for larger and complex molecules and could be very useful where experimental results are difficult to obtain as evident in the present case of aqueous DNA molecules.

3. Results and discussion

In this section, we present the results on Q_{inel}, Q_{ion}, Q_{el} and Q_T for the aqueous DNA compounds, by employing SCOP, CSP-ic and 2p-SEM. Numeric data for the CSs are provided in Appendix vide Tables 6–8 We also report various correlations (section 3.3) of peak ionisation leading to prediction of dipole polarisability (α) and dielectric constant

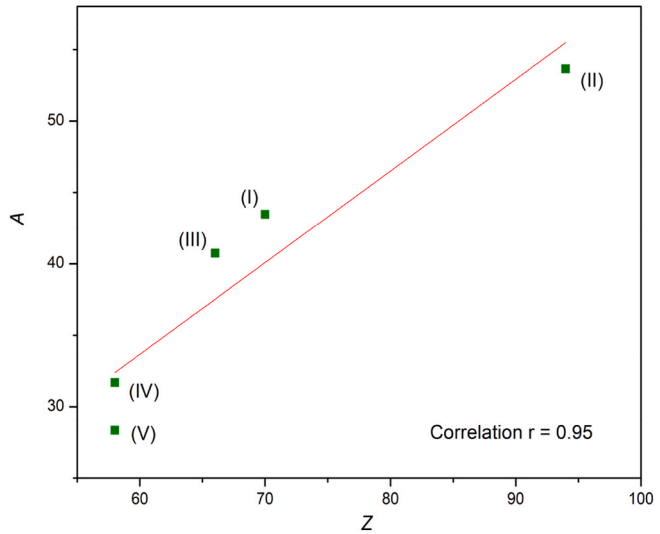

Fig. 1. Parameter A vs Z.

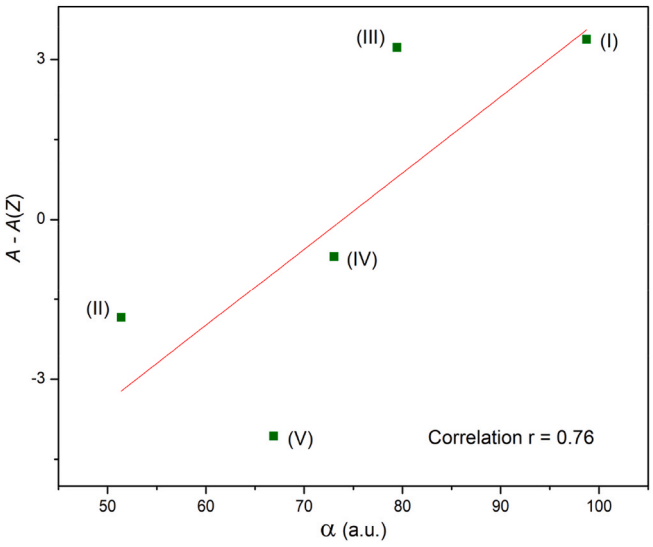

Fig. 2. A - $A(Z)$ vs α

(ε) for all the present aqueous molecules.

3.1. Inelastic contributions

Through Figs. 3–7, Q_{inel} and Q_{ion} are displayed for the investigated aqua-DNA constituents as a function of the electron energy along with the available results for condensed phase molecules (Tan et al., 2004, 2018; De Vera et al., 2021).

Top curves show total inelastic cross sections, Q_{inel}. Tan et al. (Tan et al., 2004) have reported the Q_{inel} data for the case of DNA in water using dielectric response theory and Penn's approximation. They took

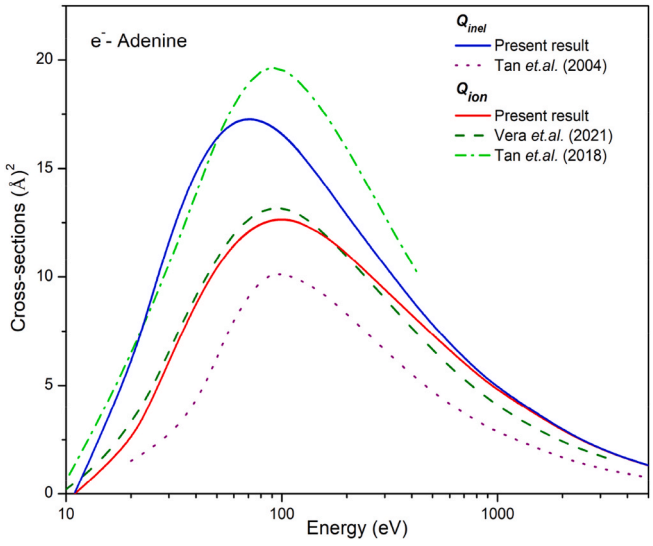

Fig. 3. Inelastic interaction CSs for Adenine
Blue solid: Present Q_{inel}; dot: Tan et al. Q_{inel} (Tan et al., 2004); red solid: Present Q_{ion}; olive green dash dot: Vera et al. Q_{ion} (De Vera et al., 2021); short dash: Tan et al. Q_{ion} (Tan et al., 2018).

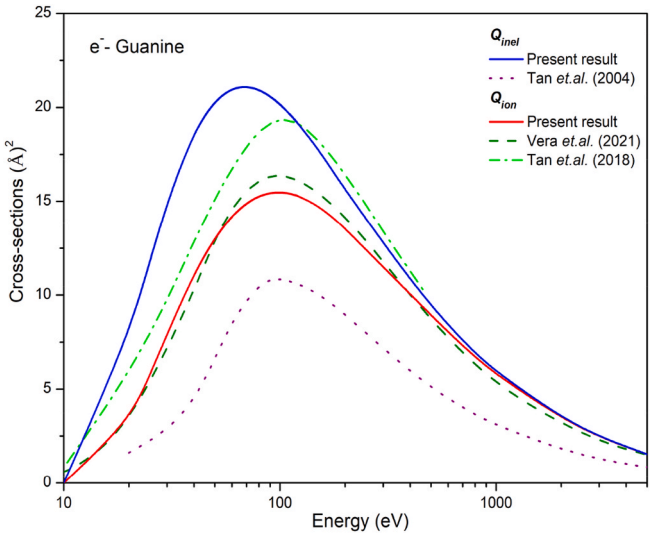

Fig. 4. Inelastic interaction CSs for Guanine
Blue solid: Present Q_{inel}; dot: Tan et al. Q_{inel} (Tan et al., 2004); red solid: Present Q_{ion}; olive green dash dot: Vera et al. Q_{ion} (De Vera et al., 2021); short dash: Tan et al. Q_{ion} (Tan et al., 2018).

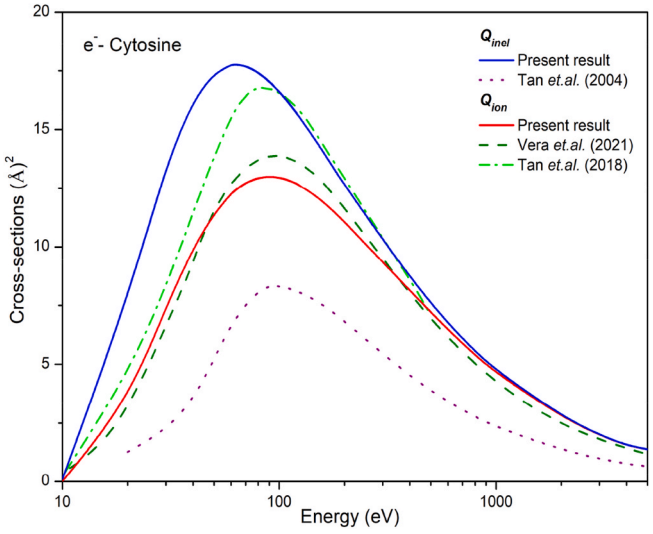

Fig. 5. Inelastic interaction CSs for Cytosine
Blue solid: Present Q_{inel}; dot: Tan et al. Q_{inel} (Tan et al., 2004); red solid: Present Q_{ion}; olive green dash dot: Vera et al. Q_{ion} (De Vera et al., 2021); short dash: Tan et al. Q_{ion} (Tan et al., 2018).

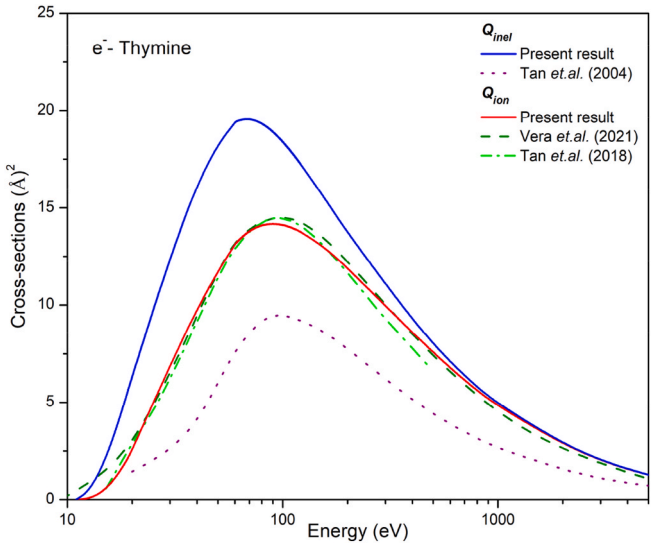

Fig. 6. Inelastic interaction CSs for Thymine
Blue solid: Present Q_{inel}; dot: Tan et al. Q_{inel} (Tan et al., 2004); red solid: Present Q_{ion}; olive green dash dot: Vera et al. Q_{ion} (De Vera et al., 2021); short dash: Tan et al. Q_{ion} (Tan et al., 2018).

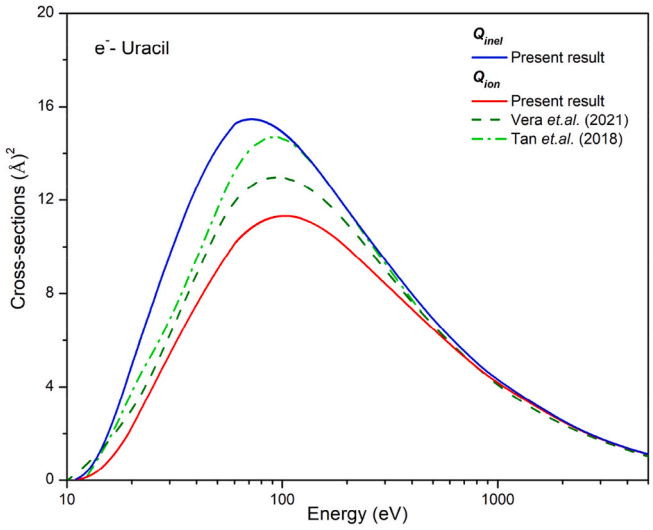

Fig. 7. Inelastic interaction CSs for Uracil Blue solid: Present Q_{inel}; dot: Tan et al. Q_{inel} (Tan et al., 2004); red solid: Present Q_{ion}; dash: Vera et al. Q_{ion} (De Vera et al., 2021); dash dot: Tan et al. Q_{ion} (Tan et al., 2018).

an equivalent unit of DNA molecule in water environment with 50% Guanine-Cytosine and 50% Adenine-Thymine and then separated into 5 constituents of DNA. However, their Q_{inel} underestimate present Q_{inel} and have lower values than even all the reported Q_{ion}.

Tan et al. (Tan et al., 2018) and Vera et al. (De Vera et al., 2021) have reported the Q_{ion} data for condensed DNA bases using the methodologies which underlines the dielectric response theory. The present results of Q_{ion} are observed to be in good accord with those of Vera et al. (De Vera et al., 2021) except in the case of Uracil. The minute deviation at the peak value of Q_{ion} may be because of the consideration of the different phases for the molecules.

As can be seen, the data of Tan et al. (Tan et al., 2018) overestimates both, present data and those of Vera et al. (De Vera et al., 2021) except for Thymine, in which case they show matching.

It is important to compare Q_{ion} for aqua and gas phase (Vinodkumar et al., 2003). Hence, apart from condensed phase results, the present aqueous phase Q_{ion} results are also compared with those of recent gas phase data (Rahman and Krishnakumar, 2015, 2016; Shafranyosh et al., 2015; Champion, 2013; Bull et al., 2014; van der Burgt et al., 2014; Minaev et al., 2014; van der Burgt, 2014, 2015) as shown in Figs. 8–12. As can be observed from the Figs. 8–12, gas phase results overestimate the present aqua phase data. This difference is because of the different threshold values for condensed and gas phase DNA compounds.

3.2. Elastic contributions

We have computed the elastic CSs (Q_{el}) and the total CSs (Q_T) for the electron energies from molecular IE to 5000 eV using the SCOP and 2p-SEM approach.

Figs. 13–17 show the Q_{el} and Q_T plots against the incident electron energies for aqueous Adenine, Cytosine, Guanine, Thymine and Uracil, respectively. We also show recent data of Q_{el} and Q_T in the gas phase.

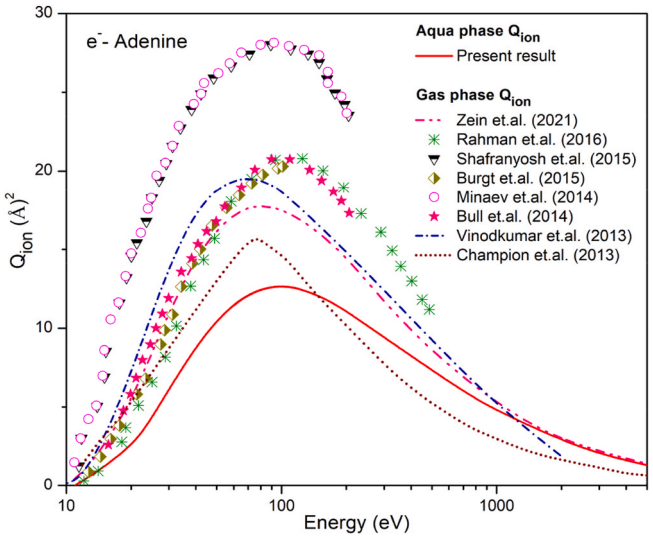

Fig. 8. Q_{ion} for Adenine in aqua and gas phase
Solid: Present Q_{ion} (aqua phase); pink dash dot: Zein et al. (Zein et al., 2021); asterisk: Rahman et al. (Rahman and Krishnakumar, 2016); inverted half-filled triangles: Shafranyosh et al. (Shafranyosh et al., 2015); half-filled diamonds: Burgt et al. (van der Burgt, 2015); open circles: Minaev et al. (Minaev et al., 2014); filled stars: Bull et al. (Bull et al., 2014); short dash dot: Vinodkumar et al. (Vinodkumar and Limbachiya, 2013); short dot: Champion (Champion, 2013).

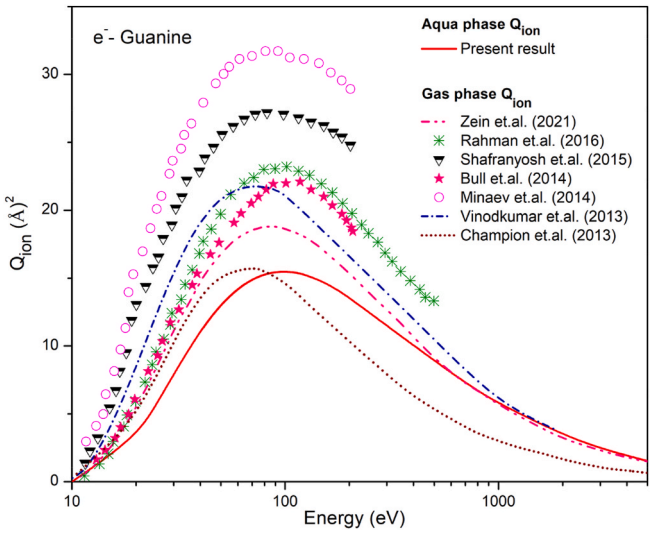

Fig. 9. Q_{ion} for Guanine in aqua and gas phase
Solid: Present aqua phase result; pink dash dot: Zein et al. (Zein et al., 2021); asterisk: Rahman et al. (Rahman and Krishnakumar, 2016); inverted half-filled triangles: Shafranyosh et al. (Shafranyosh et al., 2015); open circles: Minaev et al. (Minaev et al., 2014); filled stars: Bull et al. (Bull et al., 2014); short dash dot: Vinodkumar et al. (Vinodkumar and Limbachiya, 2013); short dot: Champion (Champion, 2013).

The results obtained from 2p-SEM and those from SCOP formalism are seen in good agreement with each other confirming the recently developed 2p-SEM method for larger and complex molecules.

The Q_{el} results from both the methodologies (2p-SEM and SCOP) are observed to be in excellent accord with each other for all the present studied molecules, which validate the newly proposed 2p-SEM formalism even for the aqueous phase molecules.

The gas phase results of Aouina (Aouina and Chaoui, 2018), Vinodkumar et al. (Vinodkumar et al., 2014b), Mokrani et al. (Mokrani et al., 2020) and Gurung (Devi Gurung and Ariyasinghe, 2017) are seen to be deviated at low energy side, which is due to the fact that at lower energies these Q_{el} and Q_T are highly sensitive to threshold values as well as polarisabilities. We observe that Q_{el} data of Zein et al. (Zein et al., 2021) shows significant deviation from the other existing Q_{el} data, mainly at the lower to intermediate energies. This deviation then reduces as we move towards high energy regime.

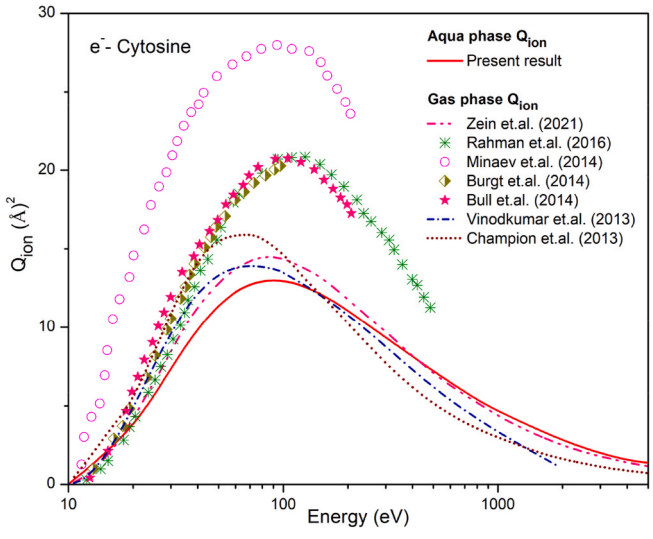

Fig. 10. Q_{ion} for Cytosine in aqua and gas phase
Solid: Present aqua phase result; Solid: Present aqua phase result; pink dash dot: Zein et al. (Zein et al., 2021); asterisk: Rahman et al. (Rahman and Krishnakumar, 2016); open circles: Minaev et al. (Minaev et al., 2014); half-filled diamonds: Burgt (van der Burgt, 2014); filled stars: Bull et al. (Bull et al., 2014); short dash dot: Vinodkumar et al. (Vinodkumar and Limbachiya, 2013); short dot: Champion (Champion, 2013).

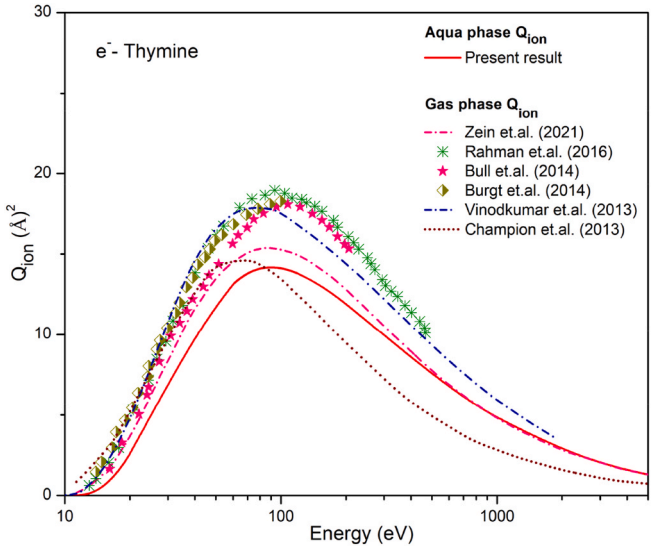

Fig. 11. Q_{ion} for Thymine in aqua and gas phase
Solid: Present aqua phase result; Solid: Present aqua phase result; pink dash dot: Zein et al. (Zein et al., 2021); asterisk: Rahman et al. (Rahman and Krishnakumar, 2016); half-filled diamonds: Burgt et al. (van der Burgt et al., 2014); filled stars: Bull et al. (Bull et al., 2014); short dash dot: Vinodkumar et al. (Vinodkumar and Limbachiya, 2013); short dot: Champion (Champion, 2013).

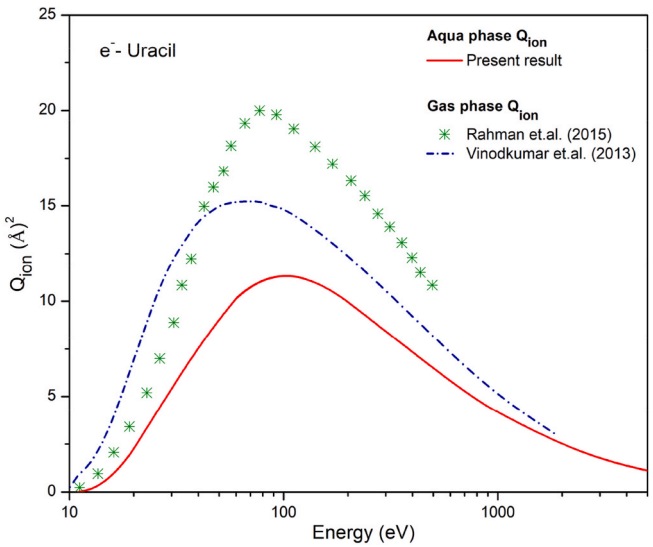

Fig. 12. Q_{ion} for Uracil in aqua and gas phase
Solid: Present aqua phase result; asterisks: Rahman (Rahman and Krishnakumar, 2015); short dash dot: Vinodkumar et al. (Vinodkumar and Limbachiya, 2013).

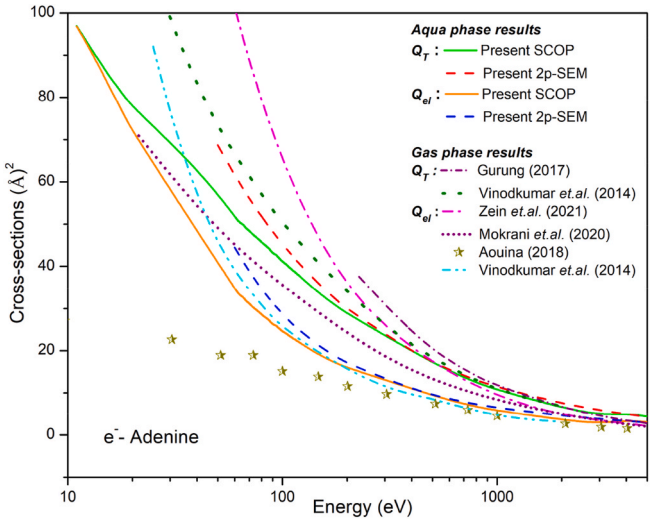

Fig. 13. Elastic and total interaction CSs for Adenine
Aqua phase results
Green solid: Present SCOP Q_T; red dash: Present 2p-SEM Q_T; Present SCOP Q_{el}; blue dash: Present 2p-SEM Q_{el}
Gas phase results
Short dash dot: Gurung Q_T (Devi Gurung and Ariyasinghe, 2017); olive green dot: Vinodkumar et al. Q_T (Vinodkumar et al., 2014b); pink dash dot: Zein et al. Q_{el} (Zein et al., 2021); short dot: Mokrani et al. Q_{el} (Mokrani et al., 2020); half-filled stars: Aouina Q_{el} (Aouina and Chaoui, 2018); dash dot: Vinodkumar et al. (Vinodkumar et al., 2014b).

3.3. Various correlations: prediction of polarisability (α) and dielectric constant (ε)

We have used the calculated total ionisation cross sections to compute useful parameters, polarisability (α) and dielectric constant (ε) for aqua-DNA molecules which are not found in literature.

3.3.1. Polarisability (α)

According to Harland's proposed qualitative dependency nature of the maximum ionisation CSs, ($Q_{ion(m)}$) with its polarisability (α)

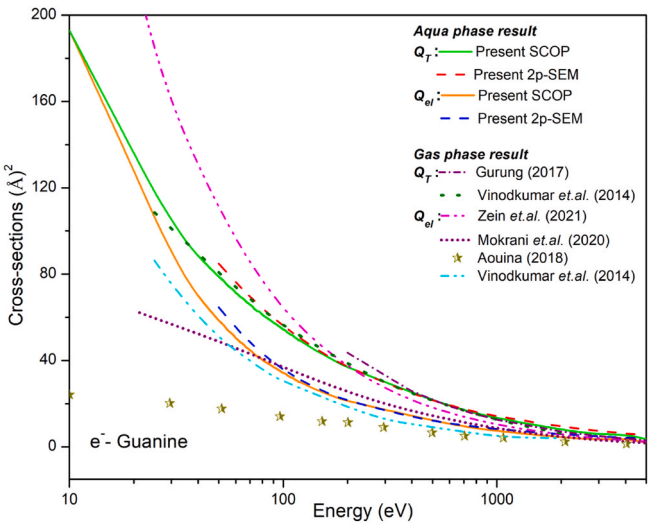

Fig. 14. Elastic and total interaction CSs for Guanine
Aqua phase results
Green solid: Present SCOP Q_T; red dash: Present 2p-SEM Q_T; Present SCOP Q_{el}; blue dash: Present 2p-SEM Q_{el}
Gas phase results
Short dash dot: Gurung Q_T (Devi Gurung and Ariyasinghe, 2017); olive green dot: Vinodkumar et al. Q_T (Vinodkumar et al., 2014b); Pink dash dot: Zein et al. Q_{el} (Zein et al., 2021); short dot: Mokrani et al. Q_{el} (Mokrani et al., 2020); half-filled stars: Aouina Q_{el} (Aouina and Chaoui, 2018); dash dot: Vinodkumar et al. (Vinodkumar et al., 2014b).

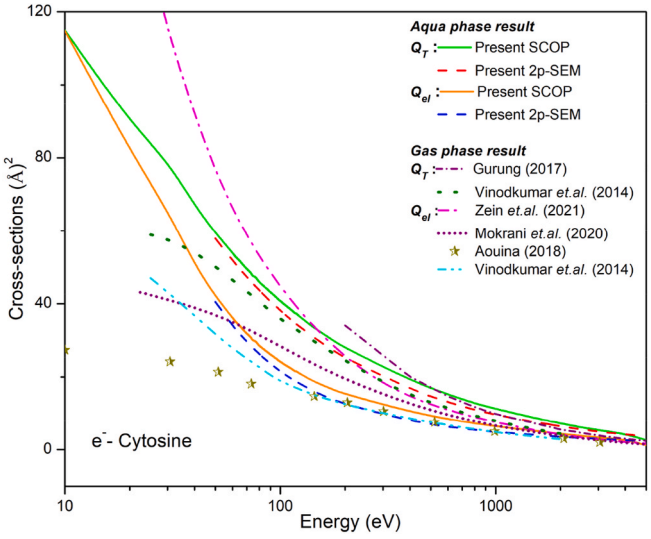

Fig. 15. Elastic and total interaction CSs for Cytosine
Aqua phase results
Green solid: Present SCOP Q_T; red dash: Present 2p-SEM Q_T; orange solid: Present SCOP Q_{el}; blue dash: Present 2p-SEM Q_{el}
Gas phase results
Short dash dot: Gurung Q_T (Devi Gurung and Ariyasinghe, 2017); olive green dot: Vinodkumar et al. Q_T [53]; pink dash dot: Zein et al. Q_{el} (Zein et al., 2021); short dot: Mokrani et al. Q_{el} (Mokrani et al., 2020); half-filled stars: Aouina Q_{el} (Aouina and Chaoui, 2018); dash dot: Vinodkumar et al. (Vinodkumar et al., 2014b).

(Harland and Vallance, 1997),

$$Q_{ion(\mathrm{m})} = \frac{e}{4\varepsilon_o}\sqrt{\frac{\alpha}{\Delta}} \tag{10}$$

Harland proposed the Δ will be equal to *IE* in case of gas phase of the

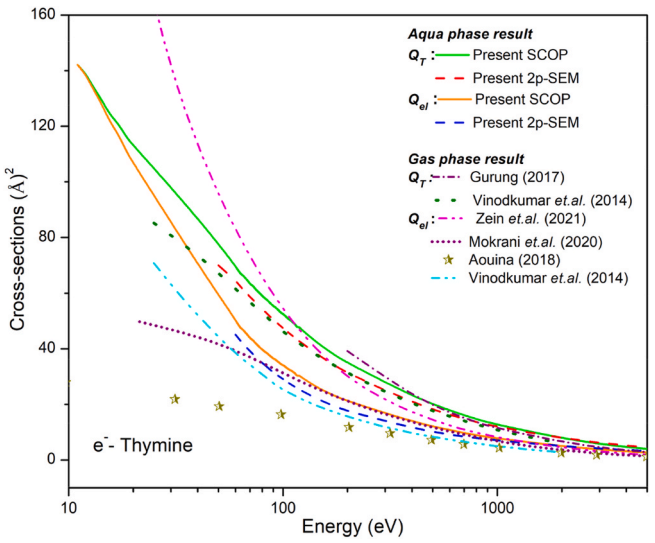

Fig. 16. Elastic and total interaction CSs for Thymine
Aqua phase results
Green solid: Present SCOP Q_T; red dash: Present 2p-SEM Q_T; orange solid: Present SCOP Q_{el}; blue dash: Present 2p-SEM Q_{el}
Gas phase results
Short dash dot: Gurung Q_T (Devi Gurung and Ariyasinghe, 2017); olive green dot: Vinodkumar et al. Q_T (Vinodkumar et al., 2014b); pink dash dot: Zein et al. Q_{el} (Zein et al., 2021); short dot: Mokrani et al. Q_{el} (Mokrani et al., 2020); half-filled stars: Aouina Q_{el} (Aouina and Chaoui, 2018); dash dot: Vinodkumar et al. (Vinodkumar et al., 2014b).

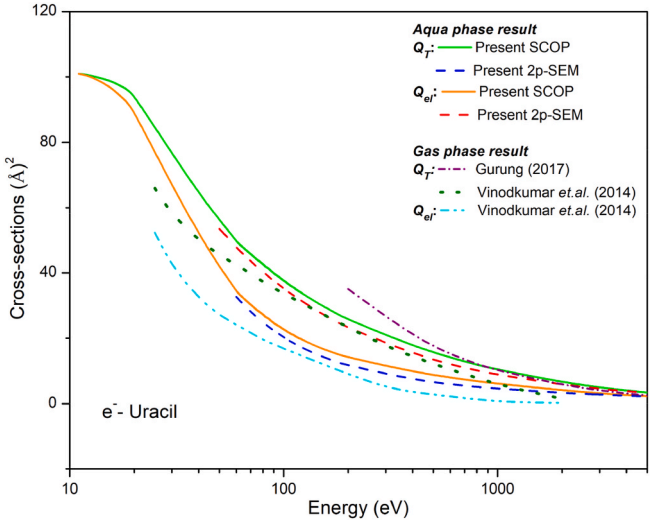

Fig. 17. Elastic and total interaction CSs for Uracil
Aqua phase results
Green solid: Present SCOP Q_T; red dash: Present 2p-SEM Q_T; orange solid: Present SCOP Q_{el}; blue dash: Present 2p-SEM Q_{el}
Gas phase results
Short dash dot: Gurung Q_T (Devi Gurung and Ariyasinghe, 2017); olive green dot: Vinodkumar et al. Q_T (Vinodkumar et al., 2014b); dash dot: Vinodkumar et al. (Vinodkumar et al., 2014b).

target system. While, in the present case of aqueous phase species, the $\Delta = IE + E_{gap}$, and the ionisation of the system actually occurs when the incoming energy is greater than the threshold value, $\Delta = IE + E_{gap}$.

Using this equation (10), we have predicted the α values for the present studied targets as given in the Table 4.

From the table it can be observed that the present predicted α for the aqueous molecules find good agreement with those of Nakagawa (2007), who calculated the α for condensed molecules.

Table 4
Predicted polarisability α (Å^3).

Target	Δ (eV)	$Q_{ion(m)}$ (Å^2)	Predicted α (Å^3)	Reference value of α for condensed phase (Å^3) (Nakagawa, 2007)
Adenine	10.25	12.65	11.54	14.33
Guanine	9.60	15.47	16.17	15.26
Thymine	10.60	14.17	14.99	13.35
Cytosine	10.85	12.99	12.88	11.47
Uracil	11.25	11.32	10.15	10.41

3.3.2. Dielectric constant (ε)

The two expressions for dielectric constant (ε) have been derived in the present work using the dependency of the $Q_{ion(m)}$ on α and ε. The first proposed expression of dielectric constant as a function of $Q_{ion(m)}$, derived using the dependency of $Q_{ion(m)}$ with α (equation (10)) and the Clausius-Mosotti (CM) equation,

$$\frac{\varepsilon-1}{\varepsilon+2} = C\cdot\left(Q_{ion(m)}\right)^2 N\Delta \tag{11}$$

where, C is the constant $= \frac{64\pi}{3}\left(\frac{\varepsilon_0}{e}\right)^2$ and N is the number density of the molecule.

Secondly, the Onsager dielectric equation (Onsager, 1936; Valiskó and Boda, 2005), which works well for the case of liquids is given by,

$$\frac{\varepsilon-1}{\varepsilon+2} = \frac{4\pi}{3}\alpha N + \frac{(\varepsilon-\varepsilon_\infty)(2\varepsilon+\varepsilon_\infty)}{\varepsilon(\varepsilon_\infty+2)^2} \tag{12}$$

This equation is thought to be more applicable in the present aqueous phase study, and again the equation of dielectric constant as a function of $Q_{ion(m)}$ is proposed as,

$$\frac{\varepsilon-1}{\varepsilon+2} = C\cdot\left(Q_{ion(m)}\right)^2 N\Delta + \frac{(\varepsilon-\varepsilon_\infty)(2\varepsilon+\varepsilon_\infty)}{\varepsilon(\varepsilon_\infty+2)^2} \tag{13}$$

where, ε_∞ is the high frequency dielectric constant, which can be obtained from the CM equation. The computed ε values are listed in Table 5.

Form the Table 5 and it can be observed as expected that the ε values computed through equation (13), are in good agreement with those of Szarek (2017).

Conclusion

The aqueous phase of DNA is explored here for several molecular processes upon electron impact, as it is a more realistic phase of DNA due to the presence of H-bonds. Radiation induced damage assessment of DNA due to the single and double strand breaks requires electron interacting with aqueous DNA inelastically. Present study quantifies various interaction processes in response to the impact of electrons on aqueous DNA constituents, viz., Adenine, Guanine, Thymine, Cytosine and Uracil through cross-sections. In order to provide Q_{el} and Q_T results for these biomaterials we have proposed a method 2p-SEM and

Table 5
Computed dielectric constants (ε).

Target	$Q_{ion(m)}$ (Å^2)	Dielectric constant (ε) (vide equation (11))	Dielectric constant (ε) (vide equation (13))	Reference value of ε for condensed phase (Szarek, 2017)
Adenine	12.65	2.22	1.00	1.59
Guanine	15.47	3.23	0.85	1.77
Thymine	14.17	3.39	0.99	1.59
Cytosine	12.99	2.84	1.03	1.71
Uracil	11.32	2.29	0.98	–

encouraging results are observed (Figs. 13–17). The proposed expression for Q_T (equation (9)) is applicable for the larger molecular systems ($55 < Z < 95$) and wider energy range. Numeric data for the CSs are provided in Appendix vide Tables 6–8 Further, from the correlation study of molecular ionisation, we have computed molecular polarisability and dielectric constant. The dielectric constant is obtained from the Q_{ion} using the Clausius-Mosotti (CM) and Onsager approaches (vide equations (11) and (13) respectively). The computed results are compared with previous data. In absence of previous study involving aqueous DNA constituents, this estimation of various cross-sections, computation of polarisability and dielectric constant may prove to be very useful.

CRediT author statement

Smruti Parikh: Data curation, Writing- Original draft preparation, Formal analysis, Conceptualization, Methodology, software. **Dhaval Chauhan:** Data curation, Methodology. **Nirav Thakkar:** Formal analysis. **Chetan Limbachiya:** Reviewing and Editing, Validation, Visualization, Investigation, Supervision.

Declaration of competing interest

The authors declare that they have no known competing financial interests or personal relationships that could have appeared to influence the work reported in this paper.

Data availability

Data will be made available on request.

APPENDIX

Table 6
Numeric data for cross-sections of Aqueous Adenine and Guanine (in Å^2)

E_i (eV)	Adenine					Guanine				
	Q_{ion}	Modified SCOP		2p-SEM		Q_{ion}	Modified SCOP		2p-SEM	
		Q_{el}	Q_T	Q_{el}	Q_T		Q_{el}	Q_T	Q_{el}	Q_T
10	–	–	–	–	–	0.00	192.94	192.95	–	–
11	0.004	96.82	96.88	–	–	0.021	188.95	189.16	–	–
20	2.35	72.02	77.85	–	–	3.27	128.23	136.08	–	–
40	8.76	48.42	63.27	–	–	11.04	70.00	88.51	–	–
60	11.46	34.79	51.86	44.49	61.56	14.17	50.40	71.35	55.34	76.29
70	12.08	31.17	48.43	38.87	56.13	14.87	44.76	65.84	48.47	69.55
80	12.43	28.59	45.76	34.64	51.80	15.25	40.28	61.20	43.28	64.20
100	12.65	24.60	41.18	28.73	45.31	15.47	34.26	54.41	36.00	56.15
400	8.25	11.04	19.91	10.86	19.72	10.04	14.30	25.07	13.67	24.44
800	5.54	6.74	12.47	7.29	13.01	6.71	8.56	15.48	9.20	16.13
1000	4.79	5.81	10.72	6.47	11.38	5.78	7.34	13.27	8.18	14.10
3000	2.07	2.69	4.78	3.80	5.89	2.48	3.17	5.66	4.80	7.30
5000	1.33	3.07	4.40	3.00	4.33	1.53	2.00	3.54	3.84	5.37

Table 7
Numeric data for cross-sections of Aqueous Cytosine and Thymine (in Å^2)

E_i (eV)	Cytosine					Thymine				
	Q_{ion}	Modified SCOP		2p-SEM		Q_{ion}	Modified SCOP		2p-SEM	
		Q_{el}	Q_T	Q_{el}	Q_T		Q_{el}	Q_T	Q_{el}	Q_T
10	0.01	114.81	114.92	–	–	–	–	–	–	–
11	0.08	109.80	110.29	–	–	0.001	142.10	142.12	–	–
20	3.42	82.11	89.88	–	–	2.55	106.87	113.23	–	–
40	9.94	50.70	66.94	–	–	10.01	70.34	87.17	–	–
60	12.26	36.26	54.00	34.14	51.88	13.13	50.41	69.81	45.06	64.46
70	12.71	31.81	49.49	29.62	47.29	13.79	43.97	63.52	39.21	58.76
80	12.93	28.52	45.93	26.25	43.65	14.09	39.72	59.05	34.91	54.24
100	12.95	24.15	40.75	21.58	38.18	14.12	34.05	52.44	29.05	47.44
400	8.13	10.45	19.12	7.95	16.62	8.58	13.73	22.93	11.45	20.65
800	5.40	7.23	12.78	5.41	10.97	5.60	8.88	14.67	7.84	13.62
1000	4.64	6.46	11.21	4.84	9.59	4.81	7.74	12.66	6.99	11.92
3000	1.98	3.35	5.34	2.97	4.96	2.03	3.78	5.82	4.12	6.16
5000	1.37	1.23	2.60	2.27	3.65	1.29	2.69	3.98	3.24	4.54

Table 8
Numeric data for cross-sections of Aqueous Uracil (in Å^2)

E_i (eV)	Uracil				
	Q_{ion}	Modified SCOP		2p-SEM	
		Q_{el}	Q_T	Q_{el}	Q_T
11	0.007	100.96	100.99	–	–
20	2.24	89.44	94.39	–	–
40	7.69	50.97	64.10	–	–
60	10.14	34.53	49.79	32.63	47.88
70	10.73	30.30	45.75	28.20	43.65
80	11.08	27.23	42.62	24.90	40.29
100	11.32	22.71	37.62	20.34	35.24
400	7.33	9.78	17.69	7.43	15.34
800	4.83	6.90	11.91	5.11	10.12
1000	4.15	6.14	10.42	4.58	8.85
3000	1.76	3.20	4.98	2.80	4.58
5000	1.12	2.31	3.43	2.25	3.37

References

Aouina, N.Y., Chaoui, Z.-E.-A., 2018. Simulation *of Positron and electron elastic mean free Path and diffusion Angle on DNA Nucleobases from 10 eV to 100 KeV*. Surf. Interface Anal. 50, 939.

Baei, M.T., Taghartapeh, M.R., Lemeski, E.T., Soltani, A., 2014. A computational study of adenine, Uracil, and cytosine adsorption upon AlN and BN nano-cages. Phys. B Condens. Matter 444, 6.

Bass, A., Sanche, L., 1998. Absolute and effective cross-sections for low-energy electron-scattering processes within condensed matter. Radiat. Environ. Biophys. 37, 243.

Boudaïffa, B., Cloutier, P., Hunting, D., Huels, M.A., Sanche, L., 2002. Cross sections for low-energy (10-50 EV) electron damage to DNA. Radiat. Res. 157, 227.

Bull, J.N., Lee, J.W.L., Vallance, C., 2014. Absolute *electron total ionization cross-sections: molecular Analogues of DNA and RNA Nucleobase and sugar constituents*. Phys. Chem. Chem. Phys. 16, 10743.

Champion, C., 2013. Quantum-mechanical predictions of electron-induced ionization cross sections of DNA components. J. Chem. Phys. 138, 184306.

Cox, H.L., Bonham, R.A., 1967. Elastic electron scattering amplitudes for neutral atoms calculated using the partial wave method at 10, 40, 70, and 100 KV for Z = 1 to Z = 54. J. Chem. Phys. 47, 2599.

Crespo-Hernández, C.E., Arce, R., Ishikawa, Y., Gorb, L., Leszczynski, J., Close, D.M., 2004. Ab initio ionization energy thresholds of DNA and RNA bases in gas phase and in aqueous solution. J. Phys. Chem. A 108, 6373.

De Vera, P., Abril, I., Garcia-Molina, R., 2021. Excitation and ionisation cross-sections in condensed-phase biomaterials by electrons down to very low energy: application to liquid water and genetic building blocks. Phys. Chem. Chem. Phys. 23, 5079.

Devi Gurung, Meera, Ariyasinghe, W.M., 2017. Total electron scattering cross sections of some important biomolecules at 0.2 – 6.0keV energies. Radiat. Phys. Chem. 141, 1.

Di Felice, R., Calzolari, A., Molinari, E., Garbesi, A., 2002. Ab initio study of model guanine assemblies: the role of (formula presented) coupling and band transport. Phys. Rev. B Condens. Matter 65, 1.

Fernando, H., Papadantonakis, G.A., Kim, N.S., Lebreton, P.R., 1998. Conduction-band-edge ionization thresholds of DNA components in aqueous solution. Proc. Natl. Acad. Sci. U. S. A. 95, 5550.

García, G., Manero, F., 1997. Correlation of the total cross section for electron scattering by molecules with 10-22 electrons, and some molecular parameters at intermediate energies. Chem. Phys. Lett. 280, 419.

Goodhead, D.T., 1994. Initial events in the cellular effects of ionizing radiations: clustered damage in DNA. Int. J. Radiat. Biol. 65, 7.

Gop, S., Sutradhar, R., Chakraborty, S., Sinha, T.P., 2019. The study of energetic and electronic properties of metal-adenine complex in solvent phase: a density functional theory approach. In: AIP Conference Proceedings, vol. 2162. American Institute of Physics Inc.

Hara, S., 1967. The scattering of slow electrons by hydrogen molecules. J. Phys. Soc. Jpn. 22, 710.

Harland, P.W., Vallance, C., 1997. Ionization cross-sections and ionization efficiency curves from polarizability volumes and ionization potentials. Int. J. Mass Spectrom. Ion Process. 171, 173.

Helmholtz Association of German Research Centres. Water molecules characterize the structure of DNA genetic material. https://www.sciencedaily.com/releases/2011/04/110426091122.htm#citation_apa.

Joshipura, K.N., Vinodkumar, M., 1996. *Cross Sections and other Parameters of e^- - H_2O scattering (Ei≥50eV)*. Pramana - J. Phys. 47, 57.

Joshipura, K.N., Vaishnav, B.G., Limbachiya, C.G., 2006. Ionization and excitation of some atomic targets and metal oxides by electron impact. Pramana - J. Phys. 66, 403.

Joshipura, K.N., Gangopadhyay, S., Limbachiya, C.G., Vinodkumar, M., 2007. Electron impact ionization of water molecules in ice and liquid phases. J. Phys. Conf. Ser. 80, 012008.

Khesbak, H., Savchuk, O., Tsushima, S., Fahmy, K., 2011. The role of water H-bond imbalances in B-DNA substate transitions and peptide recognition revealed by time-resolved FTIR spectroscopy. J. Am. Chem. Soc. 133, 5834.

Limbachiya, C., Vinodkumar, M., Mason, N., 2011. *Calculation of electron-impact rotationally elastic total cross Sections for NH_3, H_2S, and PH_3 over the energy Range from 0.01 eV to 2 KeV*. Phys. Rev. 83, 042708.

Limbachiya, C., Vinodkumar, M., Swadia, M., Barot, A., 2014. *Electron impact total cross section Calculations for CH_3SH (methanethiol) from Threshold to 5 KeV*. Mol. Phys. 112, 101.

Limbachiya, C., Vinodkumar, M., Swadia, M., Joshipura, K.N., Mason, N., 2015. Electron-impact total cross sections for inelastic processes for furan, tetrahydrofuran and 2,5-dimethylfuran. Mol. Phys. 113, 55.

MacNaughton, J., Moewes, A., Kurmaev, E.Z., 2005. Electronic structure of the nucleobases. J. Phys. Chem. B 109, 7749.

Minaev, B.F., Shafranyosh, M.I., Yu Svida, Yu., Sukhoviya, M.I., Shafranyosh, I.I., Baryshnikov, G.V., Minaev, V.A., 2014. Fragmentation of the adenine and guanine molecules induced by electron collisions. J. Chem. Phys. 140, 175101.

Mokrani, S., Aouchiche, H., Champion, C., 2020. Elastic scattering of electrons by DNA bases. Radiat. Phys. Chem. 172, 108735.

Mozejko, P., Sanche, L., 2005. Cross sections for electron scattering from selected components of DNA and RNA. Radiat. Phys. Chem. 73, 77.

Nakagawa, S., 2007. Polarizable model potential function for nucleic acid bases. J. Comput. Chem. 28, 1538.

Nikjoo, H., Taleei, R., Liamsuwan, T., Liljequist, D., Emfietzoglou, D., 2016. Perspectives in radiation biophysics: from radiation track structure simulation to mechanistic models of DNA damage and repair. Radiat. Phys. Chem. 128, 3.

Nishimura, H., Tawara, H., 1991a. Some aspects of total scattering cross sections of electrons for simple hydrocarbon molecules. J. Physiol. Biochem.: At Mol. Opt. Phys. 24, L363.

Nishimura, H., Tawara, H., 1991b. Some aspects of total scattering cross sections of electrons for simple hydrocarbon molecules. J. Physiol. Biochem.: At Mol. Opt. Phys. 24, L363.

Onsager, L., 1936. Electric moments of molecules in liquids. J. Am. Chem. Soc. 58, 1486.

Pandya, S.H., Vaishnav, B.G., Joshipura, K.N., 2012. Electron inelastic mean free paths in solids: a theoretical approach. Chin. Phys. B 21.

Parikh, S., Limbachiya, C., 2023. Electron driven molecular processes for nucleosides. Radiat. Phys. Chem. 208, 110940.

Parikh, S., Vinodkumar, M., Limbachiya, C., 2023. Electron impact inelastic molecular processes for deuterated compounds. Chem. Phys. 565, 111766.

Rahman, M.A., Krishnakumar, E., 2015. Absolute partial and total electron ionization cross sections of Uracil. Int. J. Mass Spectrom. 392, 145.

Rahman, M.A., Krishnakumar, E., 2016. Communication: electron ionization of DNA bases. J. Chem. Phys. 144, 161102.

Shafranyosh, I.I., Svida, Yu. Yu., Sukhoviya, M.I., Shafranyosh, M.I., Minaev, B.F., Baryshnikov, G.V., Minaev, V.A., 2015. Absolute effective cross sections of ionization of adenine and guanine molecules by electron impact. Tech. Phys. 60, 1430.

Staszewska, G., Schwenke, D.W., Truhlar, D.G., 1984. Investigation of the shape of the imaginary part of the optical-model potential for electron scattering by rare gases. Phys. Rev. 29, 3078.

Swadia, M., Thakar, Y., Vinodkumar, M., Limbachiya, C., 2017. *Theoretical electron impact total cross Sections for tetrahydrofuran (C_4H_8O)*. Eur. Phys. J. D 71, 85.

Szarek, P., 2017. Electric permittivity in individual atomic and molecular systems through direct associations with electric dipole polarizability and chemical hardness. J. Phys. Chem. C 121, 12593.

Tan, Z., Xia, Y., Liu, X., Zhao, M., Ji, Y., Li, F., Huang, B., 2004. Cross sections of electron inelastic interactions in DNA. Radiat. Environ. Biophys. 43, 173.

Tan, H.Q., Mi, Z., Bettiol, A.A., 2018. Simple and universal model for electron-impact ionization of complex biomolecules. Phys. Rev. E 97, 1.

Thakkar, N., Swadia, M., Vinodkumar, M., Mason, N., Limbachiya, C., 2021. Electron induced elastic and inelastic processes for perfluoroketone (PFK) molecules. Plasma Sources Sci. Technol. 30, 085008.
Toburen, L., 1998. Ionization and charge-transfer: basic data for track structure calculations. Radiat. Environ. Biophys. 37, 221.
Turner, J.E., Paretzke, H.G., Hamm, R.N., Wright, H.A., Ritchie, R.H., 1982. Comparative study of electron energy deposition and yields in water in the liquid and vapor phases. Radiat. Res. 92, 47.
Valiskó, M., Boda, D., 2005. Dielectric constant of the polarizable dipolar hard sphere fluid studied by Monte Carlo simulation and theories. Condens. Matter Phys. 8, 357.
van der Burgt, P.J.M., 2014. Electron impact fragmentation of cytosine: partial ionization cross sections for positive fragments. Eur. Phys. J. D 68, 135.
van der Burgt, P.J.M., 2015. Electron impact fragmentation of adenine: partial ionization cross sections for positive fragments. Eur. Phys. J. D 69, 173.
van der Burgt, P.J.M., Mahon, F., Barrett, G., Gradziel, M.L., 2014. Electron impact fragmentation of thymine: partial ionization cross sections for positive fragments. Eur. Phys. J. D 68, 151.
Vinodkumar, M., Limbachiya, C., 2013. Electron impact total and ionization cross-sections for DNA based compounds. Mol. Phys. 111, 215.
Vinodkumar, M., Joshipura, K.N., Limbachiya, C.G., Antony, B.K., 2003. *Electron impact Ionization of H_2O Molecule in crystalline ice*. Nucl. Instrum. Methods Phys. Res. B 212, 63.
Vinodkumar, M., Joshipura, K.N., Limbachiya, C., Mason, N., 2006. Theoretical calculations of the total and ionization cross sections for electron impact on some simple biomolecules. Phys. Rev. 74, 022721.
Vinodkumar, M., Bhutadia, H., Limbachiya, C., Joshipura, K.N., 2011. *Electron impact total ionization cross Sections for H_2S, PH_3, HCHO and HCOOH*. Int. J. Mass Spectrom. 308, 35.
Vinodkumar, M., Limbachiya, C., Barot, M., Swadia, M., Barot, A., 2013a. Electron impact total ionization cross sections for all the components of DNA and RNA molecule. Int. J. Mass Spectrom. 339–340, 16.
Vinodkumar, M., Limbachiya, C., Barot, A., Mason, N., 2013b. Computation of electron-impact rotationally elastic total cross sections for methanol over an extensive range of impact energy (0.1 – 2000 eV). Phys. Rev. 87, 012702.
Vinodkumar, M., Limbachiya, C., Desai, H., Vinodkumar, P.C., 2014a. Electron-impact total cross sections for phosphorous triflouride. Phys. Rev. 89, 062715.
Vinodkumar, M., Limbachiya, C., Barot, M., Barot, A., Swadia, M., 2014b. Electron impact total cross sections for components of DNA and RNA molecules. Int. J. Mass Spectrom. 360, 1.
Antonio Zecca, Grzegorz P. Karwasz, and R. S. Brusa, *Total-Cross-Section Measurements For Electron Scattering by NH_3, SiH_4, and H_2S in the Intermediate-Energy Range*, vol. 45, (1992)..
Zein, S.A., Bordage, M.C., Francis, Z., Macetti, G., Genoni, A., Dal Cappello, C., Shin, W. G., Incerti, S., 2021. Electron transport in DNA bases: an extension of the geant4-DNA Monte Carlo toolkit. Nucl. Instrum. Methods Phys. Res. B 488, 70.
Zhang, X., Sun, J., Liu, Y., 1992. A new approach to the correlation polarization potential-low-energy electron elastic scattering by He atoms. J. Physiol. Biochem.: At Mol. Opt. Phys. 25, 1893.

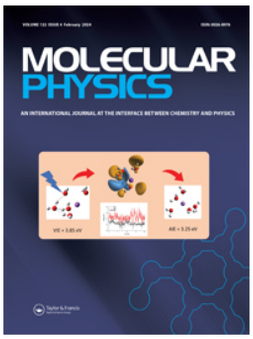

Taylor & Francis
Taylor & Francis Group

Molecular Physics

An International Journal at the Interface Between Chemistry and Physics

ISSN: (Print) (Online) Journal homepage: www.tandfonline.com/journals/tmph20

Theoretical investigation of electron interaction processes for furfural ($C_5H_4O_2$) and p-benzoquinone ($C_6H_4O_2$)

Dhaval Chauhan, Smruti Parikh, Nirav Thakkar & Chetan Limbachiya

To cite this article: Dhaval Chauhan, Smruti Parikh, Nirav Thakkar & Chetan Limbachiya (13 Feb 2024): Theoretical investigation of electron interaction processes for furfural ($C_5H_4O_2$) and p-benzoquinone ($C_6H_4O_2$), Molecular Physics, DOI: 10.1080/00268976.2024.2314706

To link to this article: https://doi.org/10.1080/00268976.2024.2314706

MOLECULAR PHYSICS e2314706
https://doi.org/10.1080/00268976.2024.2314706

Taylor & Francis
Taylor & Francis Group

RESEARCH ARTICLE

Theoretical investigation of electron interaction processes for furfural ($C_5H_4O_2$) and p-benzoquinone ($C_6H_4O_2$)

Dhaval Chauhan[a], Smruti Parikh[a], Nirav Thakkar[b] and Chetan Limbachiya[a]

[a]Department of Applied Physics, The M. S. University of Baroda, Vadodara, India; [b]Department of Physics, Sheth M. N. Science College, Patan, India

ABSTRACT

The present study aims to quantify the electron-induced inelastic and elastic processes for molecules of industrial relevance, furfural and p-benzoquinone. We have computed inelastic cross-sections (Q_{inel}), elastic cross-sections (Q_{el}) and total cross-sections (Q_T) through spherical complex optical potential (SCOP) formalism, from ionisation energy (IE) to 5000 eV. The continuum and discrete contributions of the Q_{inel} have been calculated in terms of ionisation (Q_{ion}) and excitation ($\sum Q_{exc}$) cross-sections, respectively, by employing the complex scattering potential-ionisation contribution (CSP-iC) method. A novel 2-parameter semi-empirical method (2p-SEM), a useful approach applicable for the large molecules $55 < Z < 95$ for calculating Q_T, has been proposed and validated. Computed results are compared with previous experimental and theoretical data. We have also estimated the dielectric constant (ε) using various methods and correlations with molecular ionisation for these applied molecules.

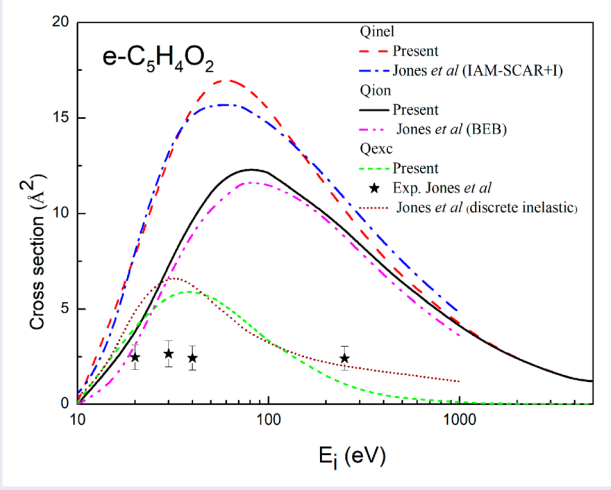

ARTICLE HISTORY
Received 18 May 2023
Accepted 31 January 2024

KEYWORDS
2-parameter semi-empirical method (2p-SEM); SCOP; CSP-ic; dielectric constant (ε); cross-sections

1. Introduction

A situation in which the rising global need for energy must be fulfilled while voicing concerns about climate change has ignited interest in devising new or improved (in terms of sustainability and low-cost) technologies over the last few decades, particularly for the conversion of lignocellulosic biomass into several biomaterials including biofuels [1–3]. Among all the issues to be surmounted, 'biomass recalcitrance' is the major contributor to the high price of converting lignocellulose into biomaterials with a high value. Theoretical and experimental studies conducted to deal with this issue found that radicals and free electrons produced within atmospheric pressure plasmas can aid in the breakdown of biomass through inducing dissociations, excitations and other fragmentation events [4,5]. In light of this, we have

CONTACT Chetan Limbachiya cglimbachiya-apphy@msubaroda.ac.in Department of Applied Physics, The M. S. University of Baroda, Vadodara 390001, India

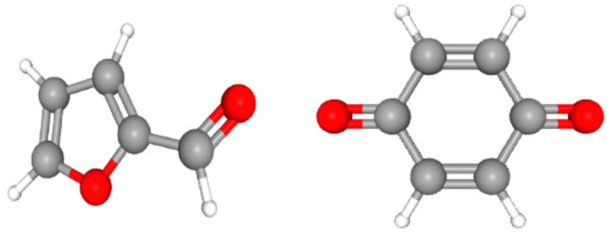

(A) Furfural ($C_5H_4O_2$) (B) p-benzoquinone ($C_6H_4O_2$)

Figure 1. Chemical structure of the molecules (https://pubchem.ncbi.nlm.nih.gov).

conducted the electron collision study with furfural, generated from the species of lignocellulose and a potential substitute for petrochemicals [6]. The chemical structure of the molecules is shown in Figure 1.

2-furaldehyde or furfural ($C_5H_4O_2$) is an essential component of green chemistry, as well as in petroleum, agrochemicals, pharmaceuticals and plastics [7]. Furthermore, it has been recognised as a crucial base chemical [6,8] for the commercialisation of bio-refineries. To provide a greater yield of biofuel conversion, biomass is first treated using electron beam irradiation techniques or atmospheric pressure plasma [3,4]. This and other modelling plasma applications [9] point to the requirement for precise and thorough electron scattering data for furfural [10].

Furthermore, with rising of the energy consumption, worldwide difficulties related to collecting and storing energy sustainably are becoming increasingly important. Knowing and imitating nature may allow developments that could assist in addressing these issues. The principal method for conversion of the energy on Earth is oxygenic photosynthesis, in which H_2O and CO_2 are transformed into O_2 and sugars [11]. Hence, improving our knowledge of these photosynthetic pathways may spur advancements in photocatalysis and photovoltaics [12] as well as the development of hybrid photo-bio electrochemical technologies [13]. Within the cellular respiration and electron transport sequence of photosynthesis, quinones [14] are crucial molecular components since they are capable of performing a reversible reduction process. As a result, they are proving to be a viable option as a long-term, cost-effective material in energy-storage and harvesting systems, such as artificial photosynthetic platforms, dye-sensitised solar cells, phototransistors, rechargeable batteries, plasmonic light harvesting and pseudo-capacitors [14]. The development of bio-inspired energy conversion and harvesting devices can be facilitated by an understanding of the special properties of quinone and its derivatives [14]. In this context, p-benzoquinone (pBQ), the simplest quinone, has served as a prototype structure in a variety of research seeking to understand the electrochemical and photo-induced behaviour of quinones in general [14].

A previous study on electron interactions with furfural and parabenzoquinone includes experimental studies of electron excitation [15] for 20-250 eV and total cross-sections measured using electron transmission technique [16] for 7-20 eV and Transmission-beam attenuation measurements [17] for 1-200 eV. Theoretical results are obtained by Binary-encounter-bethe (BEB) [10] methods, the Schwinger multichannel method with pseudopotentials (SMCPP) [17,18], Independent atomic model with Screening corrected additivity rule including interference (IAM-SCAR + I)[10]. A theoretical group [19] has used a well-established R-matrix method to study the elastic and inelastic collisions between electron and p-benzoquinone at low energy 0 eV to 8 eV.

For the present work, we have focused on these two molecules which have gained recent interest and studied their electron interaction processes for energies from molecular ionisation threshold to 5000 eV. We have quantified various electron-induced molecular processes for these compounds of great industrial applications. These processes are elastic and inelastic including excitations and ionisation.

2. Theoretical methodology

In this electron interaction study, we have computed various cross-sections using the established SCOP method and extracted ionisation cross-sections through the CSP-ic method. Furthermore, we have proposed a novel approach 2p-SEM, which is applicable for the larger and more complex molecules $55 < Z < 95$ for a wide energy range of 50 eV to 5000 eV.

2.1. Spherical complex optical potential formalism (SCOP)

To calculate Q_{inel} and Q_{el}, we have employed spherical complex optical potential formalism with group additivity rule [20,21] since present molecules have a larger physical size. This approach has been thoroughly discussed in our previous articles [21–23]. The complex potential is given as

$$V_{opt} = V_{real} + iV_{Ima} \tag{1}$$

The effects of static potential (V_s), exchange potential (V_{ex}) and polarisation potential (V_{pol}) are included through the real part of the complex potential (V_{real}) and inelastic effects are incorporated through the imaginary potential (V_{Ima}). To construct these potentials the primary input is the charge den$V_{opt} = V_{real} + iV_{Ima}$sity of

the target [24]. For exchange effects [25], the proposed model has been employed and for polarisation, Zhang *et al.* model potential is used.

$$V_{opt}(E_i, r) = V_{st}(r) + V_{ex}(E_i, r) + V_{pol}(E_i, r) + iV_{abs}(E_i, r) \quad (2)$$

To account inelastic effect, the quasi-free modified model potential [26] is used. The final V_{opt} is then fed into the Schroedinger equation, which is then solved numerically employing the partial wave approximation to compute the Q_{inel}, Q_{el} and finally Q_T. There are mainly two contributions that sum up to the Q_{inel}

$$Q_{inel}(E_i) = \sum Q_{exc}(E_i) + Q_{ion}(E_i) \quad (3)$$

where Q_{Ion} is the total ionisation cross-sections for all the permitted ionisation processes. $\sum Q_{exc}$ incorporates all the allowed electronic excitation processes.

2.2. Complex scattering potential-ionisation contribution (CSP-ic)

As the energy is increased above the ionisation energy, the $\sum Q_{exc}$ becomes less relevant than the Q_{ion}. Hence, we have

$$Q_{inel} \geq Q_{ion} \quad (4)$$

In the complex scattering potential-ionisation contribution (CSP-ic) formalism [27,28] we define a ratio$R(E_i) = Q_{ion}/Q_{inel}$. This ratio increases from zero at energy$E_i \leq IE$ (ionisation energy) and keeps growing as the incoming energy goes up, eventually approaching unity at very high energies. Thus, we may mathematically represent these criteria as

$$R(E_i) = \begin{cases} 0, \textit{ for } E_i \leq IE \\ R_P, \textit{ for } E_i = E_P \\ \sim 1, \textit{ for } E_i \gg E_P \end{cases} \quad (5)$$

The opening of the ionisation channel occurs at the molecule's ionisation energy (IE) as shown in the first condition of Equation (5). However, as needed by the third condition, ionisation predominates at very high energy and excitation cross-sections significantly decrease leading to $R(E_i) = R_P$. Q_{inel} attains maximum value, at this energy E_P, where E_P stands for incident energy at which $R(E_i) = 1$. According to theoretical predictions [20,29,30] and experimental findings for stable compounds [31], R_p is in the range of 0.7 and 0.8. Due to this characteristic, the theory is classified as semi-empirical and a range of 10-15% total uncertainty is introduced. Q_{ion} and Q_{exc} must be calculated with at least the accuracy demanded by users. Target properties are shown in Table 1.

Table 1. Target properties (http://www.chemspider.com).

Molecules	IE (eV)	Polarisability (α) (Å^3)	(a_0^3)
Furfural ($C_5H_4O_2$)	9.21	10.0	67.55
Parabenzoquinone ($C_6H_4O_2$)	10.01[32]	10.8	72.95

Table 2. Parameter for 50 eV–500 eV.

Targets	Adenine ($C_5H_5N_5$) (Z = 70)	Guanine ($C_5H_5N_5O$) (Z = 78)	Thymine ($C_5H_6N_2O_2$) (Z = 66)	Cytosine ($C_4H_5N_3O$) (Z = 58)	Uracil ($C_4H_4N_2O_2$) (Z = 58)
A	46.53	54.79	43.66	34.68	34.56
B	0.58	0.56	0.57	0.56	0.53

2.3. 2parameter-semi-empirical method formalism (2p-SEM)

The impact energy dependence of the Q_T for the intermediate energy[33,34] and high energy[35,36] have been previously studied and the proposed formula was as follows

$$Q_T = \frac{A}{E^B} \quad (6)$$

where parameter A is governed by molecular characteristics such as the size of the molecule and its polarisability. The value of B for the high energies, above 500 eV will be $\sim$0.7, which is proposed by Joshipura [35] and Garcia [36] for smaller molecules, i.e. for ten electrons (Z = 10) and up to Z = 22 electron systems, respectively. In the present work, this formula has been derived for large molecules with 55 < Z < 95. Also, the dependence of Q_T on E_i is different for diverse energy regimes. We have derived two different expressions for the intermediate (50 < E_i < 500 eV) and high energy regions (E_i > 500 eV) for the complex and larger molecular systems with 55 < Z < 95.

In Table 2, the parameters A and B have been tabulated for the DNA bases [37] and it is seen that the value of B is nearly the same for all the molecules and is $\sim$0.56. Our calculations reveal that the Q_T depends on energy and the dependence on incident energy is similar to that of Nishimura and Tawara [33] for 50-500 eV

$$Q_T = \frac{A}{\sqrt{E}} \quad (7)$$

However, the value of A is different for each molecule, suggesting its dependency on the number of target electrons (Z).

To observe this relation, we plotted the graph of A vs Z, as shown in Figures 2 and 3 for 50 < E_i < 500 eV and E_i > 500 eV, respectively. The linear relationship observed in Figure 2 is represented through the following

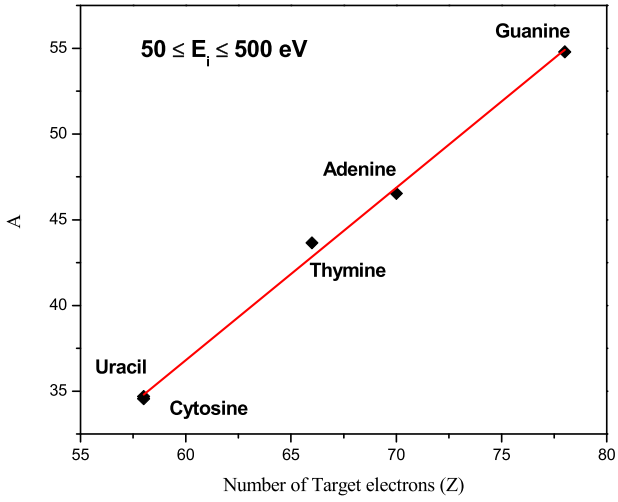

Figure 2. Parameter A vs. Z($50 \leq E_i \leq 500$ eV).

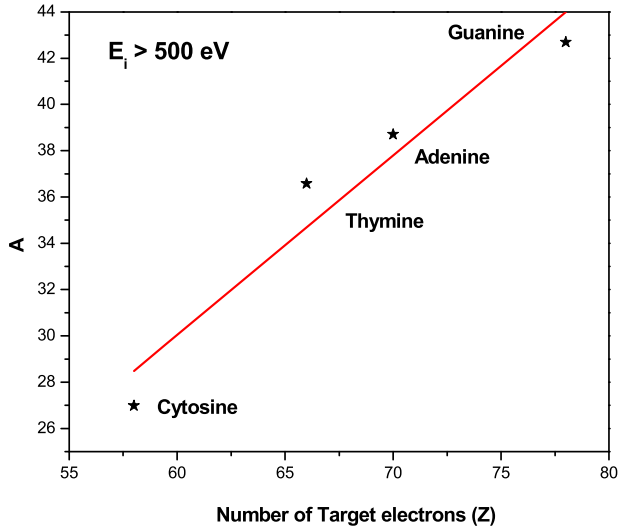

Figure 3. Parameter A vs. Z ($E_i > 500$ eV).

equation

$$A(Z) = Z - 23.54 \quad (\text{Correlation } r = 99\%) \qquad (8)$$

However, for a given Z, the precision of this approximation can be enhanced by considering the difference between the actual values of 'A' (from Table 2) and those derived from Equation (9) for each molecule. We have observed the dependency of this deviation (A – A(Z)) on the molecular size through the polarisability (α). The linear relationship between them is

$$A - A(Z) = -0.003\alpha + 0.63 \qquad (9)$$

Hence, from Equations (8) and (9), a two-parameter expression for Q_T can be formulated for the energy range from 50-500 eV

$$Q_T(E, Z, \alpha) = \frac{(Z) - 0.003(\alpha) - 22.91}{E^{0.56}} \qquad (10)$$

A similar method has been followed to derive the two-parameter expression of Q_T as a function of α and Z for the energies above 500 eV.

$$Q_T(E, Z, \alpha) = \frac{0.016(\alpha) + 0.776(Z) - 17.88}{E^{0.77}} \qquad (11)$$

We note the power of energy E is $E^{0.56}$ for lower side and $E^{0.77}$ for higher side of the incident energy.

Equations (10) and (11) provide the two-parameter expressions for Q_T for impact energy 50 eV $< E_i <$ 500 eV and $E_i >$ 500 eV, respectively allowing the estimation of Q_T for the entire energy range of the current study.

This method is employed to compute Q_{el} and Q_T for p-Benzoquinone (Z = 56) and extrapolated for Furfural (Z = 50).

3. Results and discussion

We calculated various cross-sections (Q_{inel}, Q_T, Q_{el}, Q_{ion}, and $\sum Q_{exc}$) for electron interactions with furfural ($C_5H_4O_2$) and p-benzoquinone ($C_6H_4O_2$) for the impact energy starting from IE to 5000 eV using SCOP, CSP-ic and recently developed 2p-SEM formalism. To facilitate our discussion, present results are shown in three sub-sections along with available comparisons. In sub-section 3.1, present total cross-sections are displayed in Figures 4–8. Sub-section 3.2 discusses validation of 2p-SEM and various correlations. Section 3.3 we presents the computation of the dielectric constant (ε).

3.1. Total cross-sections

Present inelastic, ionisation and excitation cross-sections for e-furfural are plotted in Figure 4.

The topmost curve shows Q_{inel}, which is compared with the only available data from Jones *et al.* [10]. They have used the Independent Atom Model with Screening Corrected Additivity Rule including the Interference (IAM-SCAR + I) method [10] for energies from 1 to 1000 eV. Throughout the energy range present Q_{inel} shows excellent accord with that of Jones *et al.* [10] except at the peak region, where present Q_{inel} slightly overestimates the IAM-SCAR + I result. Only Jones *et a. l*[10] have reported the Q_{ion} results using BEB theory and present data are seen to be in good accord with them within the mentioned 15% uncertainty of BEB[38]. The lowest curve represents the calculated $\sum Q_{exc}$. It is compared with both theoretical and experimental excitation cross-sections of Jones *et al.* [10]. Present $\sum Q_{exc}$ is close to theoretical results but overestimates of experimental

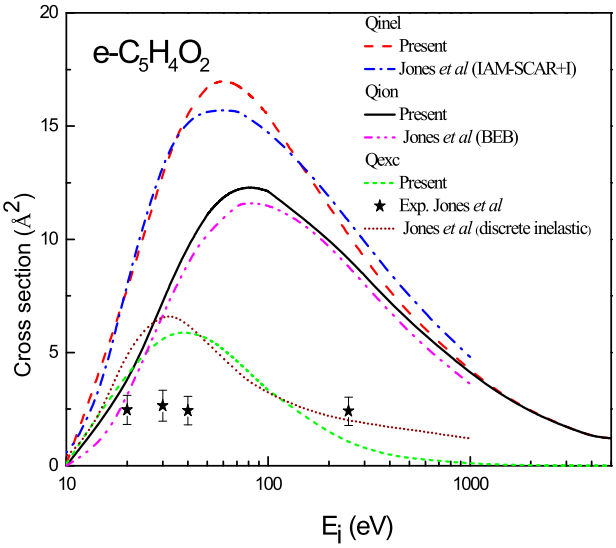

Figure 4. Q_{inel}, Q_{ion}, and $\sum Q_{exc}$ for e-$C_5H_4O_2$ Q_{inel}: Dash – Present, Dash dot – Jones *et al* [10] (IAM-SCAR + I), Q_{ion}: Solid – Present, Dash dot dot – Jones *et al.* [10], Q_{exc}: Short dash-Present, filled star – Jones *et al* [10] (exp.), Short dot- Jones *et al.* discrete inelastic.

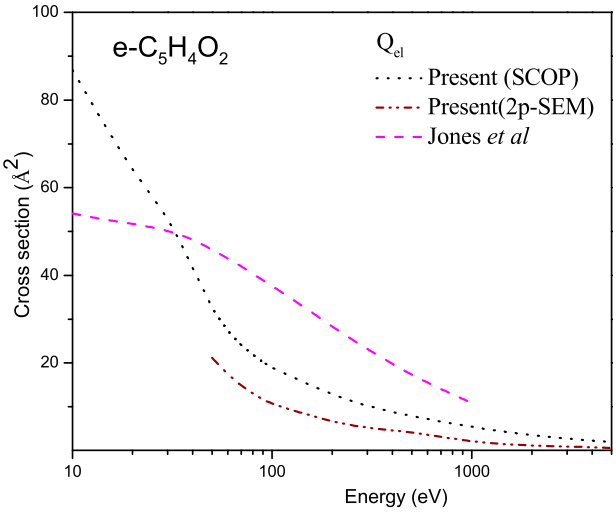

Figure 5. Q_{el} for e-$C_5H_4O_2$ Q_{el}: Dot -Present (SCOP), Dash dot dot -Present (2p-SEM), Dash - Jones *et al.* [10].

data of Jones *et al.* [10]. The experimental electronic excitation cross-sections for the bands I-VI separately and their $\sum Q_{exc}$ (band I + II + III + IV + V + VI), both are reported by Jones *et al.* [10] for the energy range 20-250 eV with the mentioned uncertainty 18% to 69%. This summed Q_{exc} is compared and seen to be of lower values as expected than present $\sum Q_{exc}$ which are calculated for all the allowed electronic excitations.

Figure 5 presents Q_{el} computed using SCOP and 2p-SEM is illustrated for the electron collision with furfural molecule. The only data of Jones *et al.* [10] for Q_{el} have been compared with the present one. At low energies, a

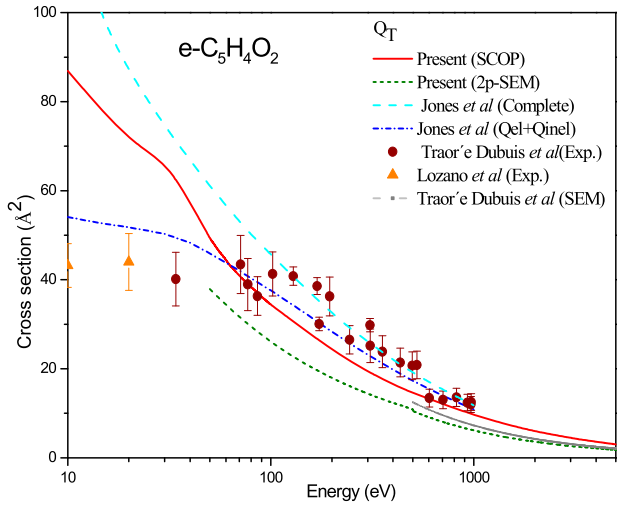

Figure 6. Q_T for e-$C_5H_4O_2$ Q_T: Solid - Present (SCOP), Short dash-Present (2p-SEM), Dash - Jones *et al.* [10] (complete), short dash dot- Jones *et al.* [10] ($Q_{el} + Q_{inel}$), solid circle- Traor´e Dubuis *et al.* [15], Solid triangle- Lozano *et al.* [16], Dash - Traor´e Dubuis *et al.* [15](SEM).

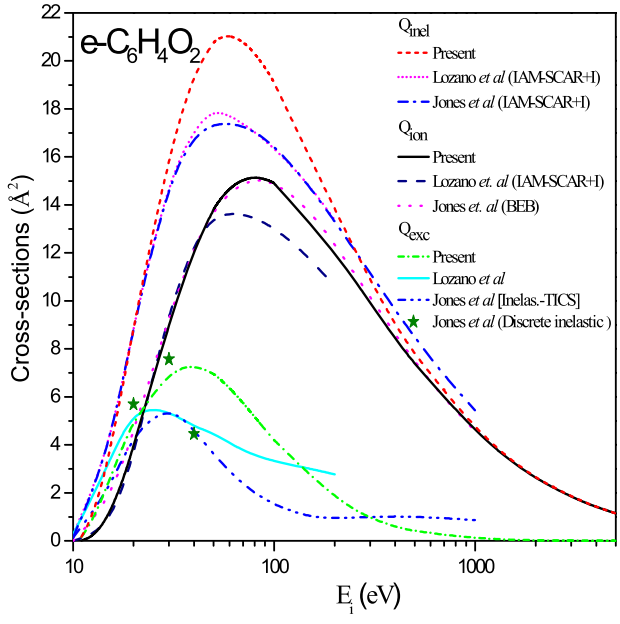

Figure 7. Q_{inel}, Q_{ion}, and $\sum Q_{exc}$ for e-$C_6H_4O_2$ [Q_{inel}: short dash -Present, short dot - Lozano *et al.* [17] (IAM-SCAR + I), dash dot - Jones *et al.* [18] (IAM-SCAR + I), Q_{ion}; solid -Present, dash -Lozano *et al.* [17] (IAM-SCAR + I), dot - Jones *et at* [18] (BEB), Q_{exc}; short dash dot -present, dash dot dot -Jones *et al.* [18] (Inelas.-TICS), solid star- Jones *et al.* [18] (Discrete inelastic)].

deviation between both of them can be observed, which is because the present Q_{el} has been calculated in the presence of inelastic channels while Jones *et al.* [10] have computed the pure Q_{el}. SCOP formalism allows for the flux competition between elastic and inelastic channels. We have computed elastic cross-sections by using the

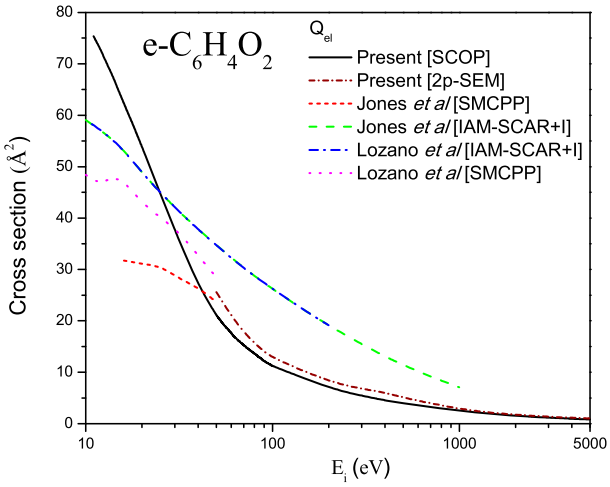

Figure 8. Q_{el} for e-$C_6H_4O_2$ Q_{el}: Solid - Present (SCOP), short dash- Present (2p-SEM), Dot- Lozano *et al.* [17] (SMCPP), dash dot - Lozano *et al.* [17] (IAM-SCAR + I), dash- Jones *et al.* [18] (IAM-SCAR + I), short dash- Jones *et at* [18] (SMCPP).

optical potential that includes an absorption potential. Hence, present elastic cross-sections are the results produced while considering the inelastic channels. Jones *et.al* [10] have reported the pure elastic cross-section data (i.e. no inelastic channels are considered in the computations). The authors reported uncertainty up to 43% at 1000 eV due to interference term added in the calculation of elastic cross-section.

The present Q_T calculated using the present SCOP method is plotted in Figure 6 with the existing data of Jones *et al.* [10], Lozano *et al.* [16] and Traoré Dubuis *et al.* [15]. The discrepancies between the present data and all the available data can be observed in Figure 6. However, the present results of Q_T show the same trend as that of Jones *et al.* [10]. While the present calculation does not involve the non-spherical effects, Jones *et al.* [10] have considered the involvement of rotational excitations in Q_T. This may be the reason for the discrepancy between the present data and the results of Jones *et al.* [10]. The experimental Q_T data of Traoré Dubuis *et al.* [15] are also seen in reasonable agreement with the present ones within the mentioned uncertainty of 4% – 22% above 50 eV[15]. Traoré Dubuis *et al.* [15] have also calculated the Q_T for energy above 500 eV, proposed by Garcia and Manero [39] for molecules having up to 22 electrons. These authors [15] claimed the SEM model has never been validated for ring molecular targets having higher atomic numbers. To estimate Q_{el} and Q_T we developed 2p-SEM and the results show a similar trend but underestimate at lower energies.

The topmost curve in Figure 7 displays the Q_{inel} for e^--$C_6H_4O_2$ collision with data from Lozano *et al.* [17] and Jones *et al.* [18]. Both authors[17,18] have employed the IAM-SCAR + I approach. Except for the peak region, present results show good agreement with the existing ones. Present ionisation cross-sections compared with available theoretical data obtained from IAM-SCAR + I [17] and BEB[18] approaches are shown in Figure 7. In Figure 7, it can be observed that the present Q_{ion} data matches excellently well with the result of Jones *et al.* [18]. However, the data of Lozano *et al.* [17] underestimate both, the present and Jones *et al.* [18] results. The data of Lozano et al. which are up to 200 eV underestimate both. Also in Figure 7, we represent $\sum Q_{exc}$ computed through the present methodology along with the available comparisons. The theoretical excitation cross-sections calculated using the IAM-SCAR + I method [17,18] are in good agreement with the present results below 25 eV, afterwards, they underestimate the present $\sum Q_{exc}$. Because Jones *et al.* [18] have also measured the electronic excitation cross-sections for each band 0-V from 20 to 40 eV energies. Their reported sum values have been compared here with the present $\sum Q_{exc}$ and good agreement can be observed for 20 and 30 eV.

Figure 8 presents Q_{el} for e-$C_6H_4O_2$ collision along with the available elastic results, computed using IAM-SCAR + I[17,18] and SMCPP [17,18] approach have been plotted. Up to 30 eV, present data overestimated with theoretical results. Beyond 30 eV present cross-sections show excellent matching with the data of Lozano *et al.* [17] and Jones *et al.* [18] obtained through SMCPP, while underestimating the results of IAM-SCAR + I [17]. The present 2p-SEM result shows excellent matching with the SCOP data. The total cross-sections along with available results are shown in Figure 9. Starting from the threshold to 30 eV our data underestimate theoretical results computed through [17] but show excellent matching with experimental [17] results within the uncertainty limit of ±5%. The present 2p-SEM result shows excellent matching with the current SCOP result. Present data include SCOP and 2p-SEM shows a similar trend with other available results.

3.2. Validation of 2p-SEM and various correlations

Several groups are involved in theoretical improvements to counter-balance the dearth of the experimental data, a situation that has improved but it is still challenging for many complex targets. Due to theoretical refinements, many models have been created, such as the Binary-encounter Bethe [38], the IAM-SCAR + I[40], the spherical complex optical potential [23,41] ab-initio R-matrix [42], complex Kohn and Schwinger multichannel methods [43,44] and so on. Above mentioned models are

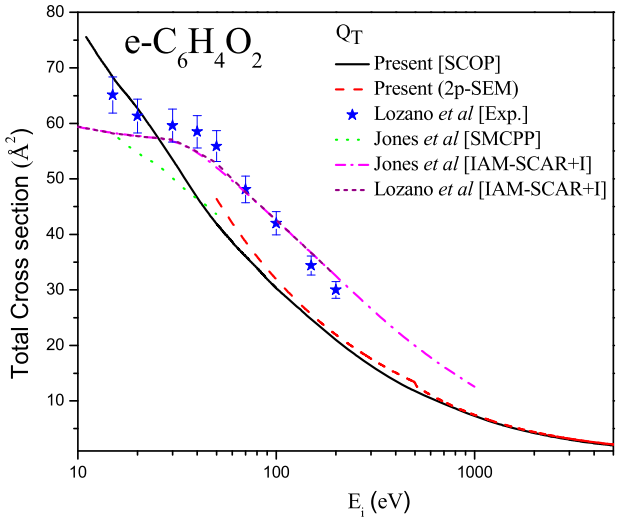

Figure 9. Q_T for e-$C_6H_4O_2$ Q_T: solid- Present, dash- Present (2p-SEM), solid star- Lozano *et al.* [17] (Exp.), dot - Jones *et al.* [18] (SMCPP), dash dot - Jones *et al.* [18] (IAM-SCAR + I), short dash - Lozano *et al.* [17] (IAM-SCAR + I).

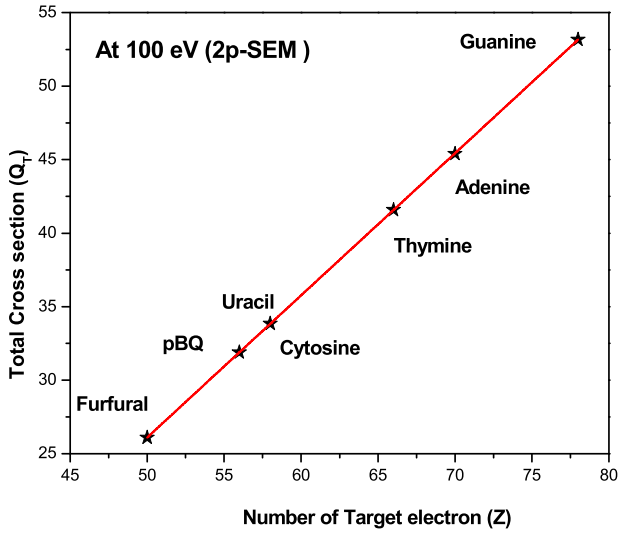

Figure 10. Correlation between Present Q_T (2p-SEM) and Z (Number of target electrons).

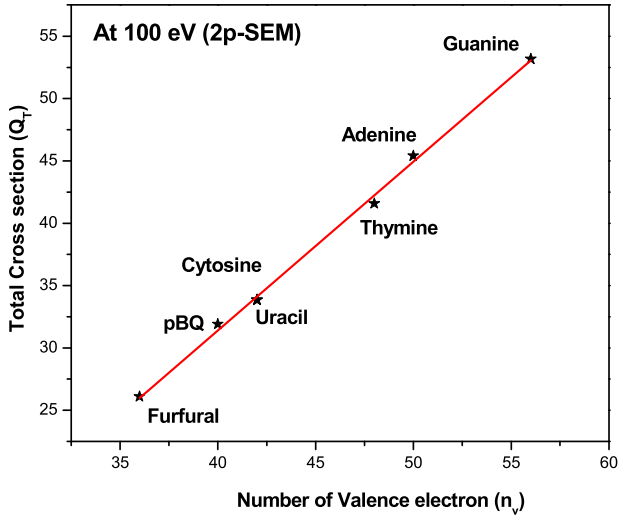

Figure 11. Correlation between Q_T (2p-SEM) and Number of valence electrons (n_v).

used to predict TCS upon electron impact within the computational complexity.

From the total electron scattering cross section data obtained through 2p-SEM, we have plotted various correlation graphs in Figures 10–15. For that we choose DNA/RNA bases [37] (Adenine, Guanine, Thymine, Cytosine), with $55 < Z < 95$. Total cross sections have been calculated analytically for the two different energy range 50 eV to 500 eV (Equation 10) and 500 eV to 5000 eV (Equation 11) as a function of the number of target electrons and the molecular polarisabilities. If there is no comparison provided by any group then the correlation is a very useful feature to evaluate the consistency and reliability of the cross sections data. The 2p-SEM method enables us to obtained reliable Q_T and Q_{el} for large and complex molecules $55 < Z < 95$ for a wide energy range 50–5000 eV.

To check the self-consistency of the present data we have plotted various graphs between Q_T(2p-SEM) vs Z (number of target electrons) and Q_T (2p-SEM) vs n_v (number of valence electrons) in Figures 10–11 at 100 eV respectively. We have shown exact correlation between them and it reflects the size dependency of target charge cloud. And also, we have plotted graph of Q_T vs polarisability (α) in Figures 12–13 at 100 eV & 1000 eV respectively. To include two ranges of energy as used in Equation 10,11. Further in Figure 14, we have shown linear correlation between Q_{ion}^{Max} and target polarisability.

3.3. Computation of dielectric constant, ε

The dielectric constant for p-benzoquinone and furfural molecules has potential applications for the study of electrical energy storage device, pseudo capacitor, photo transistor, dye-sensitised solar cells, artificial photosynthesis, rechargeable batteries, the evolution of new electronic devices and other electrical properties.

The Clausius-Mossotti equation [45] yields,

$$\frac{\varepsilon - 1}{\varepsilon + 2} = \frac{4\pi}{3} * N * \alpha \tag{13}$$

N is the number density of molecules in the material, and α is the molecular polarisability.

The number density can be calculated using the following equation [46],

$$N = \frac{N_A * \rho}{M} \tag{14}$$

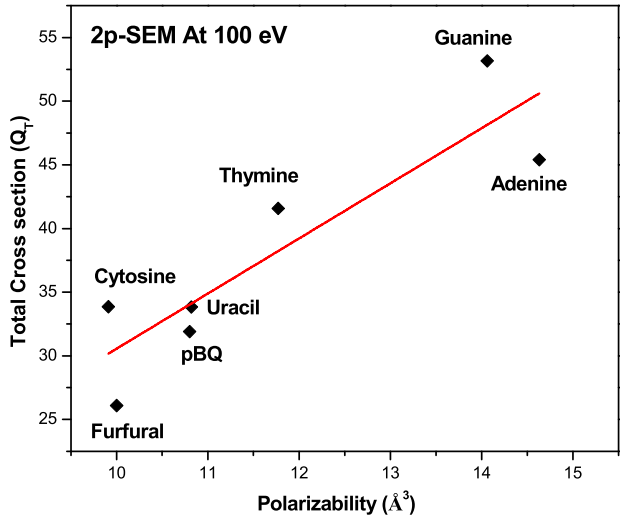

Figure 12. Correlation between Present Q_T (2p-SEM) along with the polarisability ($Å^3$).

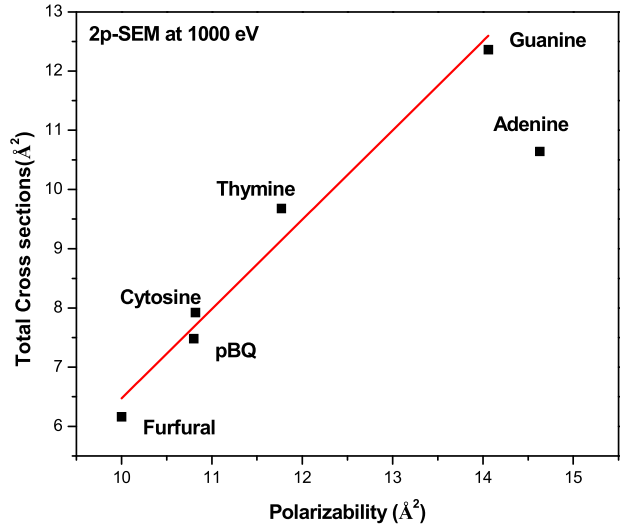

Figure 13. Correlation between Q_T and dipole polarisability (α).

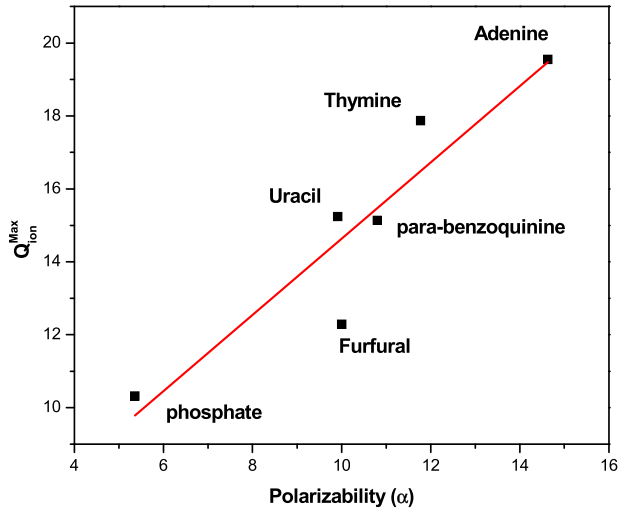

Figure 14. Correlation between $Q_{ion}{}^{Max}$ and dipole polarisability (α).

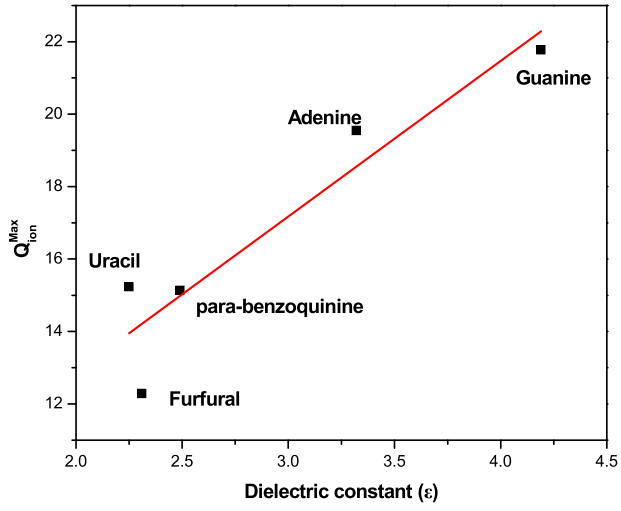

Figure 15. Correlation between $Q_{ion}{}^{Max}$ and dielectric constant (through Equation 13).

where, ρ is the density of the substance, N_A is Avogadro number (6.022×10^{23}), N is the number density of target and M is the molar mass of the molecule.

Secondly, the Onsager [47] equation yields,

$$\frac{\varepsilon - 1}{\varepsilon + 2} = \frac{4\pi}{3}\alpha N + \frac{(\varepsilon - \varepsilon_\infty)(2\varepsilon + \varepsilon_\infty)}{\varepsilon(\varepsilon_\infty + 2)^2} \tag{15}$$

where, ε_∞ is the high frequency dielectric constant.

Relation between $Q_{ion^{Max}}$ and dielectric constant (ε)

According to Harland's [48] proposed qualitative dependency nature of the $Q_{ion}{}^{Max}$ with its polarisability (α) using below Equation (16).

Then we correlate this equation with dielectric constant (using Equation 13),

$$Q_{ion^{Max}} = 11.92(\alpha) = 11.92\left(\frac{3 * (\varepsilon - 1/\varepsilon + 2)}{4\pi N * IE}\right)^{0.5} \tag{16}$$

Using above mentioned three methods, Clausius-Mossotti [45], Onsager [47] and by using the equation of Harland and vallance [48] (through Equations 13, 15,16 respectively), we have computed dielectric constant for present studied targets are shown in Table 3.

From Figure 15, we have observed linear relationship between maximum ionisation cross section and dielectric constant from Clausius- Mossootti Equation (13).

Table 3. Calculated Number density N and Dielectric constant (ε).

Mol.						Dielectric constant (ε)		
Mol.	Q_{ionMax} (Å^2)	α (10^{-24} cm^3)	ρ g/cm^3	M g/mol	N cm^{-3}	C.M. [45]	Onsager [47]	[48]
$C_5H_4O_2$	12.283	10	1.16	96.1	7.27×10^{21}	2.31	0.99	1
$C_6H_4O_2$	15.134	10.8	1.32	108.1	7.35×10^{21}	2.49	1	1

4. Conclusion

In this paper we have computed elastic, inelastic (including excitation and ionisation) and total cross sections for scattering of electrons by furfural and para-benzoquinone. The present cross sections were computed with the SCOP formalism and were compared with results available in the literature for energies above 10 eV. Furfural has many potential uses in bio-fuel, pharmaceutical, agrochemical industries, etc. whereas, p-benzoquinone is an important molecule in energy storage device, pseudo battery, artificial photosynthesis, rechargeable batteries, the evolution of new electronic devices etc. For these applied molecules, our cross-section data may be helpful in simulation. By using SCOP formalism, we quantified Q_T, Q_{el} and Q_{inel}, while Q_{ion} and $\sum Q_{exc}$ were computed through the CSP-ic method and compared with available results. A good agreement was noted between present total ionisation (Q_{ion}) through CSP-ic with BEB and IAM-SCAR + I. We have used a 2p-SEM for an energy range of 50–5 keV. This formalism may be useful for the estimation of Q_T, for those molecules/atoms whose experimental data are not available (especially due to experimental difficulties). In this paper, we have tested this method for larger and complex molecules with target electrons $55 < Z < 95$. By examining the available total electron scattering cross sections for several targets such as DNA constituents, we have observed that at intermediate to high energies the Q_T shows a significant correlation with ground state target dipole polarisability. We also computed dielectric constant ε using Clausius-Mossotti and Onsager and by making use of molecular ionisation cross sections. Furthermore, we have observed several correlations which may be helpful for the prediction of dipole polarisability and dielectric constant.

Disclosure statement

No potential conflict of interest was reported by the author(s).

References

[1] J.W. Tester, E.M. Drake, M.J. Driscoll, M.W. Golay and W.A. Peters, 2nd ed. (The MIT Press, Cambridge, 2012).

[2] J. Amorim, C. Oliveira, J.A. Souza-Correa and M.A. Ridenti, Plasma Processes Polym. **10**, 670 (2013). doi:10.1002/ppap.201200158

[3] N. Schultz-Jensen, F. Leipold, H. Bindslev and A. Thomsen, Appl. Biochem. Biotechnol. **163**, 558–572 (2011). doi:10.1007/s12010-010-9062-5

[4] J. Amorim, C. Oliveira, J.A. Souza-Corrêa and M.A. Ridenti, Plasma Process. Polym. **10**, 670 (2013).

[5] E.M. de Oliveira, R.F. da Costa, S.d. Sanchez, A.P.P. Natalense, M.H.F. Bettega, M.A.P. Lima and M.T.d.N. Varella, Phys. Chem. Chem. Phys. **15**, 1682–1689 (2013). doi:10.1039/C2CP43375C

[6] A.S. Mamman, J.-M. Lee, Y.-C. Kim, I.T. Hwang, N.-J. Park, Y.K. Hwang, J.-S. Chang and J.-S. Hwang, Biofuels, Bioprod. Biorefin. **2**, 438–454 (2008). doi:10.1002/bbb.95

[7] K. J. Zeitsch, *The Chemistry and Technology of Furfural and its Many By-Products*, 1st ed. Elsevier science (2000).

[8] H. Kobayashi and A. Fukuoka, Green Chem. **15**, 1740 (2013). doi:10.1039/c3gc00060e

[9] M.A. Ridenti, J.A. Filho, M.J. Brunger, R.F. da Costa, M.T.d.N. Varella, M.H.F. Bettega and M.A.P. Lima, Eur. Phys. J. D. **70**, 161 (2016). doi:10.1140/epjd/e2016-70272-8

[10] D.B. Jones, R.F. da Costa, M.T.d.N. Varella, M.H.F. Bettega, M.A.P. Lima, F. Blanco, G. Garcia and M.J. Brunger, J. Chem. Phys. **144**, 144303 (2016). doi:10.1063/1.4945562

[11] A. Zouni, H.-T. Witt, J. Kern, P. Fromme and N. Krauss, Nature. **409**, 739–743 (2001). doi:10.1038/35055589

[12] M. Hambourger, G.F. Moore, D.M. Kramer, D. Gust, A.L. Moore and T.A. Moore, Chem. Soc. Rev. **38**, 25–35 (2009). doi:10.1039/B800582F

[13] O. Yehezkeli, R. Tel-Vered, J. Wasserman, A. Trifonov, D. Michaeli, R. Nechushtai and I. Willner, Nature Comm. **3**, 742 (2012). doi:10.1038/ncomms1741

[14] D.B. Jones, F. Blanco, G. García, R.F. Da Costa, F. Kossoski, M.T.D.N. Varella, M.H.F. Bettega, M.A.P. Lima, R.D. White and M.J. Brunger, J. Chem. Phys. **147**, 244304 (2017). doi:10.1063/1.5010831

[15] A. Traoré Dubuis, A. Verkhovtsev, L. Ellis-Gibbings, K. Krupa, F. Blanco, D.B. Jones, M.J. Brunger and G. García, J. Chem. Phys. **147**, 054301 (2017). doi:10.1063/1.4996462

[16] A.I. Lozano, K. Krupa, F. Ferreira da Silva, P. Limão-Vieira, F. Blanco, A. Muñoz, D.B. Jones, M.J. Brunger and G. García, Eur. Phys. J. D. **71**, 226 (2017). doi:10.1140/epjd/e2017-80326-0.

[17] A.I. Lozano, J.C. Oller, D.B. Jones, R.F. Da Costa, M.T.D.N. Varella, M.H.F. Bettega, F. Ferreira Da Silva, P. Limão-Vieira, M.A.P. Lima, R.D. White, M.J. Brunger, F. Blanco, A. Muñoz and G. García, Phys. Chem. Chem. Phys. **20**, 22368–22378 (2018). doi:10.1039/C8CP03297A

[18] D.B. Jones, R.F. Da Costa, F. Kossoski, M.T.D.N. Varella, M.H.F. Bettega, G. García, F. Blanco, R.D. White, M.A.P. Lima and M.J. Brunger, J. Chem. Phys. **148**, 124312 (2018).

[19] A. Loupas and J.D. Gorfinkiel, Phys. Chem. Chem. Phys. **19**, 18252–18261 (2017). doi:10.1039/C7CP02916K

[20] M. Vinodkumar, H. Bhutadia, C. Limbachiya and K.N. Joshipura, Int. J. Mass Spectrom. **308**, 35–40 (2011). doi:10.1016/j.ijms.2011.07.017
[21] M. Vinodkumar, C. Limbachiya, A. Barot and N. Mason, Phys. Rev. A. **87**, 012702 (2013). doi:10.1103/PhysRevA.87.012702
[22] K.N. Joshipura, M. Vinodkumar, C.G. Limbachiya and B.K. Antony, Phys. Rev. A. **69**, 022705 (2004). doi:10.1103/PhysRevA.69.022705
[23] D. Chauhan and C. Limbachiya, Radiat. Phys. and Chem. **207**, 110802 (2023). doi:10.1016/j.radphyschem.2023.110802
[24] H.L. Cox and R.A. Bonham, J. Chem. Phys. **47**, 8 (1967).
[25] S. Hara, J. Phys. Soc. Jpn. **22**, 3 (1967). doi:10.1143/JPSJ.22.710
[26] G. Staszewska, D.W. Schwenke, D. Thirumalai and D.G. Truhlar, Phys. Rev. A. **28**, 2740–2751 (1983). doi:10.1103/PhysRevA.28.2740
[27] K.N. Joshipura, B.G. Vaishnav and C.G. Limbachiya, Pramana- J. Phys. **66**, 403–414 (2006). doi:10.1007/BF02704393
[28] C. Limbachiya, M. Vinodkumar, M. Swadia and A. Barot, Mol. Phys. **112**, 101–106 (2014). doi:10.1080/00268976.2013.802038
[29] H. Yadav, M. Vinodkumar, C. Limbachiya and P.C. Vinodkumar, Mol. Phys. **115**, 952–961 (2017). doi:10.1080/00268976.2017.1293306
[30] M. Vinodkumar, C. Limbachiya, H. Desai and P.C. Vinodkumar, Phys. Rev. A. **89**, 062715 (2014). doi:10.1103/PhysRevA.89.062715
[31] M.R. Chowdhury, D. Chauhan, C.G. Limbachiya, K. Tokési, C. Champion, P.F. Weck and L.C. Tribedi, J. Phys. B: At., Mol. Opt. Phys. **53**, 235201 (2020). doi:10.1088/1361-6455/abbe2b
[32] D.B. Jones, E. Ali, C.G. Ning, J. Colgan, O. Ing´olfsson, D.H. Madison and M.J. Brunger, J. Chem. Phys. **145**, 164306 (2016). doi:10.1063/1.4965919
[33] H. Nishimura and H. Tawara, J. Phys. B: At., Mol. Opt. Phys. **24**, L363–L366 (1991). doi:10.1088/0953-4075/24/15/002
[34] A. Zecca, G.P. Karwasz and R.S. Brusa, Phys. Rev. A. **45**, 2777 (1992). doi:10.1103/PhysRevA.45.2777.
[35] K.N. Joshipura and M. Vinodkumar, Pramana – J. Phys. **47**, 57 (1996). doi:10.1007/BF02847166
[36] G. García and F. Manero, Chem. Phys. Lett. **280**, 419–422 (1997). doi:10.1016/S0009-2614(97)01184-6
[37] M. Vinodkumar, C. Limbachiya, M. Barot, A. Barot and M. Swadia, Int. J. Mass Spectrom. **360**, 1–7 (2014). doi:10.1016/j.ijms.2013.12.027
[38] Y.K. Kim and M.E. Rudd, Phys. Rev. A. **50**, 3954–3967 (1994). doi:10.1103/PhysRevA.50.3954
[39] G. Garcıa and F. Maneró, Chem. Phys. Lett. **280**, 419–422 (1997). doi:10.1016/S0009-2614(97)01184-6
[40] F. Blanco, L. Ellis-Gibbings and G. García, Chem. Phys. Lett. **645**, 71–75 (2016). doi:10.1016/j.cplett.2015.11.056
[41] A. Jain, J. Chem. Phys. **86**, 1289–1300 (1987). doi:10.1063/1.452218
[42] L.A. Morgan, J. Tennyson and C.J. Gillan, Comput. Phys. Commun. **114**, 120–128 (1998). doi:10.1016/S0010-4655(98)00056-3
[43] K. Takatsuka and V. McKoy, Phys. Rev. A. **24**, 2473–2480 (1981). doi:10.1103/PhysRevA.24.2473
[44] C.W. McCurdy, T.N. Rescigno and B. Schneider, Phys. Rev. A. **36**, 2061–2066 (1987). doi:10.1103/PhysRevA.36.2061
[45] C. Kittel and D.F. Holcomb, *Introduction to Solid State Physics*, 8th ed (John Wiley and Sons Inc, 1967).
[46] P. Atkins and J. de Paula, *Atkins' Physical Chemistry* (Oxford university press (2014).
[47] L. Onsager, J. Am. Chem. Soc. **58**, 1486–1493 (1936). doi:10.1021/ja01299a050
[48] P.W. Harland and C. Vallance, Int. J. Mass Spectrom. Ion Process. **171**, 173–181 (1997). doi:10.1016/S0168-1176(97)00137-7

International Conference on Recent Advances in (Applied) Sciences & Engineering (Raise)12- 13April,2023
organized by Faculty Of Technology & Engineering, The Maharaja Sayajirao University Of Baroda

Study of Ionization Cross section, Polarizability and Dielectric Constant of C_4F_7N and $C_3F_5HO_2$

Nirav Thakkar[1], Pinal Mer[2], Chetan Limbachiya[2]

[1]*Sheth M. N. Science College, Patan-384 265;*
[2]*Dept. of Applied Physics, The M S University of Baroda, Vadodara- 390 001;*
Email: niravvv28@gmail.com
Email: pinalmer25@gmail.com
E-mail: cglimbachiya-apphy@msubaroda.ac.in

Abstract

In this Paper, we report on the results of our investigations on electron driven molecular processes for the C_4F_7N and $C_3F_5HO_2$ over a wide energy range, from the ionisation potential to 5000 eV. Due to extraordinarily low GWP of C_4F_7N, gas discharges and plasma reactors may benefit from its employment. Calculations of ionisation cross sections (Q_{ion}) are made using the Complex Scattering Potential-ionization contribution (CSP-ic) method and are shown to be in good agreement with the available data. The study involves various correlations, a prediction of dipole polarizability α, determination of the dielectric constant ε for C_4F_7N and $C_3F_5HO_2$.

Keywords: SCOP;CSP-ic

1. Introduction

Applications for fluoro- and perfluoro-organic compounds are numerous. Because of this, specific members of this family, the perfluorocarboxylic acids (PFCA), are widely distributed in the environment. They have been discovered in human and animal tissues (Moody *et.al.*, 2002), ambient waters (So *et.al.*, 2007), wastewater plants (Zhang *et.al.*, 2015) and the atmosphere (Ellis *et.al.*, 2001). Because of their bioaccumulation (Martin *et.al.*, 2003), environmental persistence, and possible danger to humans and other animals, attention has been drawn to this chemical family, primarily in the last ten years. Perfluoropropionic acid ($C_3F_5HO_2$), may not accumulate as much as longer-chain PFCAs (Martin *et.al.*, 2003) and its natural sources have yet to be identified. Nonetheless, the fact that it has been found in rainwater (Young *et.al.*, 2009) emphasises its function as an ecologically active molecule.

In high-voltage equipment, sulfur hexafluoride (SF_6) is frequently applied as an insulating gas (Li, Zhao, & Murphy, 2018). Numerous physicochemical characteristics including non-toxicity, low boiling point, and great insulating performance favour such a choice. However, SF_6 has a very large global warming potential (GWP), that is 22,800 times higher than CO_2, and it disintegrates relatively slowly in the atmosphere. SF_6 insulated equipment are extensively used in high and ultra-high- electrical voltage systems because of their excellent dependability, low electromagnetic radiation, and little land demand. Nonetheless, the failure of equipment insulation would result in enormous economic loss. C_4F_7N gas, prospective SF_6 alternative, have been extensively explored (Mantilla, Gariboldi, Grob, & Claessens, 2014) in

recent years.

Table 1 displays the difference between the dielectric strength and GWP of SF_6 and the fluoronitrile gases, where it is seen that the two gases share the same characteristics of high dielectric strength (Yu, Hou, & Wang, 2017) and low GWP (Mantilla et al., 2014).

Table 1 Comparison of the GWP and dielectric strength of SF_6 and C_4F_7N

Molecule	E_r (rel. SF_6)	GWP
C_4F_7N	2.2	2100
SF_6	1	23900

For the purpose of understanding electron avalanche and gas breakdown mechanisms, the sum of the ionisation cross sections produced by electron impacts (Q_{ion}) is a crucial variable. In figure 1 we show schematics of fluonitriles investigated in this work.

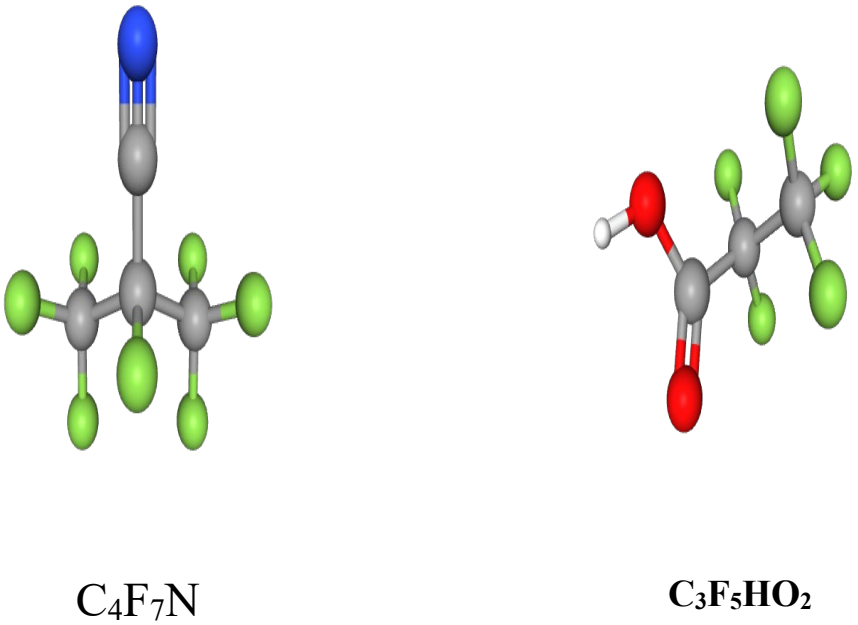

C_4F_7N **$C_3F_5HO_2$**

Fig. 1 Diagrammatic representations of C_4F_7N and $C_3F_5HO_2$ molecules
(https://pubchem.ncbi.nlm.nih.gov**)**

2. Computational Method

In this investigation, two distinct methodologies are used to calculate electron-driven molecular processes, viz. the Spherical Complex Optical Potential (SCOP)(Limbachiya, Vinodkumar, Swadia, & Barot, 2014; Thakkar, Swadia, Vinodkumar, Mason, & Limbachiya, 2021), the Complex Scattering Potential- ionisation contribution (CSP-ic) (Chauhan & Limbachiya, 2023; Joshipura, Vinodkumar, Limbachiya, & Antony, 2004).

2.1 SCOP formalism

The loss of projectile energy is a factor in all electron-molecule collisions other than the elastic, which are widely categorised in the inelastic channel. Under the fixed nuclei approach of the SCOP formalism, these interaction processes are characterised by an optical potential,

$$V_{opt}(E_i, r) = V_{st}(r) + V_{ex}(E_i, r) + V_{pol}(E_i, r) + iV_{abs}(E_i, r) \quad (1)$$

The short ranged static potential (V_{st}) quantifies the original cloud of charges in the molecular system and is constructed by employing the Hartree-Fock wave functions (Bonham, Peacher, & Cox, 1964). Exchange potential (V_{ex}) governs the exchange of the incident electrons with the target electrons. The asymptotic polarisation potential is given by an adiabatic equation(Krestyanikova & Shematovich, 2006; Yadav, Vinodkumar, Limbachiya, & Vinodkumar, 2017),

$$V_{pol} = -\frac{\alpha_d}{2r^4} - \frac{\alpha_q}{2r^6} \quad (2)$$

Here, we have disregarded the multipolar terms of higher order. The static dipole and quadrupole polarizabilities are denoted by α_d and α_q, respectively.
According to the absorption potential (V_{abs}), electronic excitation and ionisation are described by transfer of projectile flux into inelastic scattering channels.

2.2 CSP-ic formalism

The total ionisation cross section is a parameter of substantial practical relevance. Some writers created the CSP-ic approach, which involves specifying a ratio $R(E_i)$ such that (Joshipura et al., 2004; Parikh, Vinodkumar, & Limbachiya, 2023) to calculate Q_{ion}.

$$R(E_i) = \frac{Q_{ion}(E_i)}{Q_{inel}(E_i)} \quad (3)$$

The ratio $R(E_i)$ is defined as follows, where E_i represents the impact energy.

$$R(E_i) = 1 - C_1\left(\frac{C_2}{U+a} + \frac{lnU}{U}\right) \quad (4)$$

Where, $U = \frac{E_i}{I}$ and I refers to the target's ionisation potential. To calculate the three constants C_1, C_2, and a, we need to meet the following three requirements:

$$R(E_i) = \begin{cases} 0, & for\ E_i \le I \\ R_P, & for\ E_i = E_P \\ \sim 1, & for\ E_i \gg E_P \end{cases} \quad 5) \quad ($$

The opening of the ionisation channel occurs at the molecule's ionisation threshold (I). However, as needed by the third criterion, ionisation predominates at very high energy and excitation cross sections significantly decrease. The $R(E_i)=R_p$ connection holds true at the inelastic cross sections' maximum value. Specifically, value of the ratio $R(E_i)$ at impact energy E_p is denoted by the constant R_p. where the Q_{inel} are maximum. According to theoretical predictions(Kim & Stone, 2001; Limbachiya, Vinodkumar, Swadia, Joshipura, & Mason,

2015) and experimental findings for stable compounds like CH_4, H_2O(Joshipura, Vaishnav, & Limbachiya, 2006; Vinodkumar, Limbachiya, Barot, & Mason, 2013), R_p is in the range of 0.7 and 0.8.

3. Results and Discussions

Inelastic processes

As shown in figure 2, we will provide the Q_{inel}, Q_{ion}, and ΣQ_{exc} for C_4F_7N and contrast them with earlier research. In figure 3, we have plotted the Q_{ion} for $C_3F_5HO_2$ against impact energy of electrons.

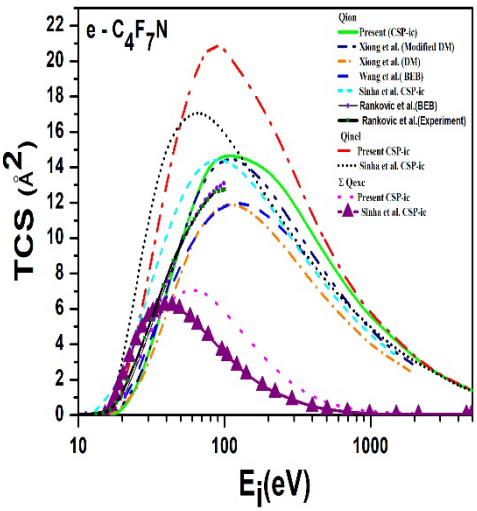

Fig. 2. Inelastic processes for C_4F_7N
line: Present Q_{ion}; Dashed: Wang et al.[12] Q_{ion} (BEB); Dash Dot Dotted: Xiong et al. (Xiong, Li, Wu, Guo, & Zhao, 2017)Q_{ion} (Modified DM); Short Dashed Dot: Xiong et al. (Xiong et al., 2017) Q_{ion} (DM); Short Dashed l: Sinha et al.(Sinha, Patel, & Antony, 2020) Q_{ion} (CSP-ic); -●- Rankovic et al.(Ranković et al., 2019)(BEB) Q_{ion}; -■- Rankovic et al.(Ranković et al., 2019)(Experiment) Q_{ion}; Dash Dotted: Present Q_{inel}; Short Dotted : Sinha et al.(Sinha et al., 2020) Q_{inel} (CSP-ic); Dotted:Present $\sum Q_{exc}$; -◀- line: Sinha et al.(Sinha et al., 2020) $\sum Q_{exc}$ (CSP-ic)

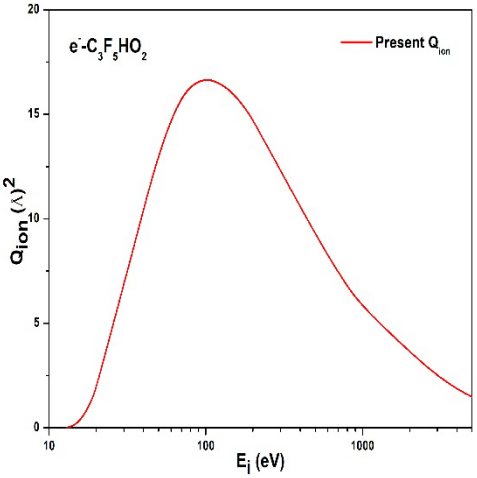

Fig. 3 Ionization cross-section for $C_3F_5HO_2$
Line: Present Q_{ion}

The cross sections for electron scattering caused by C_4F_7N are shown in Fig.2. When comparing Q_{inel} (the curve at the top) with ΣQ_{exc}, it can be seen that the data that are now accessible have a larger magnitude than the data that were published by Sinha et al.(Sinha et al., 2020) and their peaks occur at lower energies (the curve that is at the bottom). The Q_{ion} result obtained by Sinha et al. (Sinha et al., 2020) is slightly less intense than the existing data, and the peak value of the Q_{ion} result generated by Sinha et al. (Sinha et al., 2020) has less energy

than the peak value of any of the other results. According to Sinha et al.(Sinha et al., 2020), the inclusion of nuclear charge in the calculation, which affects both the position and peak value, may be the cause of this discrepancy. It was suggested that this was the cause of the change. The results of the Modified DM calculations provided by Xiong et al. (Xiong et al., 2017) are quite compatible with the existing Q_{ion} over the whole energy range that was studied. While showing reasonable agreement up to the peak of Qion, the BEB and DM findings are significantly lower than the available data beyond Q_{ion}'s peak. Beyond the peak of Q_{ion}, however, the present findings are more accurate. In addition to these findings, Rankovic et al.'s(Ranković et al., 2019) experimental data on the ionisation cross section provides results that, at lower energy, compare favourably with the current CSP-ic result.

Various Correlations: Prediction of polarizability and dielectric constant

Table 2 shows various properties including polarizability of C_4F_7N, $C_3F_5HO_2$ and perfluoroketone (PFK) ($C_xF_{2x}O$, x=5-6) (Thakkar et al., 2021) molecules that are either available in literature or predicted in this work. The data and correlations can be used to predict the polarizability of fluoroketones and fluoronitriles. The total number of electrons (n_e) decides the dimension of the molecular cloud.

Table 2: Molecular properties and predicted α

Target	n_e	Ionization Potential (eV)	Polarizability ($10^{-24}cm^{-3}$)		
			Present	**Estimated**	**Found at www.chemspider.com**
C_4F_7N	94	15.10(WANG ET AL., 2019)	6.82 (Wu et al., 2018)	7.60	8.5 (deviation 11%)
$C_5F_{10}O$	128	12.02 (ZHONG, WANG, WANG, & RONG, 2018)	8.83 (Wu et al., 2017)	9.84	10.6 (deviation 7.1%)
$C_6F_{12}O$	152	11.41 (ZHANG ET AL., 2017)	11.44 (Yu et al., 2017)	12.54	12.6 (deviation 0.4 %)
$C_3F_5HO_2$	80	11.94 (Utsunomiya *et.al.*, 1979)	-	-	7.2

Our findings confirm the linear relationship between Q_{ion} (max) and polarizability, as reported by Bart et al. (Bull, Harland, & Vallance, 2012) (figure 3). Due to this, we can now calculate polarizability for similar compounds like C_3F_5N, C_4F_7N, $C_6F_{12}O$ and $C_5F_{10}O$. In table 4, we can see a excellent matching between the predicted and the computed values, up to 95.18% for C_4F_7N and for $C_5F_{10}O$, $C_6F_{12}O$ molecules it is about 92.8% and 99.5% respectively.

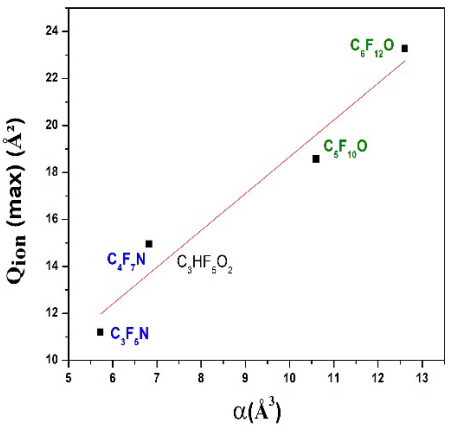

Fig.4. Variation of Q_{ion}(max) with α

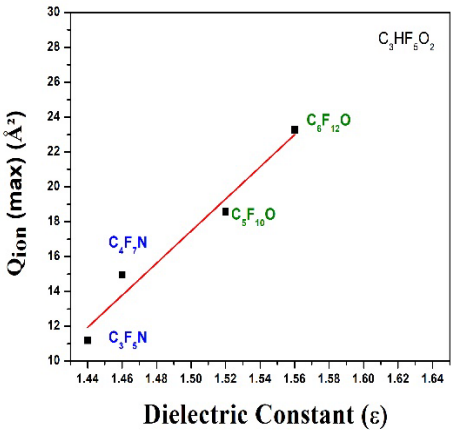

Fig.5. Variation of Q_{ion}(max) with ε

Computation of dielectric constant, ε

The dielectric constant for C_4F_7N molecules has many applications for the study of electrical energy storage, the structure of high-performance electrical insulation materials, the evolution of new electronic devices and other electrical properties.

The Clausius-Mossotti equation (Kittel & Holcomb, 1967) yields,

$$\frac{\varepsilon-1}{\varepsilon+2} = \frac{4\pi}{3} * N * \alpha \qquad (6)$$

N is the number density of molecules in the material, and α is the molecular polarizability.

The number density can be calculated using the following equation (Atkins P, Atkins PW, 2014):

$$N = \frac{N_A * \rho}{M} \qquad (7)$$

Where, ρ is the density of the substance, N_A is Avogadro number (6.022×10^{23}), N is the number density of target and M is the molar mass of the molecule.

In Table 3, we report number density and computed dielectric constant using polarizability for C_4F_7N.

Table 3: Calculated number density N and dielectric constant ε

Target	Polarizability, α ($10^{-24}cm^{-3}$)	Density of material, ρ g/cm^3	Molar mass, M g/mol	Calculated Number Density, N $molecules/cm^3$	Calculated Dielectric Constant, ε
C_4F_7N	6.82 (Wu et al., 2018)	1.5±0.1 (P, 1992)	195.03(P, 1992)	$4.6*10^{21}$	1.45
$C_3F_5HO_2$	7.2 [chemspider.com]	1.56 [chemspider.com]	164.03 [chembk.com]	$5.7*10^{21}$	1.62

We have linear relationship between polarizability and dielectric constant from Clausius-Mossotti equation (6). Since these exists linear relation between Q_{ion} (max) and polarizability (Bull et al., 2012) as seen in figure 4, we can expect linear relation between Q_{ion} (max) and the dielectric constant. We observe this feature for the studied molecules in figure 5. Thus the current study of cross section calculation upon electron impact can help predict dielectric constant for any materials of electrical applications. From figure 4 we can estimate Q_{ion}(max) from the available polarizability and it is found to be 14.20 and the Q_{ion}(max) from figure 3 is found 16.6.

As demonstrated by J. C. Devins's experiments, fluoro-nitrile organic gases like C_4F_7N can have double electric strengths than that of SF_6 (Jiao, Xiao, Zhao, & Deng, 2016). The dielectric properties of C_4F_7N lead to its potential use as a high-performance insulating gas in power equipment. The dielectric constant of C_4F_7N was found to be significantly greater to that of the SF_6, a widely employed insulating gas, which suggests that C_4F_7N could be a promising alternative for use in power equipment (Qiu et al., 2020).

References

Moody, C. A.; Martin, J. W.; Kwan, W. C.; Muir, D. C. G.; Mabury, S. A. (2002). Monitoring perfluorinated surfactants in biota and surface water samples following an accidental release of fire-fighting foam into Etobicoke Creek. Environ. Sci. Technol. 36, 545−551.

Zhang, C.; Yan, H.; Li, F.; Zhou, Q. (2015). Occurrence and fate of perfluorinated acids in two wastewater treatment plants in Shanghai, China. Environ. Sci. Pollut. Res. 22, 1804−1811.

So, M. K.; Miyake, Y.; Yeung, W. Y.; Ho, Y. M.; Taniyasu, S.; Rostkowski, P.; *et al.* (2007). Perfluorinated compounds in the Pearl River and Yangtze River of China. Chemosphere 68, 2085−2095.

Ellis, D. A.; Mabury, S. A.; Martin, J. W.; Muir, D. C. G. (2001). Thermolysis of fluoropolymers as a potential source of halogenated organic acids in the environment. Nature 412, 321−324.

Martin, J. W.; Mabury, S. A.; Solomon, K. R.; Muir, D. C. G. (2003). Dietary accumulation of perfluorinated acids in juvenile rainbow trout (Oncorhynchus mykiss). Enviro Toxicol. Chem. 22, 189−195.

Young, C. J.; Hurley, M.l.D.; Wallington, T. J.; Mabury, S. A. (2009). Atmospheric chemistry of CF3CF2H and CF3CF2CF2CF2H: Kinetics and products of gas-phase reactions with Cl atoms and OH radicals, infrared spectra, and formation of perfluorocarboxylic acids. Chem. Phys. Lett. 473, 251−256.

Utsunomiya, C.; Kobayashi, T.; Nagakura, S. (1979). Photoelectron spectra of hydrogen-bonded complexes. Bull. Chem. Soc. Jpn. 52, 3223−3225.

Atkins P, Atkins PW, de P. J. (2014). *Atkins' physical chemistry*. Oxford university press.

Bonham, R. A., Peacher, J. L., & Cox, H. L. (1964). On the calculation of multicenter two-electron repulsion integrals involving slater functions. *The Journal of Chemical Physics*, *40*(10), 3083–3086. https://doi.org/10.1063/1.1724953

Bull, J. N., Harland, P. W., & Vallance, C. (2012). Absolute total electron impact ionization cross-sections for many-atom organic and halocarbon species. *Journal of Physical Chemistry A*, *116*(1),

767–777. https://doi.org/10.1021/jp210294p

Chauhan, D., & Limbachiya, C. (2023). Electron interactions with analogous of DNA/RNA nucleobases: 3-hydroxytetrahydroFuran and α-Tetrahydrofurfuryl alcohol. *Radiation Physics and Chemistry*, *207*. https://doi.org/10.1016/j.radphyschem.2023.110802

Jiao, J., Xiao, D., Zhao, X., & Deng, Y. (2016). Analysis of the Molecules Structure and Vertical Electron Affinity of Organic Gas Impact on Electric Strength. *Plasma Science and Technology*, *18*(5), 554–559. https://doi.org/10.1088/1009-0630/18/5/19

Joshipura, K. N., Vaishnav, B. G., & Limbachiya, C. G. (2006). Ionization and excitation of some atomic targets and metal oxides by electron impact. *Pramana - Journal of Physics*, *66*(2), 403–414. https://doi.org/10.1007/BF02704393

Joshipura, K. N., Vinodkumar, M., Limbachiya, C. G., & Antony, B. K. (2004). Calculated total cross sections of electron-impact ionization and excitations in tetrahedral [Formula Presented] and [Formula Presented] molecules. *Physical Review A - Atomic, Molecular, and Optical Physics*, *69*(2), 6. https://doi.org/10.1103/PhysRevA.69.022705

Kim, Y. K., & Stone, P. M. (2001). Ionization of boron, aluminum, gallium, and indium by electron impact. *Physical Review A - Atomic, Molecular, and Optical Physics*, *64*(5), 11. https://doi.org/10.1103/PhysRevA.64.052707

Kittel, C., & Holcomb, D. F. (1967). Introduction to Solid State Physics. In *American Journal of Physics* (8th ed., Vol. 35). https://doi.org/10.1119/1.1974177

Krestyanikova, M. A., & Shematovich, V. I. (2006). Stochastic models of hot planetary and satellite coronas: A hot oxygen corona of Mars. *Solar System Research*, *40*(5), 384–392. https://doi.org/10.1134/S0038094606050030

Li, X., Zhao, H., & Murphy, A. B. (2018). SF6-alternative gases for application in gas-insulated switchgear. *Journal of Physics D: Applied Physics*, *51*(15). https://doi.org/10.1088/1361-6463/aab314

Limbachiya, C., Vinodkumar, M., Swadia, M., & Barot, A. (2014). Electron impact total cross section calculations for CH 3SH (methanethiol) from threshold to 5 keV. *Molecular Physics*, *112*(1), 101–106. https://doi.org/10.1080/00268976.2013.802038

Limbachiya, C., Vinodkumar, M., Swadia, M., Joshipura, K. N., & Mason, N. (2015). Electron-impact total cross sections for inelastic processes for furan, tetrahydrofuran and 2,5-dimethylfuran. *Molecular Physics*, *113*(1), 55–62. https://doi.org/10.1080/00268976.2014.943314

Mantilla, J. D., Gariboldi, N., Grob, S., & Claessens, M. (2014). Investigation of the insulation performance of a new gas mixture with extremely low GWP. *EIC 2014 - Proceedings of the 32nd Electrical Insulation Conference*, (June), 469–473. https://doi.org/10.1109/EIC.2014.6869432

P, D. (1992). CRC Handbook of Chemistry and Physics. In *Journal of Molecular Structure* (Vol. 268). https://doi.org/10.1016/0022-2860(92)85083-s

Parikh, S., Vinodkumar, M., & Limbachiya, C. (2023). Electron impact inelastic molecular processes for deuterated compounds. *Chemical Physics*, *565*. https://doi.org/10.1016/j.chemphys.2022.111766

Qiu, R., Zhou, W., Zheng, Y., Hu, S., Li, H., & Yu, J. (2020). A Simulation Research on Diffusion Processes of Discharging Decomposition Products of C4F7N/CO2 in Gas Insulated Transmission Lines. *7th IEEE International Conference on High Voltage Engineering and Application, ICHVE 2020 - Proceedings*, 20–23. https://doi.org/10.1109/ICHVE49031.2020.9279468

Ranković, M., Chalabala, J., Zawadzki, M., Kočišek, J., Slavíček, P., & Fedor, J. (2019). Dissociative ionization dynamics of dielectric gas C3F7CN. *Physical Chemistry Chemical Physics*, *21*(30), 16451–16458. https://doi.org/10.1039/c9cp02188d

Sinha, N., Patel, V. M., & Antony, B. (2020). Ionization cross sections for plasma relevant molecules. *Journal of Physics B: Atomic, Molecular and Optical Physics*, *53*(14). https://doi.org/10.1088/1361-6455/ab8e26

Tang, N., Chen, L., Zhang, B., & Li, X. (2020). Experimental and Theoretical Exploration of C4F7N

Gas Decomposition under Partial Discharge. *7th IEEE International Conference on High Voltage Engineering and Application, ICHVE 2020 - Proceedings*, 4–7. https://doi.org/10.1109/ICHVE49031.2020.9279726

Thakkar, N., Swadia, M., Vinodkumar, M., Mason, N., & Limbachiya, C. (2021). Electron induced elastic and inelastic processes for perfluoroketone (PFK) molecules. *Plasma Sources Science and Technology*, *30*(8). https://doi.org/10.1088/1361-6595/ac17ca

Vinodkumar, M., Limbachiya, C., Barot, A., & Mason, N. (2013). Computation of electron-impact rotationally elastic total cross sections for methanol over an extensive range of impact energy (0.1 - 2000 eV). *Physical Review A - Atomic, Molecular, and Optical Physics*, *87*(1), 1–10. https://doi.org/10.1103/PhysRevA.87.012702

Wang, F., Dun, Q., Chen, S., Zhong, L., Fan, X., & Li, L. L. (2019). Calculations of total electron impact ionization cross sections for fluoroketone and fluoronitrile. *IEEE Transactions on Dielectrics and Electrical Insulation*, *26*(5), 1693–1700. https://doi.org/10.1109/TDEI.2019.008255

Wu, Y., Wang, C., Sun, H., Murphy, A. B., Rong, M., Yang, F., … Wang, X. (2018). Properties of C4F7N-CO2 thermal plasmas: Thermodynamic properties, transport coefficients and emission coefficients. *Journal of Physics D: Applied Physics*, *51*(15). https://doi.org/10.1088/1361-6463/aab421

Wu, Y., Wang, C., Sun, H., Rong, M., Murphy, A. B., Li, T., … Niu, C. (2017). Evaluation of SF6-alternative gas C5-PFK based on arc extinguishing performance and electric strength. *Journal of Physics D: Applied Physics*, *50*(38). https://doi.org/10.1088/1361-6463/aa800b

Xiong, J., Li, X., Wu, J., Guo, X., & Zhao, H. (2017). Calculations of total electron-impact ionization cross sections for Fluoroketone C5F10O and Fluoronitrile C4F7N using modified Deutsch-Märk formula. *Journal of Physics D: Applied Physics*, *50*(44), 2–9. https://doi.org/10.1088/1361-6463/aa881d

Yadav, H., Vinodkumar, M., Limbachiya, C., & Vinodkumar, P. C. (2017). Scattering of electrons with formyl radical. *Molecular Physics*, *115*(8), 952–961. https://doi.org/10.1080/00268976.2017.1293306

Yu, X., Hou, H., & Wang, B. (2017). Prediction on dielectric strength and boiling point of gaseous molecules for replacement of SF6. *Journal of Computational Chemistry*, *38*(10), 721–729. https://doi.org/10.1002/jcc.24741

Zhang, X., Tian, S., Xiao, S., Deng, Z., Li, Y., & Tang, J. (2017). Insulation strength and decomposition characteristics of a C6F12O and N2 gas mixture. *Energies*, *10*(8). https://doi.org/10.3390/en10081170

Zhong, L., Wang, J., Wang, X., & Rong, M. (2018). Calculation of electron-impact ionization cross sections of perfluoroketone (PFK) molecules CxF2xO (x = 1-5) based on Binary-Encounter-Bethe (BEB) and Deutsch-Märk (DM) methods. *Plasma Sources Science and Technology*, *27*(9). https://doi.org/10.1088/1361-6595/aad4d2